# A Quantum Cluster Approach to Vibrational Spectra and Anderson Localization of Phonons in Disordered Harmonic Lattices



Wasim Raja Mondal

Theoretical Sciences Unit

Jawaharlal Neheru Center for Advanced Scientific Research

A thesis submitted for the degree of

*Doctor of Philosophy*

November 2019

*Abba, Maa, Rinku, Bhabi*

# Declaration

I hereby declare that the matter embodied in the thesis entitled "**A Quantum Cluster Approach to Vibrational Spectra and Anderson localization of Phonons in Disordered Lattices**" is the result of investigations carried out by me at the Theoretical Sciences unit, Jawaharlal Nehru Centre for Advanced Scientific Research, Bangalore, India under the supervision of Prof. N. S. Vidhyadhiraja and that it has not been submitted elsewhere for the award of any degree or diploma.

In keeping with the general practice in reporting scientific observations, due acknowledgement has been made whenever the work described is based on the findings of other investigators.

<div align="right">

Wasim Raja Mondal

</div>

# Certificate

I hereby certify that the matter embodied in this thesis entitled "**A Quantum Cluster Approach to Vibrational Spectra and Anderson localization of Phonons in Disordered Lattices**" has been carried out by Mr. Wasim Raja Mondal at the Theoretical Sciences Unit, Jawaharlal Nehru Centre for Advanced Scientific Research, Bangalore, India under my supervision and that it has not been submitted elsewhere for the award of any degree or diploma.

<div align="right">

Prof. N. S. Vidhyadhiraja
(Research Supervisor)

</div>

# Acknowledgements

# Synopsis

A disorder induced metal-insulator transition, where diffusive transport comes to a complete halt due to quantum interference is a universal wave-based quantum phenomenon discovered by Anderson 60 years ago. Among the models involving excitation of classical waves that are expected to exhibit Anderson localization, the oldest problem is the disordered lattice vibrational problem, which was introduced by Dyson even before the concept of electron localization. The complicated physics of phonon localization represents a challenge for analytical approaches. Also, an efficient numerical method that is compulationally feasible and can be scaled upto real material calculations for investigating Anderson localization is still lacking. This thesis opens up a new direction by introducing a new computational approach for investigating the Anderson localization of phonons in solids.

**In chapter 1**, we have introduced Anderson localization, with its past and present developments. We have discussed phonon localization and its impact in controlling the thermal transport in solids. We have highlighted the main aim of this thesis which is the development of a Green's function based quantum cluster approach for studying phonon localization.

**In chapter 2**, a Green's function formalism for lattice vibrations is presented. This Green's function formalism is extensively used in chapter 3.

**In chapter 3**, we present our development of the dynamical cluster approximation (DCA) and typical medium dynamical cluster approximation

(TMDCA) for studying mass-disordered phononic systems. It is shown that the DCA and TMDCA contain essential features of a successful cluster theory. We have demonstrated that the DCA introduces systematic and causal corrections to the single-site coherent potential approximation, whereas the TMDCA is a systematic cluster extension of the local typical medium theory. We have extensively benchmarked the DCA and TMDCA against exact diagonalization and transfer matrix method, respectively. Using the TMDCA, we have shown that in a binary alloy, the high-frequency vibrational modes localize as the impurity becomes lighter with respect to the host atoms. We also find that the low-frequency vibrational modes are the most resilient to localization.

**In chapter 4**, we have employed the TMDCA for studying the effects of short-range spatial correlations on phonon localization in mass-disordered systems by introducing pair-wise spatial correlations between neighboring lattice sites that are labeled by odd and even site indices. We find that such pair-wise correlations drastically change the Anderson transition of phonons, in the sense that, short-range correlated disorder prevents the localization of vibrational modes, and finally, a correlation driven localization-delocalization transition of phonons emerges in a three-dimen -sional disordered sample.

**In chapter 5**, we have introduced a non-trivial modification of the DCA/ TMDCA developed in chapter-3 to incorporate force-constant disorder in addition to mass disorder using the Blackman- Esterling-Berk formalism and shown that the DCA and TMDCA serve as efficient computational methods in treating both mass and force constants disorder of a binary alloy. The DCA is shown to preserve it's cluster properties, while the TMDCA successfully captures the Anderson localization of phonons. Excellent agreement of the results obtained from the DCA with exact diagonalization results of our collaborator Dr. Tom Berjlin of ORNL, USA,

for various values of mass and force constants disorder validate our formalism. We note that such benchmarking incorporating both the mass and force constants disorder has not been carried out hitherto in the literature. Using the DCA and TMDCA, the effects of mass disorder and a concomitant change in the force constants on the vibrational spectra have been carefully examined. We have uncovered the role of force constants disorder in the formation of the boson peak and character of the vibrational modes associated with the boson peak. Also, we have revealed the role of force-constants in controlling the vibrational property of the solid as experimentally found in $Ni_{1-x}Pt_x$ alloys. The interplay of mass and force constants disorder in a binary alloy is found to be non-trivial. The two types of disorder could act competitively or cooperatively depending on the frequencies of the vibrational spectra. As an alternative route to achieving strong localization, we show by a qualitative modeling of vacancies that they are capable of localizing the vibrational modes over the entire frequency region of the vibrational spectra.

**In chapter 6**, we have extended the DCA for studying disordered lattice vibrations by incorporating three branches in our formalism. We have shown that the DCA in its multi-branch form maintains important cluster properties and is a systematic extension of the previous single-site formalism that was described in Chapter 3. We have compared results that are obtained from the multi-branch DCA with exact diagonalization results and found an excellent agreement between them. Using the DCA, we have investigated the precursor effects of Anderson localization of phonons including the vectorial nature of phonons. However, as shown in this thesis, within our formalism, description of phonon localization can not be completed without observing the typical density of states. For doing so, the TMDCA for multibranch disordered phononic systems remains to be developed in future.

**In chapter 7**, we outline our overall findings in this thesis. Finally, we end our discussion with possible future directions.

# List of publications

## Publications Related to the Thesis Work

1. Localization of phonons in mass-disordered alloys: A typical medium dynamical cluster approach, **Wasim Raja Mondal**, T. Berlijn, Juana Moreno, M. Jarrell, N. S. Vidhyadhiraja, Phys. Rev. B **96**, 014203, (2017)

2. Phonon localization in binary alloys with diagonal and off-diagonal disorder: A cluster Green's function approach, **Wasim Raja Mondal**, T. Berlijn, M. Jarrell, N. S. Vidhyadhiraja, Phys. Rev. B **99**, 134203, (2019)

3. Anderson localization of phonons in spatially correlated mass-disordered systems: A typical medium dynamical cluster approach, **Wasim Raja Mondal**, N. S. Vidhyadhiraja (Manuscript under preparation)

4. A dynamical cluster approximation for studying vibrational excitations in mass-disordered systems with multiple branches, **Wasim Raja Mondal**, Yi. Zhang,H. Terletska, K.-M. Tam, T. Berlijn, N. S. Vidhyadhiraja (Manuscript under preparation)

# Other Publication by the Author

1. A multi-orbital iterated perturbation theory for model Hamiltonians and real material-specific calculations of correlated systems, Nagamalleswararao Dasari, **Wasim Raja Mondal**, Peng Zhang, Juana Moreno, Mark Jarrell, N. S. Vidhyadhiraja, Eur. Phys. J. B **69**, 202 (2016)

# Contents

# List of Figures

# Chapter 1

# Introduction

The venerable phenomenon of Anderson localization (AL)[1; 2; 3; 4; 5; 6; 7] has generated a sustained interest in the condensed matter physics community over the last five decades due to its paramount importance in diverse phenomena such as metal-insulator transitions, quantum Hall effect, mesoscopic fluctuations in small conductors, quantum chromodynamics, and quantum chaos. Although the initial focus was on electronic systems, where the quantum nature of electrons was necessary to obtain an understanding, it was quickly realized subsequently, that AL is not limited to electrons; In fact, the phenomenon should be observable with any kind of wave - quantum or classical. This thesis aims to understand the localization of phonons through a new formalism that was originally developed for electronic systems. We have organized this chapter as follows: In section 1.1, we present a general description of AL. In section 1.2, we demonstrate how the concepts of AL can explain various experimentally observed anomalous transport phenomena. In section 1.3, we discuss several direct experimental findings of AL.

## 1.1 Anderson localization

In 1958, Anderson put forward a radical proposal that a complete localization of electrons is possible in solids. Around the same time, many experiments[8; 9; 10] were trying to understand the spin diffusion in semiconductors. Notably, in 1955, Feher *et al.*[10] experimentally measured electron spin resonance of P and As in doped

Si and found that the characteristic electron spin frequency of P and As continued to exist for a time scale of the order of seconds to minutes. This unusual behavior was hard to interpret from a theoretical point of view because simple Fermi golden rule calculations predicted the expected lifetime to range from 0.1 to $10^{-6}$ s. Hence, a microscopic interpretation of this behavior was proving elusive. Anderson, in his groundbreaking paper[1], based on a viewpoint of a tight-binding model, posited that the anomaly is related to an "absence of diffusion" which originated from a random distribution of site-energies. Anderson's work has stimulated an enormous body of theoretical and experimental work on the nature of metal-insulator transitions and behavior of waves in a disordered system. We now discuss the well established notion of diffusion in a solid.
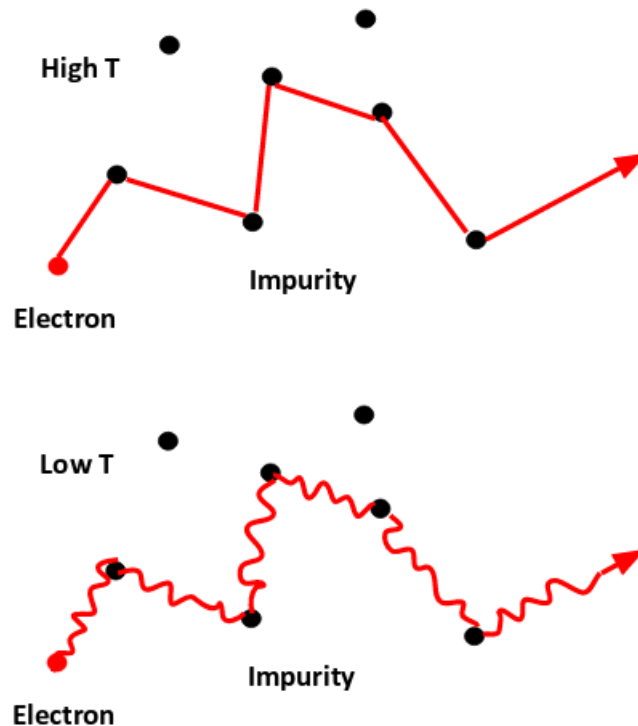


Figure 1.1: Phase coherence increases with decreasing temperature.

***Diffusion in solids***:    The concept of diffusion was well established before 1958[11]. A phenomenological framework was introduced in 1855 by Fick. In 1905, Einstein

put forward an atomistic framework based on kinetic theory, which related the zero temperature dc conductivity($\sigma$) of a solid with the diffusion constant ($D$) as $\sigma = e^2\rho(E_F)D$. Here $\rho(E_F)$ corresponds to the density of states per unit volume at the Fermi level. According to diffusion theory, D can be expressed as $D = \frac{1}{d}v_F l$, where $d, v_F$ and $l$ are the dimensionality, Fermi velocity, and mean-free path, respectively. If $D$ is not zero, the material is supposed to behave as a metal unless the Fermi level lies in a band gap. In that case, depending on the size of the gap, the material should be either an insulator or a semiconductor. The mechanism of the band-gap can be explained within a single particle picture or from electron correlation effects. However, most importantly, within the classical diffusion picture, $D$ would not be zero because $l$ cannot be zero. Even in the presence of strong disorder, $l$ may become shorter but is expected to have some minimum value. Such an expectation leads, through the diffusion equation of Einstein (which should be valid for any Markovian process), to the expectation of a minimum conductivity value. But, this picture can break down in disordered systems. In the presence of disorder, electrons diffract and scatter from impurities. Such random motion through impurity potentials dominates mainly at low temperature as illustrated in Fig1.1. Next, we describe scattering processes in disordered systems.
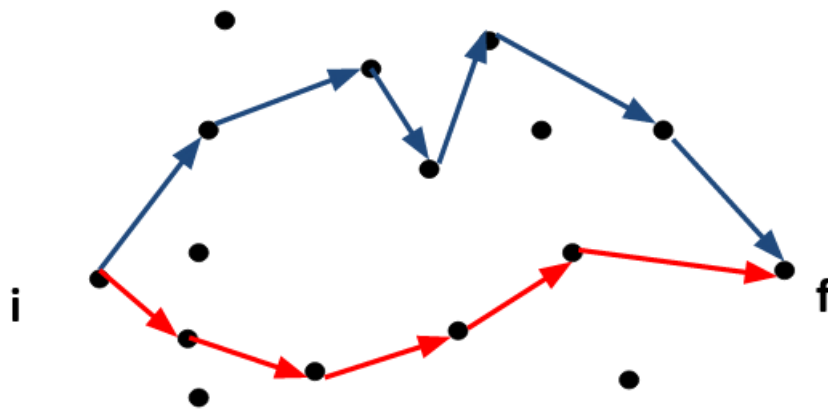


Figure 1.2: Electrons are scattered from impurities.

*Coherent backscattering*:    Let us consider single-electron propagation from lattice site $i$ to lattice site $f$ in a disordered medium. Now the question is, what is the probability that an electron, starting at $i$, will arrive at $f$? The answer is the square of the absolute value of the sum of the amplitudes for all possible paths. For example, let us consider two such paths having amplitude $A_1$ and $A_2$. In this case, the return probability $(W)$ can be expressed as

$$W = |A_1 + A_2|^2$$
$$= \underbrace{|A_1|^2 + |A_2|^2}_{\text{incoherent}} + \underbrace{2|A_1||A_2|\cos(\phi_1 - \phi_2)}_{\text{coherent}}, , \tag{1.1}$$

where the first term is the classical incoherent contribution, and the second term arises due to interference. If the phases of the interference terms become very random in a disordered medium, their sum would vanish on average, and hence this would result in diffusive transport. But the interference term can survive, too. An electron,
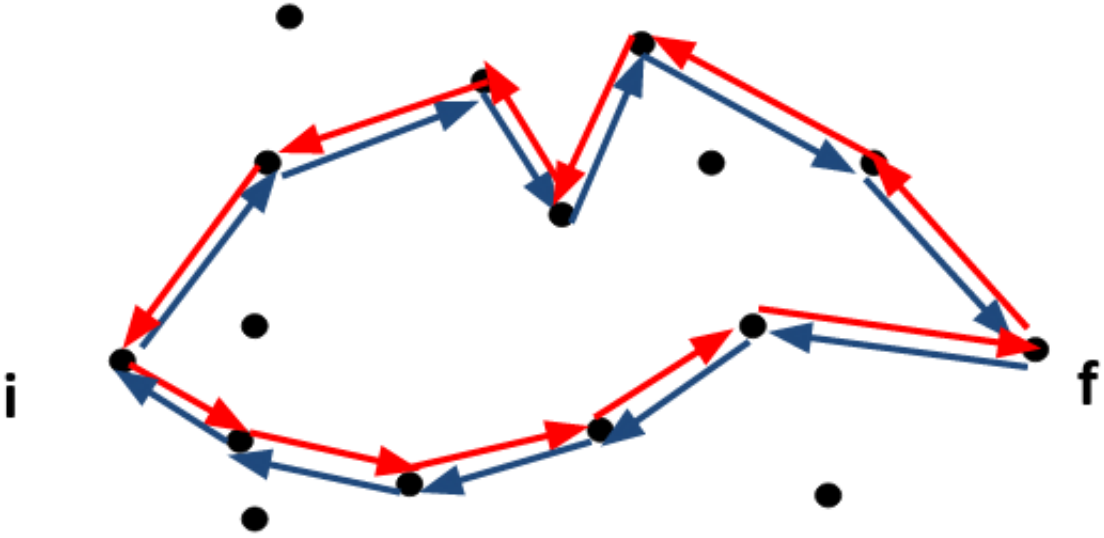


Figure 1.3: In coherent back scattering, the waves scatter coherently along two closed paths that are time reversed partners of each other. The resultant constructive interference increases the return probability significantly leading to localization.

starting from site $i$, goes to $f$ and then returns to $i$ through a scattering process. As shown in Fig. 1.3, for each randomly chosen closed path, there will exist another path

that is, simply, the time-reversed counterpart of the first ($|A_1| = |A_2|$) provided that the system is time-reversal invariant. This leads to an increased probability of the backscattering process and hence leads to localization. So, in such a case,

$$
\begin{aligned}
W &= |A_1 + A_2|^2 \\
&= |A_1|^2 + |A_2|^2 + 2|A_1||A_2| \\
&= 4|A_1|^2 .
\end{aligned}
\tag{1.2}
$$

Eq.(1.2) shows that the return probability increases by a factor of 2 compared to the case of completely incoherent scattering (when $|A_1| = |A_2|$, but the phase information is not preserved in the scattering process) . Consequently, the coherent backscattering process effectively lowers the conductance between $i$ and $f$ by enhancing the electron's likelihood of returning to its starting point $i$. Thus, electrons localize around $i$ and eventually lose their Bloch wave character. The electron can then be viewed as a standing wave that is confined around the neighborhood region of $i$ and consequently has a long lifetime. The envelope of the wave function (see fig. 1.4) develops the following form

$$
\Psi(\vec{r}) \approx e^{-\frac{|\vec{r} - \vec{r}_0|}{\xi}},
\tag{1.3}
$$

with $\xi$ as the localization length.
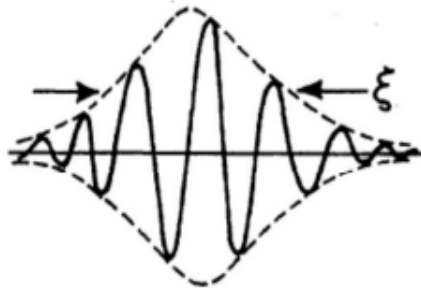


Figure 1.4: The figure is taken from Ref [2]. When localized, the wave function $\Psi(r)$ decays exponentially from some lattice site $r_0$. The wave function has an envelope of the form $|\Psi(r)| \approx \exp(|r - r_0|/\xi)$.

Such a change of the wave function can, with increasing disorder, lead to an absence of the diffusion process, and the system can transform to an Anderson insulator. In the following section, we discuss various theoretical and numerical attempts, that have led to a deeper understanding of localization.

### 1.1.1 Theoretical studies on Anderson localization

*The pre-scaling era(1958-1976)*:  Anderson[1] considered the problem of non-interacting electrons moving on a fixed, regular lattice, hopping from lattice site $i$ to its neighboring site $j$ with a fixed matrix element $t_{ij} = -t$ and on-site energies, $V_i$, being random. The Anderson model is

$$H = -t \sum_{\langle ij \rangle, \sigma} \left( c_{i,\sigma}^{\dagger} c_{j,\sigma} + \text{h.c} \right) + \sum_i \left( V_i - \mu \right) n_{i\sigma}. \tag{1.4}$$

Here, a quasiparticle on site $i$ with spin $\sigma$ is created by the operator $c_{i,\sigma}^{\dagger}$, whereas the operator $c_{j\sigma}$ annihilates a quasiparticle with spin $\sigma$ at lattice site $j$ and $n_{i,\sigma} = c_{i\sigma}^{\dagger} c_{i\sigma}$ is the on-site occupancy of spin $\sigma$. Disorder is introduced in the system through local orbital energies $V_i$, which are generally taken as quenched random variables distributed according to some specific probability distribution $P(V)$. Anderson carried out a perturbative expansion in hopping for the model given in Eq-1.4. Localization was achieved by considering the effect of coherent backscattering from higher-order expansion terms. Thus, Anderson predicted a first quantitative estimate of the strength of the disorder which is needed for the absence of diffusion in certain random lattices. But the exact value of critical disorder for localization was a debatable issue, and it was argued that systems tend to delocalize more easily than Anderson thought. Anderson, in his first treatment, had neglected "loops," i.e electron paths that return to the same lattice site[1]. Subsequently, Thouless and many others[12; 13; 14; 15] bolstered Anderson's treatment by clarifying a few subtle issues such as the so-called small denominator problem. Besides, the localization problem turned out to be more challenging to solve for higher dimensions because one had to take care of all possible paths that a particle could take. Mott explored the concept of localization in

the context of transport properties of amorphous semiconductors and introduced the concept of a mobility edge, an energy scale which separates localized states from extended states. Wegner[16] employed the renormalization group approach. Thus, a connection between Anderson localization and second-order phase transitions was already established in the pre-scaling era.

***The scaling era(1976-1979)***: During the period of 1976 to 1979, the development of a scaling theory for the Anderson localization transition had become a central theme of research in the field of disordered systems.

In 1979, the "Gang-of-four"- E.Abrahams, P.W. Anderson, D. C. Licciardello and T. V Ramakrishnan presented a scaling theory of localization[17] followed by the work of Thouless and co-workers[18; 19] and by Wegner[16]. Its central theme is that close to the transition between localized and extended states, there is only one relevant scaling variable which characterizes the critical behavior of the DC conductivity of metals close to the localization transition and the localization length for Anderson insulators. Thouless[18; 19] suggested that the conductance $G$(not conductivity) for a $L^d$ sample can be expressed in units of $\frac{e^2}{\hbar}$ and hence one can define a dimensionless conductance or "Thouless number" as; $g = G/(\frac{e^2}{\hbar})$, which is a physically measurable quantity. Wegner[16] analyzed the scaling of the conductivity ($\sigma$) for dimensionality $d \neq 2$ as $\sigma \approx (E - E_c)^{(d-2)\nu}$. With this background, the scaling theory employed a renormalization group scheme in which the scaling parameter $g$ was found to satisfy the following renormalization group (RG) equation

$$\frac{d \ln g}{d \ln L} = \beta(g), \tag{1.5}$$

where the scaling function $\beta(g)$ is a function of $g$ alone. The behavior of $\beta$ was explored in the limits of weak and strong disorder strength through the parameter $g$. In the strong disorder limit, all states were found to be be localized with an average localization-length $\xi$. So, $g(L)$ would be a decreasing function of $L$ as $g(L) \approx \exp(-L/\xi)$, which deviates strongly from expected ohmic behavior $(g \approx L^{d-2})$. Thus, in the strong disorder limit, $\beta$ becomes negative as $\beta(g) \approx \ln(g/g_c) < 0$. On the other
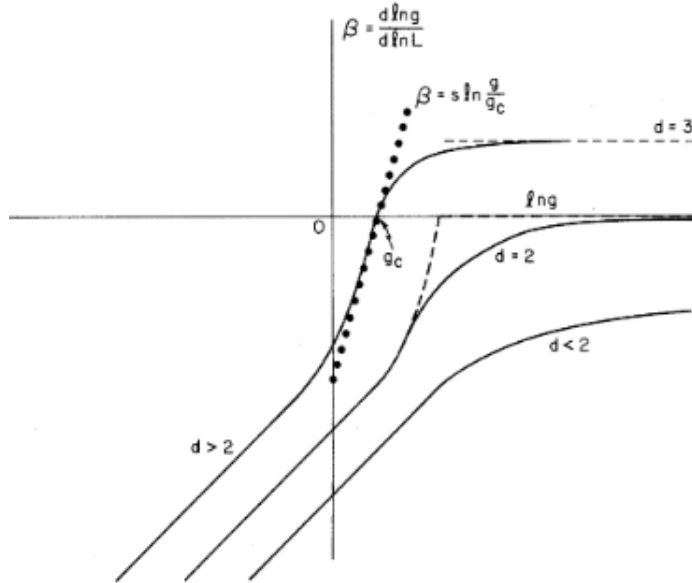
Figure 1.5: Figure is reproduced from Ref[17]. The scaling theory provides a comprehensive description of Anderson localization and Anderson transition in terms of a scaling function $\beta$, taking into account a single scaling parameter, namely the dimensionless conductance $g$. The $\beta$ function changes sign for three dimensions, while for one and two dimensions, it is negative-definite.

hand, in the weak disorder limit, $g$ reduces to an ohmic form as $g \approx L^{d-2}$ so that $\beta = d - 2$. The scaling theory proposed, quite radically, that 1D and 2D systems would be Anderson insulators for any infinitesimal disorder in the thermodynamic limit. For two dimensions, Mott believed the RG trajectory of $g$ could meet the horizontal axis at a minimum metallic conductivity. But, according to the scaling theory, the 2D trajectory approaches the axis logarithmically, but never intersects the $x$-axis, and that suggests that a two-dimensional electronic system would never be metallic. For a 3D system, $\beta$ was shown to be negative for small $g$ and positive for large $g$. Hence, a metal-insulator transition may occur at a critical conductance $g_c$ . Such a behavior of $\beta(g)$ as a function of $\ln g$ is depicted in Fig.1.5.

Thus, the scaling theory provided compelling arguments for the absence of a delocalized phase in 1D and 2D, while arguing that in 3D, a continuous metal-insulator transition can occur as a function of energy (at a mobility edge, $E_c$) or disorder ($\delta_c$) from a delocalized to a localized phase. The scaling theory also yields the critical

behavior at the Anderson transition. Analogous to a second-order phase transition, in the neighbourhood of the transition point, the scaling of two physical observables, namely the localization length ($\xi$) (for $E < E_c$) on the insulating side and dc-conductivity ($\sigma_{dc}$) (for $E > E_c$) on the metallic side was shown to be

$$\xi \propto (E_c - E)^{-\nu}$$
$$\sigma_{dc} \propto (E - E_c)^s. \tag{1.6}$$

The corresponding critical exponents follow the scaling relation $s = \nu(d - 2)$, first derived by Wigner[16].

***The post scaling era (1980-1990):*** The period starting from the eighties to the early nineties saw significant advances, including the development of numerical scaling theory, two-particle formalism and field-theoretic approaches for calculating the conductivity of disordered electronic systems.

Various numerical studies were performed to explore Anderson transition and its critical behavior. Kramer et al.[20], using exact diagonalization, numerically investigated an Anderson transition in 3D and compared it with the scaling theory. Although the agreement between the two was reasonable, in certain parameter regimes, the numerical results did not agree with the analytical results regarding the critical behavior of the Anderson transition. The predicted localization length for an Anderson insulator and zero temperature DC-conductivity of an Anderson metal differed from the scaling theory results. Various numerical calculations[21; 22] as well as a variety of approximate methods[23; 24] were employed to calculate the critical exponents, $\nu$ and $s$, which generated a lively debate. The results obtained through these methods yielded a whole range of $\nu$ and $s$[24; 25; 22] and were very sensitive to the methods used and the approximations made. The critical behavior of Anderson transition was also investigated through the "mobility edge", which separates the localized states from the extended ones. Bulka et al.[26] performed a detailed numerical analysis and obtained surprising results. They provided strong evidence of the existence of extended states beyond the band edge of the unperturbed system, which was in contrast to the

perturbative approach[23], mode-coupling theory[24], and the numerical analyses of the fractal character of the disordered wavefunction[27]. Two mechanisms of localization were proposed to explain the mobility edge[26]: (1) localization through coherent backscattering, and (2) localization due to local potential fluctuations. Economou et al. [28; 29] also discussed localization as arising from potential fluctuations in the context of Anderson localization. Bulka et al. [30; 26] argued that the behavior of mobility edge as a function of disorder could be explained through a competition of local potential fluctuations and quantum interference effects. Unfortunately, such a re-entrance behavior of mobility edge in 3D was impossible to understand in terms of the one-parameter scaling hypothesis[28; 29]. Lee[31] also questioned one-parameter scaling results for 2D.

Rather than studying the one-particle properties, Vollhardt and Wolfle[32; 33; 23] presented an alternate route for studying AL by calculating dynamical or frequency($\omega$)-dependent response function. By using a self-consistent diagrammatic expansion of the density response function, this new approach found strong agreement with the conclusions made by the one-parameter scaling theory. One of the advantages of this approach was that much of the physics of the localization problem was captured, since the approach incorporated maximally crossed diagrams, which included the contribution from coherent backscattering.

Field-theoretic approaches made a significant contribution to the localization problem [34; 35]. There have also been improvements in the perturbative approaches. For example, a perturbative $\epsilon$ expansion in $d = 2 + \epsilon$ dimensions has been computed to five-loops[36].

**The modern era (1990-present):** During the last thirty years, great progress has been made including the finding of multifractality of the wave function at the transition, classification of symmetry as well as universality classes, the criticality of the Anderson transition in higher dimensions as well as in lower dimensions, interaction effects and so on [4].

Several level statistics analyses at the metal-insulator transition have been performed using random matrix theory[37; 38]. In the delocalized phase, the level statistics correspond to the Gaussian orthogonal ensemble (GOE). On the contrary, the localized phase is characterized by Poisson statistics because the exponentially localized wave functions do not overlap with each other. Therefore, level repulsion does not occur, and the distribution of eigenenergies is similar to random points thrown on line. Numerical simulations[39; 40; 41; 42; 43] confirm such predictions. Interestingly, level statistics at the transition can be described neither by GOE nor by Poissonian[44]. Rather, a universal distribution that depends only on dimensionality characterizes such a critical point. At the transition, critical eigenstates, being neither extended nor localized, exhibit large fluctuations of wave-function amplitudes at all length scales. As a result, the spectrum becomes multifractal[45; 46; 47; 48].

The problem of how electrons in a metal become localized by disorder in the presence of non–trivial topology is intertwined with considerations of symmetry classification and universality class. The dimensionality of the system and the symmetries of the Hamiltonian define the universality class. As far as the disordered system is concerned, the Hamiltonian does not have translational symmetry. Instead, the important symmetries for the Anderson localization problem are time-reversal symmetry and spin rotation symmetry. Moreover, certain discrete symmetries may be crucial as well[49; 50]. For example, there are chiral and particle-hole symmetries in certain disordered systems[51]. Ignoring these discrete symmetries, one can define three Wigner-Dyson symmetry classes: orthogonal, unitary, and symplectic. In addition to these conventional Wigner-Dyson classes, there are three chiral classes and four Bogoliubov-de Gennes classes. So, overall, there are ten symmetry classes, including the discrete symmetries[52; 51]. With these symmetry classifications, the criticality in 2D has been explored in great detail[53]. According to the scaling theory, states are always localized in two dimensions. Such a conclusion turns out to be valid only for the orthogonal symmetry class, while the other nine symmetry classes exhibit an Anderson transition in two dimensions, including the unitary class and the symplec-

tic class. The relation between the Anderson transition and topological physics is currently an active area of research with many open questions.

The criticality of Anderson transition in higher dimensions and the critical upper dimension of the localization problem has also been explored. In analogy with continuous thermal phase transitions, the concept of universality and scaling becomes important in the proximity of a critical point. The exponents corresponding to the power law scaling functions are believed to be universal in a sense that they depend only on the university class. The value of the critical exponent for the Anderson transition in the three-dimensional orthogonal universality class has been computed to good precision. Typically, for the Anderson tight binding electronic model in 3D, where the Hamiltonian has both time reversal and spin-rotation symmetries, the critical exponent[4] is found out to be $\nu \simeq 1.57$, which is independent of disorder distribution as verified by the multifractal analysis[54], exact results of Wegner[55] and detailed finite size scaling[56]. Presently, the most accurate value of the critical exponent governing Anderson transition in 3D for systems with orthogonal symmetry is reported to be $\nu = 1.58 \pm 0.01$ as verified by several numerical studies[57; 56; 58; 59]. For the 3D unitary universality class, the critical exponent is found to be $\nu = 1.43 \pm 0.39$ or $\nu = 1.43 \pm 0.47$, whereas $\nu = 1.375 \pm 0.359$ or $\nu = 1.375 \pm 0.391$ is found for the 3D symplectic university class. Besides the prediction of critical exponents, the upper critical dimension for Anderson localization has been an active area of research[60]. The localization problem has been investigated for dimensions $d = 4$ as well as $d = 5$ [61].

Over the last few years, the consideration of localization for interacting quantum systems has given rise to the concept of many body localization. The eigenstate thermalization hypothesis (ETH)[62; 63] states that if an isolated quantum system evolves according to unitary time evolution for a long time, the system should eventually thermalize. However, the absence of thermalization for some many-particle quantum systems implies the violation of ETH. These systems are found to be localized in the Fock space, and during their time evolution, they can get trapped in very long-lived metastable states. Such localization is termed many-body localization[64; 65]. In

2006, Denis Basko, Igor Aleiner, and Boris Altshuler found that, starting from an Anderson insulator, turning on electron-electron interaction does not delocalize the insulating state. In fact, the Anderson insulating state is very different from any other insulating state such as band/Mott insulators in the sense that the conductivity remains strictly zero even at finite but low temperatures. Followed by this work, many theoretical studies [66; 67; 68; 69; 70] have been done to understand many-body localization. Currently, it is a very active field of research with many open questions: (1) How stable is the many-body localized state? (2) What is the mechanism of transition between quantum thermalization and many-body localization? (3) How do we understand quantum thermalization in the presence of interaction?

To conclude this section, significant progress in understanding the physics of Anderson transition has been accomplished due to the developments of several analytical theories and large-scale numerical simulations. However, the subject is still more alive than ever with many challenges and disputes.

## 1.2    Anderson localization in experiments

The theoretical understanding of Anderson localization paves the way for explaining a large body of experimental observations. A short list of such experimental signatures constitutes the next topic of our discussions.

**Amorphous semiconductors**    The low-temperature conductivity of amorphous semiconductors follows Mott's celebrated $T^{-1/4}$ law[40]. The variable range hopping theory could explain such behavior. It suggests a strong relationship between the level of hopping conductance and the concentration of localized states around the chemical potential. This argument has been employed to explain the low-temperature transport properties of many amorphous materials[71; 72].

**One dimensional thin wires**    Experimentally measured conductance or the resistance of thin wires of metallic samples shows anomalous fluctuations as a function

of chemical potential, magnetic field, or impurity configuration at very low temperatures $\leq 1K$[73; 74; 75; 76]. These fluctuations could not be characterized by usual noise, which are random time-dependent changes in the resistance. Lee et al.[77] explain these results. Localization theory explains the transport properties of several one-dimensional systems, including metallic nanowires[78] and single-walled carbon nanotubes[79].

**Anderson localization in two dimensions**  The dimension $d = 2$ is generally believed to be the lower critical dimension for Anderson localization. Two dimensional systems are also considered as the paradigm for weak localization. Due to such interesting properties, experiments in two dimensional systems have attracted special attention [80]. Experimental investigations on metallic thin films[81; 82; 83; 84; 85] reveal anomalous transport behavior including the temperature dependence as well as the magnetic field dependence of the resistance. These experimental observations can be explained by the theory of weak localization. In recent times, Anderson localization in two dimensions has been experimentally studied using an atomic quasi-periodic kicked rotor which is equivalent to a two-dimensional Anderson-like model[86]. It has been experimentally found that the localization length depends exponentially on the strength of disorder which is in good agreement with the self-consistent theory for the two dimensional Anderson localization.

**Metal-insulator transition**  A disorder-induced metal-insulator transition (MIT) was found in phosphorus-doped silicon, Si:P as well as the photoconductor $Al_xGa_{1-x}As$ [87; 88]. For both materials, measurement of the dielectric susceptibility and the conductivity give an insight into the insulating and metallic side of the transition, respectively. In the experiment, the tuning parameter was the magnitude of the uniaxial stress applied to the Si:P sample at a fixed doping level or the concentration of the doping atoms. On the other hand, the concentration of charge carriers was tuned via optical excitation in $Al_xGa_{1-x}As$. Increasing carrier concentration

reduces the electron-correlation-to-Fermi-energy ratio, and doping also induces disorder because dopant atoms randomly occupy lattice sites. Therefore, this MIT is considered as a manifestation of an Anderson transition. The critical exponents for this transition were found to be equal on both sides. For the Si:P samples and other uncompensated doped materials, the absolute value of critical exponent came out as close to 0.5, whereas exponents of the order of 1 were found for $Al_xGa_{1-x}$, and other amorphous materials as well as compensated semiconductors. Two characteristics of transitions were distinguished. The first category includes the transitions that can be characterized by the exponent close to 0.5. This kind of transition occurs in uncompensated doped semiconductors. The second type includes the transition, which is characterized by the exponent close to 1. This transition exists in the larger group of systems including amorphous metals, amorphous semiconductors, and compensated doped semiconductors. However, finding MIT in three-dimensional crystalline solids by varying a degree of disorder is a challenging experimental task. A disorder driven MIT was found in polycrystalline semiconducting $GeTe-Sb_2Te_3$ system[89; 90; 91] and polycrystalline FeSe:Cu [92]. The three-dimensional single crystals of $Li_xFe_7Se_8$ have been found to be perfect Anderson insulators[93] wherein strong disorder is introduced by doping $Li$ into a clean crystal of $Fe_7S_8$.

**Quantum Hall effect**    Klaus von Klitzing discovered that the Hall conductance $\sigma_{xy}$ of a 2D electron gas displays quantized values, i.e plateaus in the presence of strong magnetic field[94]. A. Pruisken pointed out the connection between Anderson localization and the plateau structure[95]. Using field theory, he showed that the quantum Hall effect could be described by a $\sigma$ model with an additional, topological term. The transitions between quantum Hall plateaus for the integer quantum Hall effect systems are in fact Anderson transitions belonging to the unitary universality class. The exponent for such transitions has been explored both experimentally[96] and numerically. Experimentally, the critical exponent is found to be $\nu \approx 2.38$, whereas theoretically predicted critical exponent is $\nu \approx 2.6$[97; 98; 99; 100; 101] for

the Chalker-Coddington model[102]. The reason for this discrepancy could be the absence of electron-electron interactions in the numerical simulations.

## 1.3   Direct observation of Anderson localization

Despite the research over many decades, a direct observation of Anderson localization of electrons has remained devilishly hard to validate experimentally. It has been realized that classical waves are potentially better suited to observe the phenomenon of Anderson localization directly. For electrons or other quantum particles (e.g., cold atoms), one has to perform experiments at very low temperatures to minimize the effects of inelastic scattering, which destroys phase coherence. There are no such difficulties in dealing with classical waves. Moreover, classical waves have a certain advantage that the analog of electron-electron interactions (nonlinearities) can be avoided by choosing appropriate materials and power levels. Again, most important is the versatility of experiments in dealing with classical waves, where measurement as a function of both space and time are feasible, reveals much-needed information about localization by looking into total transmittance at a single frequency. The latter technique is equivalent to measuring the overall sample conductance for electronic systems, which has been widely used for studying electronic localization. For classical waves, one can measure the statistical distribution of the intensity, the complex amplitude of the waves, and their temporal response. These properties are believed to be strongly influenced by localization. Notably, the localized regime shows large, non-Gaussian fluctuations of the complex field amplitude and long-range correlations in the intensity pattern. The experimental search for observing the localization of classical waves started actively in the late '80s. The group of Akira Ishimaru, of George Maret and Lagendijk observed weak localization of light around 1986 and later[103; 104; 105; 105]. These works stimulated further experimental investigations for observing the localization of classical waves such as light and sound. Both acoustic and electromagnetic wave localization were found in one- and two- dimensional systems, as well as in quasi-1D waveguides[106; 107; 108; 109; 110]. Anderson localization

of matter waves have also been observed[111]. But, finding localization in higher dimensions was proving elusive. It is particularly important because one can observe a real transition from propagating to localized modes only in higher dimensions like 3D. In spite of several tour-de-force experiments in optics[112; 113; 114], observation of Anderson localization in three dimensions remained a hard problem due to technical difficulties. For example, preparing strong scattering samples is laborious. In recent times, tremendous progress has been made using ultrasound experiments to unambiguously demonstrate Anderson localization in three dimensions. Hu et. al.[115] first observed the localization of ultrasound in a 3D elastic network. The network is formed by brazing the aluminum beads together with weak elastic links. They used a point like source of ultrasound energy at the edge of the sample and looked into spreading of elastic energy in the transverse direction. According to the conventional Brownian random-walk picture, the expansion should grow with the square root of time. But, transverse confinement of elastic energy has been observed, confirming localization. Thus, direct observation of sound localization has been achieved experimentally.

## 1.3.1 Anderson localization of phonons

Interest in phonon localization has rekindled due to the direct experimental findings in recent times. The concept of localization of these classical mobile entities is not surprising. If quantum interference is the dominant mechanism for Anderson localization in a disordered medium, it must be applicable to lattice vibrational waves, too. John, Sompolinsky, and Stephen[116] introduced such ideas using continuum field theory and renormalization-group techniques in 1983. Followed by this work, Kirkpatrick[117] gave a theory for the localization of sound in two and three dimensional systems of random hard scatterers using a diagrammatic technique.

It is now recognized that the Anderson localization of phonons contains all the rich features of the Anderson localization-delocalization transition and it can be more easily experimentally probed than electrons. For example, ultrasound is particularly well-appropriate for time-dependent studies because one can get long-time scales over which energy can be monitored. Hence, phonon localization comes across as an

ideal phenomenon to validate the theoretical predictions of localization theory against experiments.

A knowledge of phonon localization finds applications in various branches of research. A rich understanding of the phase diagram of disordered vibrations is significant for acoustic metamaterials[118; 119; 120]. Phonon localization has also been invoked to explain the low-temperature thermal properties of glasses[121; 122; 123; 124; 125; 126].

The reduction of heat transport to ultra-low levels is a much-needed task for thermoelectrics which can produce electricity by converting waste heat into electricity. In recent times, various strategies have been put forward to design high-efficiency thermoelectric materials, where its efficiency is defined through figure of merit ($ZT$) as $ZT = \frac{\sigma S^2 T}{\kappa_e + \kappa_{ph}}$; where $S$ refers to Seebeck coefficient, $T$ is the temperature, $\sigma$ stands for electrical conductivity, $\kappa_e$ and $\kappa_{ph}$ define the thermal conductivity due to electrons and phonons, respectively. One of the common ways is to control electronic properties[127] using quantum wells and wires so that $S$ and $\sigma$ increases, which will eventually increase $ZT$. But, most new methods have been emphasizing the reduction of thermal conductivity through nano-structuring[128]. Another approach is alloying, which can induce phonon localization. Combining the strategy of alloying and nanoparticles can significantly improve thermoelectric efficiencies[128]. Tuning phonon localization in the super-lattice structure geometry can also be an effective way to increase $ZT$ value. In this kind of superlattice geometry, interfaces act as scattering centers. So, the interface structures produce strong scattering of phonons, which reduce their mean-free path. For example, $Bi_2Te_3/Sb_2Te_3$ and PbSe/PbTe quantum dot superlattices show promising thermoelectric properties[129; 130].

The idea of controlling phonon propagation fosters many opportunities in phononics. Uni-directional phonon propagation may be used for creating acoustic diodes[131; 132]. Recently, a strategy to achieve simultaneous localization of mechanical and optical waves through acoustic and optical cavities has attracted much attention for enhancing light and sound interaction. It creates the possibility of a new class

acoustic-optical crystal which makes possible, a combined control of phonons and photons[133; 134; 135; 136; 137].

In the following chapter, we provide a detailed description of our development of a Green's function based approach to phonon localization. The solution to the resulting equations is obtained through cluster methods, namely the dynamical cluster approximation (DCA) and typical medium DCA, which allow us to obtain a thermodynamic limit description of Anderson localization of phonons.

# Chapter 2

# Green's function theory of lattice vibrations

Atoms or molecules in a solid vibrate about their equilibrium positions. Since the atoms are connected by chemical bonds, the displacement of one atom about its equilibrium position influences the motion of neighboring atoms. Such coupled vibrational motion in crystals are called lattice vibrations. The quanta of these lattice vibrations are termed phonons, which are particle-like elementary excitations that carry energy and momentum. They play a significant role in many characteristic properties of matter such as infrared, Raman, and neutron scattering spectra, specific heat, thermal conductivity, electrical conductivity, optical and dielectric properties, diffusion mechanisms, phase change phenomena, and so on. This chapter is devoted to building a Green's functions based theory to understand lattice vibrations in the presence of disorder. We organize this chapter as follows: In section 2.1, we discuss an adiabatic theory of lattice vibrations. In section 2.2, we describe a Green's function theory of lattice vibrations. In section 2.3, we draw a comparison between the electronic and phononic systems. In section 2.4, we present our conclusions of this chapter.

## 2.1 An adiabatic theory of lattice vibrations

### 2.1.1 Born–Oppenheimer or adiabatic and harmonic approximation

A theory of lattice vibrations begins with the Born-Oppenheimer (B-O) or the adiabatic approximation. There are $N \approx 10^{23}$ ions interacting strongly with $N$ electrons. Fortunately, thanks to the adiabatic or the Born-Oppenheimer approximation, we have a natural expansion parameter for this problem, which is the ratio of the electronic mass ($m$) to the ionic mass($M$):

$$\frac{m}{M} << 1, \tag{2.1}$$

that helps us to achieve a reliable theory of lattice vibrations. From the Newton's third law, the forces on the ions and electrons can be assumed to be $F \approx Ze^2/a^2$, where $a$ is the lattice constant. So, we write,

$$F \approx Ze^2/a^2 \approx m\omega_{\text{electron}}^2 a \approx M\omega_{\text{ion}}^2 a. \tag{2.2}$$

It suggests that

$$\frac{\omega_{\text{ion}}}{\omega_{\text{electron}}} \approx (\frac{m}{M})^{1/2} \approx 10^{-3}. \tag{2.3}$$

Therefore, it is justified to consider that the ions are almost stationary during electronic thermalization. This is known as the Born-Oppenheimer or adiabatic approximation.

The B-O approximation however, is not sufficient to make the theory of lattice vibrations analytically tractable, hence the harmonic approximation is necessary. It is generally assumed that the excursions of each atom from its equilibrium position are small in magnitude compared to the inter-atomic distance. Therefore, a Taylor's expansion of the potential energy about the equilibrium inter-atomic distance of the system may be carried out. The harmonic approximation consists of a truncation of the series at the quadratic term. Hence, it reduces the many-body problem to an effective one-body problem. However, as is obvious, such a truncation neglects anharmonic corrections arising due to phonon-phonon scattering, and hence is valid

only in a limited parameter range. Nevertheless, we will argue that our formalism, based on Green's functions, is highly suited, through the use of diagrammatic perturbation theory, to incorporate higher order terms, and even include for example, electron-phonon scattering.

### 2.1.2 Model

The Hamiltonian for a non-disordered lattice within the harmonic approximation is written as

$$H = \sum_{\alpha i l} \frac{p_{i\alpha}^2(l)}{2M_i} + \frac{1}{2} \sum_{\alpha\beta ll'ij} \Phi_{ij}^{\alpha\beta}(l,l')u_\alpha^i(l)u_\beta^j(l')\,, \tag{2.4}$$

where $p_{i\alpha}(l)$ and $u_\alpha^i(l)$ represents, respectively, the momentum and the displacement (from the equilibrium position) of a site $i$ belonging to the unit cell $l$ along the Cartesian coordinate $\alpha = (x, y, z)$ direction. The index $i$ runs from 1 to $N_{\text{cell}}$ where the latter denotes the number of atoms in the basis. We assume that the force-constant tensor, $\Phi$, is a function of $|\mathbf{R}_i(l) - \mathbf{R}_j(l')|$, where $\mathbf{R}_i(l)$ is the position of ion $i$ in unit cell $l$.

### 2.1.3 Force constants

The force constants are defined as

$$\Phi_{\alpha\beta}^{ij}(l,l') = \frac{\partial^2 \Phi_{\text{potential}}}{\partial u_\alpha^i(l)\partial u_\beta^j(l')}\bigg|_0, \tag{2.5}$$

where $\Phi_{\text{potential}}$ is the potential energy of an arbitrary crystal and the subscript 0 signifies that the derivatives have to be performed in the configuration in which all atoms occupy their equilibrium positions. The invariance of the potential energy under rotations, translations, and interchange of equivalent particles lead to various symmetry properties of the force-constants. Two such important properties are

$$\Phi_{\alpha\beta}^{ij}(l,l') = \Phi_{\beta\alpha}^{ji}(l',l) \tag{2.6}$$

and

$$\sum_{l'} \Phi_{\alpha\beta}(l,l') = 0. \tag{2.7}$$

The detailed calculations are given in Appendix-A.

## 2.1.4 Dynamical matrix

Another useful quantity is the dynamical matrix, $D^{ij}_{\text{mat},\alpha\beta}(\mathbf{k})$. The matrix elements $\{D^{ij}_{\text{mat},\alpha\beta}(\mathbf{k})\}$ are labelled by the Cartesian axes $(\alpha, \beta = x, y, z)$ as well as the atom indices $(i, j)$. It is defined as the Fourier transform of the force-constant matrix as

$$D^{ij}_{\text{mat},\alpha\beta}(\mathbf{k}) = = \frac{1}{\sqrt{M_i M_j}} \sum_{ll'} \Phi^{ij}_{\alpha\beta}(l, l') \exp\left(i\mathbf{k}.(\mathbf{R}_l - \mathbf{R}_{l'})\right). \tag{2.8}$$

The dynamical matrix satisfies some important properties. Most importantly, it is Hermitian (see Appendix-A for detailed derivation), i.e. ,

$$D^{ji}_{\text{mat},\beta\alpha}(\mathbf{k}) = \left(D^{ij}_{\text{mat},\alpha\beta}\right)^*(\mathbf{k}). \tag{2.9}$$

Hence, eigenvalues are real and eigenvectors can be chosen to satisfy the orthonormality and closure conditions for the normal modes.

## 2.1.5 Normal modes

A vibrational motion can be characterized by inspecting its normal modes. A normal mode of a vibrating system represents a pattern of motion in which all parts of the system vibrate coherently with the same frequency maintaining a fixed phase relation. Normal mode frequencies, and eigenvectors can be determined by the secular equation

$$\sum_{j\beta} D^{ji}_{\text{mat},\beta\alpha}(\mathbf{k}) u^j_\beta(\mathbf{k}) = \omega^2(\mathbf{k}) u^i_\alpha(\mathbf{k}). \tag{2.10}$$

## 2.1.6 Phonon density of states

The number of phonon modes per unit volume in the interval $\omega$ and $\omega + d\omega$ is defined as phonon density of states (phonon DOS). Mathematically, it can be expressed as the integral over the Brillouin zone, which runs through all $3N_{\text{at}}$ phonon bands, considering $N_{\text{at}}$ is the number of atoms in the unit cell as

$$g(\omega^2) = \sum_{\alpha=1}^3 \int_{BZ} \delta[\omega^2 - \omega^2_{\mathbf{k}}] d\mathbf{k}, \tag{2.11}$$

where each $\mathbf{k}$ represents a point in the first Brillouin zone and the integral is taken over the first Brillouin zone.

The shape of the phonon DOS at low frequencies ($\omega \to 0$) for the d dimensional lattice according to Debye scaling predictions can be given as

$$g(\omega) \propto \omega^{d-1} \text{ for } \omega \to 0. \tag{2.12}$$

## 2.2   A Green's function theory of lattice vibrations

An exact description of lattice vibrations in a disordered system is a challenging task. A disordered medium does not preserve the translational invariance and the concept of phonons as plane waves or quasi-particles are no longer valid in it. Due to the loss of lattice periodicity with the introduction of the disorder, no other relations of force constants except given in Eq. (2.6) and Eq.(2.7) can be derived. Therefore, obtaining the normal modes and the characteristic frequencies by exactly diagonalizing the disordered Hamiltonian as shown in our previous discussions is a computationally expensive task. The additional task of disorder averaging compounds the computational expense. As an alternative, Green's function based mean-field theory serves as an effective tool for studying disordered systems. Green's functions are computationally less expensive to compute and can be directly related to experimental observable. For example, the observable in spectroscopic experiments such as inelastic neutron scattering or tunneling spectroscopy are closely related to Green's functions.

The Green's functions and their spectral representation for disordered lattice vibrations have been extensively discussed in the literature. However, for completeness, we re-derive some of those results here.

The Hamiltonian for a mass disordered lattice within the harmonic approximation is written down as

$$H = \sum_{\alpha i l} \frac{p_{i\alpha}^2(l)}{2M_i(l)} + \frac{1}{2} \sum_{\alpha \beta l l' i j} \Phi_{ij}^{\alpha\beta}(l,l') u_\alpha^i(l) u_\beta^j(l') , \tag{2.13}$$

where the symbols and indices are described in subsection 2.1.2. The retarded displacement-displacement Green's functions, represented by,

$$i D_{\alpha\beta}^{ij}(l,l',t) = \langle\langle u_\alpha^i(l,t); u_\beta^j(l',0) \rangle\rangle , \tag{2.14}$$

24

may be found through the equation of motion formalism. Using the Heisenberg equation of motion, we get

$$i\frac{\partial}{\partial t}\langle\langle u_\alpha^i(l,t); u_\beta^j(l',0)\rangle\rangle = i\delta(t)\langle[u_\alpha^i(l,t), u_\beta^j(l',0)]\rangle$$

$$+ \langle\langle[u_\alpha^i(l,t), H]; u_\beta^j(l',0)\rangle\rangle. \quad (2.15)$$

Now, since $[u_\alpha^i(l,t), H] = ip_{i\alpha}(l)/M_i(l)$, Eq. (2.15) can be written as

$$\frac{\partial}{\partial t}\langle\langle u_\alpha^i(l,t); u_\beta^j(l',0)\rangle\rangle = 0 + \langle\langle\frac{p_{i\alpha}(l,t)}{M_i(l)}; u_\beta^j(l',0)\rangle\rangle. \quad (2.16)$$

A similar consideration for the momentum-displacement Green's function, $\langle\langle p_{i\alpha}(l,t); u_\beta^j(l',0)\rangle\rangle$, yields

$$i\frac{\partial}{\partial t}\langle\langle\frac{p_{i\alpha}(l,t)}{M_i(l)}; u_\beta^j(l',0)\rangle\rangle = i\delta(t)\langle\left[\frac{p_{i\alpha}(l)}{M_i(l)}, u_\beta^j(l')\right]\rangle$$

$$+ \langle\langle\left[\frac{p_{i\alpha}(l,t)}{M_i(l)}, H\right]; u_\beta^j(l',0)\rangle\rangle. \quad (2.17)$$

Since

$$\left[\frac{p_{i\alpha}(l,t)}{M_i(l)}, H\right] = -i\sum_{\gamma,l''j'}\frac{\Phi_{j'i}^{\gamma,\alpha}(l'',l)}{M_i(l)}u_\gamma^{j'}(l'',t), \quad (2.18)$$

Eq. (2.17) reduces to

$$i\frac{\partial}{\partial t}\langle\langle\frac{p_{i\alpha}(l,t)}{M_i(l)}; u_\beta^j(l',0)\rangle\rangle = -i\frac{1}{M_i(l)}i\delta(t)\delta_{ij}\delta(l,l')\delta_{\alpha\beta}$$

$$-i\frac{1}{M_i(l)}\sum_{\gamma,l''j'}\Phi_{j'i}^{\gamma,\alpha}(l'',l)\langle\langle u_\gamma^{j'}(l'',t); u_\beta(l',0)\rangle\rangle. \quad (2.19)$$

Taking derivative with respect to time on both sides of Eq. (2.16) and using Eq. (2.19), we get

$$\frac{\partial^2}{\partial t^2}\langle\langle u_\alpha^{(i)}(l,t)u_\beta^{(j)}(l',0)\rangle\rangle = -\frac{1}{M_i(l)}i\delta(t)\delta_{ij}\delta_{\alpha\beta}\delta(l,l')$$

$$-\frac{1}{M_i(l)}\sum_{\gamma,l''j'}\Phi_{j'i}^{\gamma,\alpha}(l'',l)\langle\langle u_\gamma^{j'}(l'',t); u_\beta^j(l',0)\rangle\rangle. \quad (2.20)$$

Using the definition of Green's function (Eq. (2.14)), we can re-write Eq. (2.20) as

$$M_i(l)\frac{\partial^2}{\partial t^2}D_{\alpha\beta}^{ij}(l,l',t) = -\delta(t)\delta_{\alpha\beta}\delta_{ll'}\delta_{ij} - \sum_{\gamma,l''j'}\Phi_{j'i}^{\gamma\alpha}(l'',l)D_{\gamma\beta}^{j'j}(l'',l',t). \quad (2.21)$$

Transforming to frequency space and using the symmetry relations of the force-constant matrix ($\Phi_{j'i}^{\gamma\alpha} = \Phi_{ij'}^{\alpha\gamma}$), finally, Eq. (2.21) can be written as

$$M_i(l)\omega^2 D_{\alpha\beta}^{ij}(l,l',\omega) = \delta_{\alpha\beta}\delta_{ll'}\delta_{ij} + \sum_{\gamma,l''j'} \Phi_{ij'}^{\alpha\gamma}(l,l'')D_{\gamma\beta}^{j'j}(l'',l',\omega). \qquad (2.22)$$

## 2.2.1 Normalization condition in mass-disordered systems

To obtain the normalization condition for the Green's function in the presence of mass-disorder, we expand the displacement (u) and momentum (p) in terms of normal modes as follows[138],

$$u(l,t) = \frac{1}{\sqrt{2M(l)}}\sum_s B^{(s)}(l)\sqrt{\frac{1}{\omega_s}} \times \left[b_s\exp(-i\omega_s t) + b_s^\dagger\exp(i\omega_s t)\right] \qquad (2.23)$$

$$p(l,t) = \frac{1}{i}\sqrt{\frac{M(l)}{2}}\sum_s B^{(s)}(l)\sqrt{\omega_s} \times \left[b_s\exp(-i\omega_s t) - b_s^\dagger\exp(i\omega_s t)\right] \qquad (2.24)$$

Here, $b_s$ and $b_s^\dagger$ are the phonon destruction and creation operators for the $s^{\text{th}}$ normal mode, respectively. Hence, they follow commutation algebra for bosons i.e $\left[b_s, b_{s'}^\dagger\right] = \delta_{ss'}$. The normal modes $B^s(l)$ are defined by a quantum number s, which take $3p$ values for a three dimensional system with $p$ ions in the basis. The normal modes satisfy orthonormality and completeness relations, namely

$$\sum_l B^{(s)}(l)B^{(s')}(l) = \delta_{ss'}$$
$$\sum_s B^{(s)}(l)B^{(s)}(l') = \delta_{ll'}. \qquad (2.25)$$

Inverting Eq. (2.24) to get the phonon creation ($b_s^\dagger$) and annihilation operators ($b_s$) in terms of displacement and momentum operators in frequency space, we get (using Eqs. 2.25),

$$b_s = \sum_l B^s(l)\frac{1}{\sqrt{2M(l)\omega_s}}\Big(M(l)\omega_s u(l,\omega) + ip(l,\omega)\Big) \qquad (2.26)$$

$$b_s^\dagger = \sum_l B^s(l)\frac{1}{\sqrt{2M(l)\omega_s}}\Big(M(l)\omega_s u(l,\omega) - ip(l,\omega)\Big). \qquad (2.27)$$

Using the definition of displacement-displacement Green's function as given in Eq. (2.14), we get

$$iD(l, l', \omega) = i \frac{1}{\sqrt{M(l)M(l')}} \sum_s B^s(l) B^s(l') \frac{1}{(\omega^+)^2 - \omega_s^2}. \tag{2.28}$$

Thus, the normalization condition in mass-disordered systems is

$$-\frac{\mathrm{Im}}{\pi} \int_0^\infty d\omega \, (2\omega^+) \sqrt{M(l)} \, D(l, l', \omega) \sqrt{M(l')} = \delta_{ll'}. \tag{2.29}$$

## 2.3   A comparison between the electronic and phononic systems

We begin the comparison between the phononic and electronic systems by comparing the respective Hamiltonians. Let us re-write the non-disordered Hamiltonian for lattice vibrations in terms of just the displacement ($u$) for a single atom basis as

$$H = \sum_{\alpha l} \frac{1}{2} M \frac{\partial}{\partial t} [u_\alpha(l, t)] \frac{\partial}{\partial t'} [u_\alpha(l, t')] + \frac{1}{2} \sum_{\alpha \beta l l'} \Phi^{\alpha\beta}(l, l') u_\alpha(l, t) u_\beta(l', t') . \tag{2.30}$$

We assume the time dependence of $u$ is of the form

$$u_\alpha(l, t) = u_\alpha(l) \exp(i\omega t) . \tag{2.31}$$

Substituting Eq .(2.31) into Eq .(2.30), we get

$$H = -\sum_{\alpha i l} \frac{1}{2} M \omega^2 u_\alpha(l) \exp(i\omega t) u_\alpha(l) \exp(i\omega t') + \frac{1}{2} \sum_{\alpha \beta l l'} \Phi^{\alpha\beta}(l, l') u_\alpha(l, t) u_\beta(l', t') \tag{2.32}$$

Again, Eq .(2.32) can be simplified to

$$H = -\sum_{\alpha l} \frac{1}{2} M \omega^2 u_\alpha(l, t) u_\alpha(l, t') + \frac{1}{2} \sum_{\alpha \beta l l'} \Phi^{\alpha\beta}(l, l') u_\alpha(l, t) u_\beta(l', t') . \tag{2.33}$$

Next, we consider electronic systems. The Anderson model for electronic systems reads as

$$H = \sum_{l\sigma} \epsilon_l c_{l\sigma}^\dagger c_{l\sigma} - \sum_{ll'\sigma} t_{ll'} (c_{l\sigma}^\dagger c_{l'\sigma} + c_{l'\sigma}^\dagger c_{l\sigma}) , \tag{2.34}$$

where $c_{l\sigma}$ creates a quasiparticle with spin $\sigma$ at site l and $c_{l'}$ destroys that quasiparticle at site $l'$. The diagonal $\epsilon$ is the on-site energy and $t_{ll'}$ represents the hopping constant between site $l$ and $l'$.

Now, we are ready to carry out a comparison between the lattice vibration model for phonons and the Anderson model for electrons. Comparing Eq .(2.33) and Eq .(2.34), we can easily identify a one to one correspondence between the phononic system and the electronic system. We note that the on-site energy of the electronic system is equivalent to the on-site mass of the phononic system. Mathematically, we write as

$$M\omega^2 \equiv \epsilon . \tag{2.35}$$

We also observe that the off-diagonal hopping for the electronic system is equivalent to the off-diagonal force-constants for the phononic system. Hence, we can mathematically write as

$$\Phi \equiv t . \tag{2.36}$$

We find that the branches of the phononic system are equivalent to the spins of the electronic system, too. Hence,

$$\alpha \equiv \sigma . \tag{2.37}$$

With this one to one mapping, we can readily explore the structural similarities of the Green's function for phonons and electrons. The correlation function $\langle\langle c(t); c^\dagger(t')\rangle\rangle$ of the electronic system is similar to the correlation function $\langle\langle u(t); u(t')\rangle\rangle$ of the phononic system.

$$\langle\langle u(t); u(t')\rangle\rangle \equiv \langle\langle c(t); c^\dagger(t')\rangle\rangle . \tag{2.38}$$

Hence, the retarded Green's function $(G(\mathbf{k}))$ for the electronic system is equivalent to the retarded displacement-displacement $(D(\mathbf{k}))$ Green's function for the phononic system. So

$$D(\mathbf{k}) \equiv G(\mathbf{k}). \tag{2.39}$$

The retarded displacement-displacement Green's function of the phononic system is defined as

$$D(\mathbf{k}) = -i\theta(t - t')\langle u_{\mathbf{k}}(t); u_{\mathbf{k}'}(t')\rangle$$
$$= \frac{1}{\omega^2 - \omega_{\mathbf{k}}^2}, \qquad (2.40)$$

where $\omega_{\mathbf{k}}^2$ is the dispersion of the phononic system and the retarded Green's function of the electronic system is defined as

$$G(\mathbf{k}) = -i\theta(t - t')\langle c_{\mathbf{k}}(t); c_{\mathbf{k}}(t')\rangle$$
$$= \frac{1}{\omega - \epsilon_{\mathbf{k}}}, \qquad (2.41)$$

where $\epsilon_{\mathbf{k}}$ is the dispersion of the electronic system. Thus, we have explored the similarities and differences between the electronic tight-binding Hamiltonian and the lattice vibrations Hamiltonian. A remarkable difference is seen in the correspondence of the band dispersion of electrons and the ionic mass term of the phonons. The former is a constant, depending only on the band structure, and the hopping integrals, while the latter is a frequency dependent term, and contributes strongly to the energy dependence of the Green's function, and also to the localization/delocalization of low and high energy phonons, as will be described in more detail, later in chapter 3. There are sum rules for the force-constants of the phononic systems, whereas no such sum rule exists for the hopping integrals of the electronic systems.

## 2.4   Conclusions

We have presented a detailed description of Green's functions for lattice vibrations. We have argued that the knowledge of such Green's functions is essential, especially for disordered systems. In particular, it is computationally less expensive to calculate, and is much more directly related to experimental observables as compared to other existing exact wavefunction based methods. We have also given a comparison between the Green's function for disordered lattice vibrations with the Green's function for disordered electronic systems, which enables us to understand that the Green's

function, like electronic systems, can be useful for constructing quantum cluster theories for disordered phononic systems. In the next chapter, we will develop such Green's function based quantum cluster methods for studying phonon localization in disordered solids.

# Chapter 3

# Localization of phonons in mass-disordered alloys: A typical medium dynamical cluster approach

As discussed in chapter 1, a theoretical understanding of AL remains a challenging research topic though it has been pursued extensively over the years. In this context, several computational techniques including exact diagonalization (ED), transfer matrix method, kernel polynomial method, [139; 140; 141; 142; 20; 143; 144; 145; 146; 56] and renormalization group method [147; 148; 149] have been developed and applied. A majority of these studies deal, however, with electronic systems, and less attention has been paid to other relevant elementary excitations, such as phonons, despite being accessible to experiment and having various applications like in high-performance thermoelectric materials design.

The present work aims to apply a recently developed framework, namely the dynamical cluster approximation (DCA) and typical medium dynamical cluster approximation (TMDCA), to investigate the AL of phonons in mass-disordered alloys. We have organized this chapter as follows. In section 3.1, we briefly introduce the problem and review the relevant work on phonon localization before delving into the formalism in the next section. In section 3.2, we describe a model for a mass-disordered lattice and the formalism employed to solve the model. We will validate the DCA and TMDCA against exact diagonalization and transfer matrix method respectively

in section 3.3. Subsequently in section 3.4, the typical density of states, computed through TMDCA, is used to discuss the physics of phonon localization. Conclusions are presented in the final section of this chapter.

## 3.1 Introduction

A random substitution of ions in a crystal lattice creates local disturbances, the extent of which depends on both the size and chemical nature of the impurity ions. As a result, real space perturbations of a given unit cell can propagate to neighboring unit cells and be extended over a characteristic length scale $\xi$. If this length scale is comparable to the system size, the normal modes of the disordered system are termed extended, and adiabatic continuity can be expected to connect the disordered system with the clean case. However, it may happen that, at and beyond some critical value of the disorder strength, some or all of these modes remain confined over a finite localization length, implying a real space localization of such modes.

This kind of disorder-induced confinement of lattice waves indicates localization of phonons. If impurities are heavier than host atoms, the phonon spectrum will be, in general, shifted towards low-frequency regions. Lighter impurities, on the other hand, can lead to more interesting effects. New states corresponding to the vibration of guest atoms can appear in frequency regions where no levels of the host crystal were present. Hence new impurity bands isolated from the host-dominated spectra may be observed in the phonon spectrum. Thus, a small amount of disorder in lattice vibrations can change the physical properties of the material.

Extensive theoretical attempts to investigate isotopic disorder exist and some even predate Anderson's work on localization. Most of these may be classified as either Green's function based approaches or computational methods. The former include perturbative, semi-analytical approaches[150; 151; 138; 152; 153; 154; 155; 156; 157; 158; 159; 160; 161; 162; 163; 164] and continuum field theory based approaches[116; 165]. Early perturbative methods utilized either the impurity concentration, or the deviation from a mean mass as a small parameter. Later ap-

proaches were based on the coherent potential approximation (CPA) and the average T-matrix approximation (ATA). More recently, Ghosh et al. [164] developed the itinerant coherent-potential approximation (ICPA) which satisfies translational invariance, unitarity, and analyticity of physical properties. The ICPA has two additional advantages. First, it can capture the physics of multi-site correlations. Second, it can incorporate both mass and spring disorder simultaneously. In this connection, the ICPA is one of the most successful extensions of the CPA to predict the vibrational density of states of realistic binary alloy systems. Nevertheless, the ICPA is not able to capture the AL of phonons.

Approximate theories such as the CPA or the ATA may be used to get a qualitative insight. However, these are often based on uncontrolled approximations, and their region of validity is always in question. This is where numerically exact methods such as exact diagonalization (ED)[166; 167] and transfer matrix method (TMM)[168] prove their mettle and provide very useful benchmarks for approximate theories. Recently, Monthus and Garel [169] use ED for relatively large system sizes to investigate the localization of phonons in mass-disordered systems. Using finite size-scaling methods for the low-frequency part of the spectrum, they show that the single-parameter scaling theory of localization, originally developed for electronic systems applies to phononic systems as well. Pinski et al. [168] employ the TMM to obtain the mobility edge as a function of mass and spring disorder in three-dimensional systems. They find a close correspondence between the electronic and phonon systems. The main drawback of ED and TMM is that their computational expense scales exponentially with system size.

Despite extensive investigations over decades, a method that fulfills all of the following set of requirements has not yet been developed: (1) The method should systematically approach the thermodynamic limit. (2) It should reproduce exact diagonalization results for both the main vibrational spectrum and the impurity modes. (3) It should be applicable over the full alloy regime, i.e., for all defect concentrations. (4) It should be able to handle both mass (diagonal) and spring (off-diagonal) disorder on an equal footing. (5) It should capture the AL of phonons, including the

33

dependence of the mobility edge on the disorder. (6) It should be relatively computationally inexpensive in order to be useful for investigations of phonon localization in real materials, which necessarily involve multiple branches, and mass as well as spring disorder.

The lack of a single method satisfying all the criteria mentioned above for phononic systems motivates us to adapt the dynamical cluster approximation (DCA) and the typical medium DCA (TMDCA) for disordered phononic systems to capture the Anderson localization of phonons since these methods have been shown to work extraordinarily well in electronic systems [170; 171; 172; 173] .

The main difficulty inhibiting the development of such a method for the study of Anderson localization of phonons lies in finding a single particle order parameter to characterize the Anderson transition in disordered phononic systems. Recently, a typical medium theory (TMT) [174] for electronic systems proposes the local density of states (LDOS) as an appropriate quantity to look at for the study of Anderson localization of electrons. The local density of states, defined as $\rho_l(\omega) = \sum_n \delta(\omega - \omega_n)|\psi_n(l)|^2$, changes from continuous to discrete upon the system transiting from an itinerant to a localized state. On the insulating side of the transition, the spectrum consists of delta functions. Here, the typical value of the LDOS vanishes, whereas the globally averaged density of states (ADOS) does not, nor is it critical at the Anderson transition. Hence, the TMT adopts the typically averaged DOS (TDOS), as an order parameter for the study of the Anderson localization of electrons. In spite of the success of the TMT in describing localized electron states, it suffers shortcomings due to its single-site character. For example, the TMT does not provide a proper description of the critical behavior of the Anderson localization transition in three dimensions for disordered electronic systems since it is not able to capture the effects of non-local coherent back-scattering.

Recently, an extension of the TMT that includes non-local dynamical correlations, called the typical medium dynamical cluster approximation(TMDCA),[171] has been developed for disordered electronic systems. It incorporates the typical medium within the dynamical cluster approximation (DCA) scheme. The TMDCA

possesses all features of a successful cluster theory such as the systematic incorporation of non-local correlations, and it captures the critical behavior of the Anderson localization transition including the correct value of critical disorder strength and re-entrant behavior of the mobility edge.

The present TMDCA method for electronic systems utilizes the fact that the LDOS is a continuum in the metallic state; whereas it is composed of a set of delta-functions in an insulator, so that the typical value of the LDOS, averaged over disorder locations, is zero. This same idea is equally applicable to phonons or the localization of any propagating waves. So, we can consider that the typical value of the LDOS remains a valid order parameter for phononic systems. Based on this concept, we establish a TMDCA formalism for the study of Anderson localization of phonons.

We end this introduction with two questions: (1) (a) How well do the DCA and the TMDCA formalisms do when compared with exact methods like ED and TMM? (b) To what extent are the requirements of a successful method, that are mentioned above, fulfilled by the DCA and the TMDCA? (2) What new insights into the localization of phonons does the calculation of typical density of states give? These questions will be addressed at the appropriate places in this chapter. In the following section, we describe a model for a mass disordered lattice within the harmonic approximation and the formalism employed to solve the model.

## 3.2   Method

As discussed in chapter 2, the Hamiltonian for the ionic degrees of freedom of a disordered lattice in the harmonic approximation can be written in terms of momentum ($p$) and displacement ($u$) operators, as

$$H = \sum_{\alpha il} \frac{p_{i\alpha}^2(l)}{2M_i(l)} + \frac{1}{2} \sum_{\alpha\beta ll'ij} \Phi_{ij}^{\alpha\beta}(l,l')u_\alpha^i(l)u_\beta^j(l') \,, \tag{3.1}$$

where symbols and indices are described in chapter 2.

The retarded displacement-displacement Green's functions,

$$iD_{\alpha\beta}^{ij}(l,l',t) = \langle\langle\, u_\alpha^i(l,t); u_\beta^j(l',0)\,\rangle\rangle \tag{3.2}$$

corresponding to the above Hamiltonian can be obtained using their frequency dependent counterparts given by the solution of the following coupled linear equations:

$$M_i(l)\omega^2 D_{\alpha\beta}^{ij}(l, l', \omega) = \delta_{\alpha\beta}\delta_{ll'}\delta_{ij} + \sum_{\gamma, l''j'} \Phi_{ij'}^{\alpha\gamma}(l, l'')D_{\gamma\beta}^{j'j}(l'', l', \omega). \tag{3.3}$$

The detailed calculations are given in chapter 2. With a single composite index, $\lambda = (\alpha, l, i)$, we can write the above equation in a matrix representation and obtain a formal solution for the Green's function (Eq. 3.2) as

$$M_0\hat{D}(\omega) = \left[\omega^2\mathbb{1} - \hat{\Phi}M_0^{-1} - \omega^2\hat{V}\right]^{-1}, \tag{3.4}$$

where $M_0$ includes the masses of the ions in the unit cell of the clean lattice with respect to which the mass disorder potential, $\hat{V}$, is given as

$$\left(\hat{V}\right)_{\lambda,\lambda'} = \left(1 - M_\lambda M_{0\lambda'}^{-1}\right)\delta_{\lambda,\lambda'}. \tag{3.5}$$

Note that the masses have been assigned a Cartesian index purely for notational convenience, *i.e.* the mass of the $i^{\text{th}}$ atom in the $l^{\text{th}}$ unit cell does not, naturally, depend on $\alpha$, the direction.

In this work, we consider an isotropic simple cubic lattice with a monoatomic basis ($M_{0\lambda} = M_0$) and a spring constant tensor $\Phi$ truncated at nearest-neighbors:

$$\Phi^{\alpha\beta}(l, l') = \delta_{\alpha\beta}(\Phi_D\delta_{l,l'} + \Phi_{nn}\delta_{\mathbf{R}_{l'},\mathbf{R}_l+\vec{\delta}}), \tag{3.6}$$

where $\Phi_D$ and $\Phi_{nn}$ are the diagonal, and the nearest neighbor component of the tensor, respectively, and $\vec{\delta}$ is a vector connecting a site to its nearest neighbors.

We consider two kinds of mass disorder in Eq. 3.5, namely (1) binary isotopic disorder, where the random masses $M_\lambda$ are either $M_{\text{imp}}$ or $M_0$ with concentrations $c$ and $(1-c)$, respectively, and (2) a uniform (box) disorder, where $(1 - M_\lambda/M_0) \in [-V, V]$ with equal probability for any value in that interval and $0 < V \leq 1$ representing the strength of disorder . Binary isotopic disorder is a special case of binary disorder, since the latter may involve substitutions that may induce spring disorder in addition to mass disorder. Most experimental studies involve disorder in a binary alloy. Hence,

we perform calculations for this disorder distribution. However, a comprehensive validation of the numerical schemes requires us to compare our results with the available results for the box distribution. Thus, the two distributions are needed to complete our study.

In the absence of mass disorder, i.e $\hat{V} = 0$, corresponding to a clean, monoatomic lattice, all ionic masses are identical, hence $M_i(l) = M_0$ and $i = 1$ for all $l$ lattice sites. In such a case, the system is translationally invariant, hence transforming to $\mathbf{k}$-space using

$$M_0 D^{(0)}_{\alpha\beta}(l, l', \omega) = \sum_{\mathbf{k}} D^{(0)}_{\alpha\beta}(\mathbf{k}, \omega) e^{i\mathbf{k}\cdot(\mathbf{R}_l - \mathbf{R}_{l'})},$$

Eq. 3.3 simplifies to

$$\bar{D}^{(0)}(\mathbf{k}, \omega) = \left[\omega^2 \mathbb{1} - \bar{F}(\mathbf{k})\right]^{-1} \tag{3.7}$$

where the 'bar' represents a matrix in the Cartesian basis (e.g. $3 \times 3$ in three dimensions), and $\bar{F}(\mathbf{k})$ is related to $\hat{\Phi}$ through

$$(\bar{F}(\mathbf{k}))_{\alpha\beta} = \sum_{l'} \frac{\Phi_{\alpha\beta}(l, l')}{M_0} e^{i\mathbf{k}\cdot(\mathbf{R}_l - \mathbf{R}_{l'})}.$$

Thus, with the specific form for $\Phi$ given by Eq. 3.6, the Green's function in the clean limit reduces to

$$\bar{D}^{(0)}(\mathbf{k}, \omega) = \left(\omega^2 - \omega_{\mathbf{k}}^2\right)^{-1} \mathbb{1}, \tag{3.8}$$

where the dispersion is given by

$$\omega_{\mathbf{k}}^2 = \omega_0^2 \left(\sin^2 \frac{k_x}{2} + \sin^2 \frac{k_y}{2} + \sin^2 \frac{k_z}{2}\right), \tag{3.9}$$

with $\omega_0 = \sqrt{4\gamma/M_0} = 1$ being our unit of energy and $\gamma = -\Phi_D = 6\Phi_{nn}$; the latter equality stems from sum rules that need to be satisfied by the spring constant tensor. The choice of $\omega_0 = 1$ implies that the bandwidth of the non-interacting spectrum is $\sqrt{3}$. Since all the branches have identical dispersion, we will drop the branch index ($\alpha$) henceforth in this work. Thus, Eq. (3.4) may be written as a Dyson equation:

$$\hat{D}^{-1}(\omega) = \left(\hat{D}^{(0)}(\omega)\right)^{-1} - \omega^2 \hat{V}. \tag{3.10}$$

As discussed in chapter 2, the connection to disordered electronic systems can now be made. The non-interacting electronic Green's function in a clean lattice is given by $G^{(0)}(\mathbf{k}, \omega) = (\omega^+ - \epsilon_\mathbf{k})^{-1}$, where $\epsilon_\mathbf{k} = -2t(\cos(k_x) + \cos(k_y) + \cos(k_z))$ is the electronic dispersion in a cubic lattice with nearest-neighbor hopping $t$. By noting that the phonon dispersion (Eq. (3.9)) can be mapped to the electronic dispersion through $\omega_\mathbf{k}^2 = 6\gamma/M_0 + \gamma\epsilon_\mathbf{k}/(M_0 t)$, the similarity between $G^{(0)}$ and $D^{(0)}$ (Eq. (3.8)) becomes immediately clear.

A major difference between the localization of phonons and electrons emerges from the form of the Dyson equation. In the electronic case, $\hat{V}$ represents site-disorder and the Dyson equation reads $\hat{G}^{-1}(\omega) = \left(\hat{G}^{(0)}(\omega)\right)^{-1} - \hat{V}$, while in the phonon case, the perturbation term is $\omega^2\hat{V}$ (Eq. (3.10)), which creates a significant difference in the localization of phonons *vs* electrons. For example, localizing low energy acoustic modes should be almost impossible because the modulating factor of $\omega^2$ implies that the disorder potential becomes vanishingly small at low energies, hence leaving the acoustic modes almost unperturbed. The implication for high-frequency modes is also clear: the disorder potential increases without bound; hence high-frequency modes are expected to get localized even for relatively weak disorder. Further differences will be pointed out in the results section.

There are several methods to solve the Dyson equation (Eq. (3.10)). Diagrammatic methods employing an infinite resummation of a certain class of diagrams are one choice[175]. The CPA, which reduces the lattice problem to an effective single-site problem, is another. Alternatively, one can choose a finite system with periodic boundary conditions and solve for the Green's function exactly. Each of these methods has specific advantages and disadvantages. For example, the diagrammatic methods are often uncontrolled approximations and may violate sum rules and/or yield unphysical spectra.

Finite system calculations, though exact, suffer from a large computational expense. Hence, a method is needed that is computationally feasible, systematically approaches the thermodynamic limit and is fully causal. The dynamical cluster approximation (DCA) is one such method. It has been applied very successfully to

investigate a variety of fermionic and bosonic models. In this chapter, we extend the DCA to study phonons in mass-disordered systems. We now describe the DCA for phonons in some detail below.

### 3.2.1 Dynamical cluster approximation (DCA) for phonons

The advent of dynamical mean field theory (DMFT) led to a sort of revolution in the understanding of quantum many body lattice systems. However, since DMFT ignores non-local dynamical correlations, several phenomena such as d-wave superconductivity, Anderson localization, and low dimensional physics are out of scope of this framework. Hence, quantum cluster approaches, that go beyond DMFT, have assumed great importance. One such approach, that is based on momentum space clusters, is the dynamical cluster approximation (DCA).

The DCA may be viewed as an approximation to the wave-vector sums that occur in Feynman-Dyson Perturbation Theory (FDPT). Here, the first Brillouin zone containing $N$ wavenumbers $\mathbf{k}$ is broken into $N_c$ non-overlapping coarse graining cells. We then approximate the integrals associated with each diagram by its sum of average/coarse-grained estimates of the integrand within each cell. There is considerable freedom in how this is done. For example, if the integrand is composed of the product of two functions of the integration variable, do we take the product of the two averages, or the average of the products to define the approximate value in the cell? Since these two approximations have the same error provided that the number of such cells is large, we can use this freedom to simplify the approximation. To do this, we define the many-to-few mapping $M(\mathbf{k}) = \mathbf{K}$, where $\mathbf{K}$ labels the cells including $\mathbf{k}$, so that $\mathbf{k} = \mathbf{K} + \tilde{\mathbf{k}}$, where $\tilde{\mathbf{k}}$ labels the wave-numbers within each cell. The corresponding transformation of the Lie algebra is $\bar{c}_{\mathbf{k}} = \sum_{\tilde{\mathbf{k}}} c_{\mathbf{K}+\tilde{\mathbf{k}}}$. It is easy to see that this transformation preserves the Lie algebra. So it maps bosons onto bosons and fermions onto fermions. The mapping is not canonical though since information is lost in the process. Nevertheless, this mapping ensures that FDPT may be used to analyze lattice plus the quantum impurity problem. Under this transformation, all points within each cell are considered to be equivalent, and are mapped to a single

point $\mathbf{K}$. So, each Green's function within the cell may be replaced by its average value within the cell. Equivalently, each $G(\mathbf{k})$ in a Feynman graph may be replaced by its coarse grained analog. More significantly, each sum over $\mathbf{k}$ is replaced by a sum over $\mathbf{K}$ thereby dramatically reducing the complexity of the problem of order $N$ to order $N_c$. The associated FDPT is the same as a small self-consistently embedded periodic cluster problem. Once the cluster problem is solved, we calculate the corresponding irreducible self energy and vertex functions. We use them in the Dyson and Bethe-Salpeter equation to calculate the single-particle spectra and the two-particle susceptibilities.

For example, the DMFT framework may be represented as a mapping of the entire first Brillouin zone to just one momentum at the centre for the zone. The main simplification in the DMFT framework is the absence of momentum conservation at the vertices in the Feynman diagrams, thus leading to a local self-energy. The DCA targets this lacuna of DMFT and replaces the Dirac delta function that represents true momentum conservation at the vertices by a Laue function that conserves momentum, but only for the cluster momenta. This brings back the momentum dependence in the Green's functions and self-energy, lost at the DMFT level. Thus, as the number of clusters increases, the Brillouin zone is sampled more densely, and hence the thermodynamic limit is systematically approached. We refer the reader to review articles [170; 176] for details of the DCA, and its applications to a variety of problems.

An algorithm that implements the DCA for solving Eq. (3.10) for phonons is given below:

1. The computational scheme begins with an initial guess for the hybridization function $\Gamma_{\text{old}}(\mathbf{K}, \omega)$. Such a guess can be obtained either through a previous calculation or through a coarse-graining of the non-disordered Green's function (Eq. (3.8)):

$$\Gamma_{\text{old}}(\mathbf{K}, \omega) = \omega^2 - \bar{\omega}_{\mathbf{K}}^2 - \left( \sum_{\tilde{\mathbf{k}}} D^{(0)}(\mathbf{K} + \tilde{\mathbf{k}}, \omega) \right)^{-1}, \qquad (3.11)$$

where $\tilde{\mathbf{k}}$ runs over the momenta of the cell centered at the cluster momentum $\mathbf{K}$, and $\bar{\omega}_{\mathbf{K}}^2$ is the coarse-grained dispersion given by

$$\bar{\omega}_{\mathbf{K}}^2 = \frac{N_c}{N} \sum_{\tilde{\mathbf{k}}} \omega_{\mathbf{K}+\tilde{\mathbf{k}}}^2 \,, \tag{3.12}$$

where $\omega_{\mathbf{k}}^2$ is given in Eq. (3.9).

2. The hybridization function is used to calculate the cluster excluded Green's function $\mathcal{D}(\mathbf{K}, \omega)$ as

$$\mathcal{D}(\mathbf{K}, \omega) = \frac{1}{\omega^2 - \bar{\omega}_{\mathbf{K}}^2 - \Gamma_{\text{old}}(\mathbf{K}, \omega)} \,. \tag{3.13}$$

3. The cluster excluded Green's function in momentum space is Fourier transformed to real space:

$$M_0 \mathcal{D}(l, l', \omega) = \sum_{\mathbf{K}} \mathcal{D}(\mathbf{K}, \omega) \exp\left(i\mathbf{K} \cdot (\mathbf{R}_l - \mathbf{R}_{l'})\right). \tag{3.14}$$

4. Next, we generate a large number of configurations of the disorder potential $(\hat{V})$ for a given distribution, namely binary isotopic or box disorder.

5. For each disorder configuration $\hat{V}$, the mass-weighted Dyson equation is used to compute the cluster Green's function, given by

$$D^c(l, l', \omega) = \sqrt{1 - (\hat{V})_l} \left[(\hat{\mathcal{D}}(\omega))^{-1} - \omega^2 \hat{V}\right]_{ll'}^{-1} \sqrt{1 - (\hat{V})_{l'}} \,, \tag{3.15}$$

which is then averaged over all disorder configurations:

$$D_{\text{DCA}}^c(l, l', \omega) = \left\langle D^c(l, l', \omega) \right\rangle \tag{3.16}$$

where $\langle ... \rangle$ denotes an algebraic average. As explained in chapter 2, the mass-weighting is essential in order to ensure a proper normalization of the spectral functions in the presence of disorder. In practice, we have generated about 600-1000 disorder configurations for each simulation, and have verified the robustness of our results with respect to the number of configurations.

6. The average cluster Green's function obtained in Eq. (3.16) is Fourier transformed to momentum space, and then used to compute the coarse-grained lattice Green

function:

$$D^{CG}(\mathbf{K}, \omega) = \frac{N_c}{N} \sum_{\tilde{\mathbf{k}}} \left[ (D^c_{\mathrm{DCA}}(\mathbf{K}, \omega))^{-1} + \Gamma_{\mathrm{old}}(\mathbf{K}, \omega) - \omega^2_{\mathbf{K}+\tilde{\mathbf{k}}} + \bar{\omega}^2_{\mathbf{K}} \right]^{-1}. \qquad (3.17)$$

The disorder averaged spectral function, termed the ADOS may be defined as

$$\mathrm{ADOS}(\omega^2) = -\frac{2\omega}{N_c\pi} \mathrm{Im} \sum_{\mathbf{K}} D^c_{\mathrm{DCA}}(\mathbf{K}, \omega). \qquad (3.18)$$

7. A new hybridization function is found through

$$\Gamma_{\mathrm{new}}(\mathbf{K}, \omega) = \Gamma_{\mathrm{old}}(\mathbf{K}, \omega) + \xi \left[ (D^{CG}(\mathbf{K}, \omega))^{-1} - (D^c_{\mathrm{DCA}}(\mathbf{K}, \omega))^{-1} \right] \qquad (3.19)$$

where $\xi$ is a linear mixing parameter used for improving the convergence.

Self-consistency is achieved when $||\Gamma_{\mathrm{new}}(\mathbf{K}, \omega) - \Gamma_{\mathrm{old}}(\mathbf{K}, \omega)||$ reaches numerical tolerance (in practice, about 0.005). We have checked that such a condition is sufficient to obtain converged Green's functions and self-energies. If the self-consistency condition is satisfied, the iterations end, else we impose $\Gamma_{\mathrm{old}} = \Gamma_{\mathrm{new}}$ and go back to step-2. In practice, we add a small imaginary broadening factor ($\omega \to \omega + \iota\eta; \eta \sim 10^{-3}$) to real frequencies for accelerating convergence.

Though the DCA possesses several advantages over the CPA, both are unable to capture the Anderson localization. The arithmetic averaging used for computing the cluster Green's function (Eq. (3.16)) in step-5 leads to this inability. The typical medium DCA developed for electronic systems has been demonstrated to capture Anderson localization. We describe the extension of DCA to TMDCA for phonons below.

## 3.2.2 Typical Medium Dynamical Cluster Approximation (TMDCA) for phonons

As mentioned above, the DCA employs algebraic averaging over disorder configurations, while in the TMDCA, the effective medium is constructed via geometric averaging. The ansatz for computing the typical density of states remains the same as in the electronic case, namely:

$$\rho^c_{\mathrm{typ}}(\mathbf{K}, \omega) = \exp\left( \frac{1}{N_c} \sum_{l=1}^{N_c} \langle \ln \rho^c(l, \omega) \rangle \right) \times \left\langle \frac{\rho^c(\mathbf{K}, \omega)}{\frac{1}{N_c} \sum_l \rho^c(l, \omega)} \right\rangle \qquad (3.20)$$

where

$$\rho^c(l,\omega) = -\frac{2\omega}{\pi}\mathrm{Im}\, D^c(l,l,\omega)$$

$$\rho^c(\mathbf{K},\omega) = -\frac{2\omega}{\pi}\mathrm{Im}\, D^c(\mathbf{K},\omega)$$

are the local and momentum dependent spectral functions respectively, computed from the unaveraged cluster Green function $D^c(l,l',\omega)$ (Eq. (3.15)).

The disorder-averaged typical Green's function can be calculated from the typical density of states (Eq. (3.20)), using the Hilbert transform as

$$D^c_{\mathrm{typ}}(\mathbf{K},\omega) = \mathcal{P}\int d\omega' \frac{\rho^c_{\mathrm{typ}}(\mathbf{K},\omega')}{\omega^2 - \omega'^2} - i\frac{\pi}{2\omega}\rho^c_{\mathrm{typ}}(\omega)\,, \qquad (3.21)$$

and the corresponding typical density of states, termed the TDOS is given by

$$\mathrm{TDOS}(\omega^2) = -\frac{2\omega}{N_c\pi}\mathrm{Im}\sum_{\mathbf{K}} D^c_{\mathrm{typ}}(\mathbf{K},\omega)\,. \qquad (3.22)$$

The TMDCA implementation is almost identical to that of the DCA, except that the typical Green's function is obtained by combining Eqs. (3.15), (3.20) and (3.21)
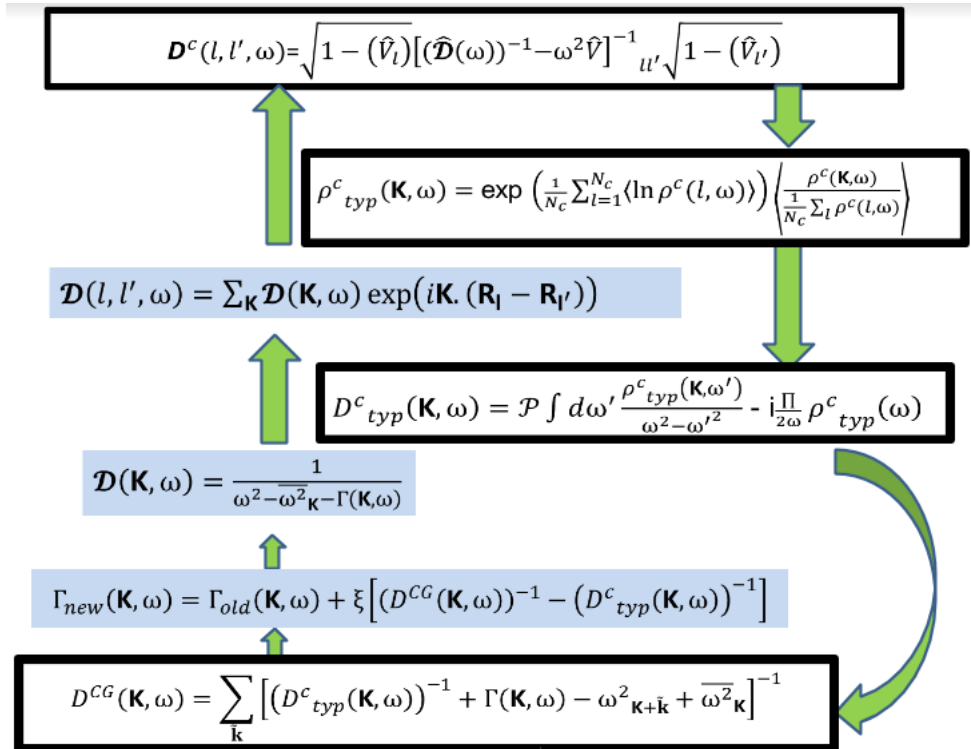


Figure 3.1: Self-consistency loop of the TMDCA for phonons.

43

and in Eqs. (3.17) and (3.19), the $D_{\mathrm{DCA}}^c$ is replaced by $D_{\mathrm{typ}}^c$. The flowchart of the algorithm is presented in Fig. 3.1. Apart from the typical Green's function, $D_{\mathrm{typ}}^c$, an average Green's function, denoted by $D_{\mathrm{typ}}^{\mathrm{ave}}$ can also be computed within the TMDCA using Eq. (3.16) in the final iteration of the TMDCA self-consistency cycle. An interpretation of such a Green's function is that it yields the physical density of states, while the typical density of states acts as an order parameter for the Anderson localization transition.

## 3.3 Benchmarking DCA and TMDCA

The first step to establish any new method is to benchmark it against previous exact results. This will be the objective of this section. The DCA and TMDCA benchmarks are established separately in subsections 3.3.1 and 3.3.2 respectively.

### 3.3.1 Dynamical Cluster Approximation

Fig. 3.2 shows a direct comparison of the density of states obtained from the DCA with results from exact diagonalization (ED) [167] for a binary isotopic alloy system in three dimensions at various values of disorder potential ($V$) and concentrations ($c$). The disorder averaged density of states can be obtained from the DCA cluster Green's function $D_{\mathrm{DCA}}^c$ (Eq. (3.16)) and is given by Eq. (3.18).

The DCA calculations have been performed for a simple-cubic lattice with different cluster sizes, namely $N_c = 1, 8, 64, 125$. In the ED calculations [167], the DOS was calculated for a $6 \times 6 \times 25$ randomly disordered simple-cubic lattice. The left panels of Fig. 3.2 show the evolution of the spectrum with increasing (from top to bottom) concentration ($c$) of light impurities (with $M_{imp} = M_{host}/2$, hence $V = 0.5$). The two-peaked structure of the spectrum, seen for all concentrations, is reflective of the binary mass distribution. The spectral weight of the higher frequency band is seen to grow with increasing $c$, while the low-frequency band shrinks. For $c \gtrsim 0.5$, the system may be viewed as the dual of the original system, i.e., a binary alloy with a

lighter host and heavier impurities. The transfer of spectral weight is natural since lighter impurities should have higher characteristic frequencies.
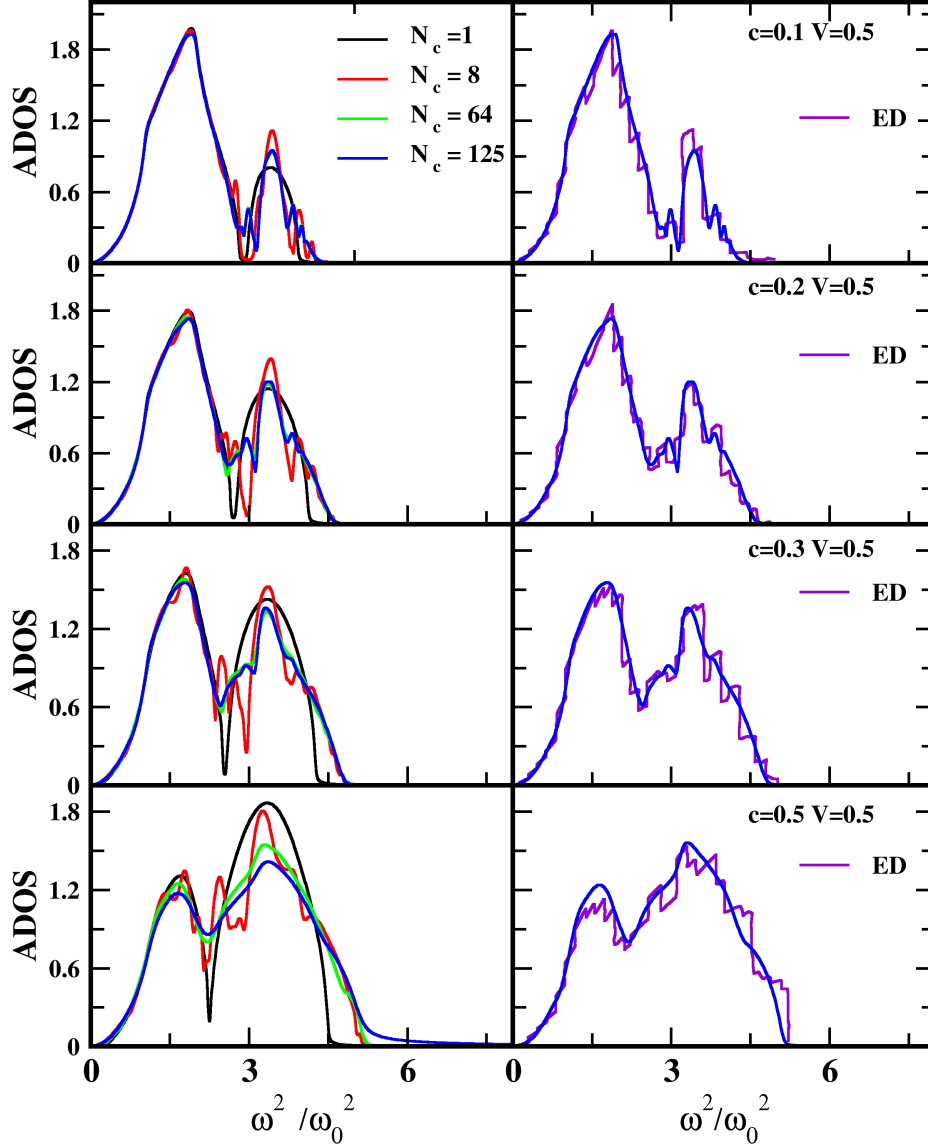


Figure 3.2: Comparison of the density of states obtained from the DCA and exact diagonalization (ED) methods (taken from Ref [167]) for a binary isotopic alloy system in three dimensions at a fixed mass ratio ($V = 0.5$) and various values of concentration ($c$). The left panel shows the DCA results for increasing impurity concentration $c$ (from top to bottom). Each panel illustrates the evolution of the spectrum with increasing cluster size. The right panel shows a comparison of the $N_c = 125$ DCA result with ED for the same parameters. The agreement between the DCA and ED is seen to be excellent, whereas there is strong disagreement between $N_c = 1$ results and ED results.

The DCA for a single-site cluster ($N_c = 1$) reduces to the CPA. The left panels of Fig. 3.2 also shows that results from the CPA are quite different from those at higher $N_c$, thus emphasizing the need to incorporate non-local dynamical correlations. Nevertheless, we note that the CPA roughly captures the overall shape. There are two problems, however. At the lowest frequencies, the CPA spectral function exhibits a gap, while the DCA spectra (for higher $N_c = 64, 125$) do not. In fact, even the $N_c = 8$ spectrum is gapped, albeit with a smaller gap as compared to the CPA. The reason for this spurious gapped behavior is that the correct sum rules are obeyed only in the thermodynamic limit. The second problem is that in the high-frequency region, the CPA spectrum comprises an almost separated impurity band with a cusp-like non-analytic feature. This feature is again in contrast with results of higher $N_c$, which shows that the spectrum is continuous and broad. Moreover, we observe that results for $N_c = 64$ and $N_c = 125$ are hardly different for all concentrations, suggesting that the convergence with respect to increasing in cluster size is achieved for a cluster as small as $4 \times 4 \times 4$.

The right panels of Fig. 3.2 show a direct comparison of results using the DCA at the highest $N_c = 125$ of the corresponding left panel with ED results [167]. In general, the computational expense in ED depends on many factors; like the number of frequencies, the length of the lattice and also on the number of atoms in a cross section of the lattice. We consider ED results from Ref [167], where they use a $6 \times 6 \times 25$ lattice and a Strum sequence method. Clearly, the agreement between the ED and DCA, even considering the fine structure of the ED results, is rather good. Thus, the DCA is not only far less expensive than the ED but is also able to yield a smooth and continuous spectrum. Furthermore, the DCA converges to the exact, thermodynamic limit result far more rapidly than the ED, which achieves convergence for much larger system sizes ($6 \times 6 \times 25$). Thus, our DCA scheme can efficiently calculate the average vibrational spectra in three dimensions for arbitrary values of impurity concentrations and disorder potential.

Given the validation of the DCA with ED, we investigate the dependence of the phonon spectrum on the impurity mass within the DCA. This is shown in figure 3.3,

where the DCA phonon spectra for increasing $V$ (implying increasingly lighter impurities) and a fixed concentration ($c = 0.5$) for $N_c = 64$ are shown. As $V \to 1$, the $M_{imp}/M_{host} \to 0$. For a clean simple cubic lattice with a 2-atom basis, where the masses of the two atoms are very different, we expect an optical phonon branch at high frequencies. If the mass of one of the atoms goes to zero, the optical phonon frequency diverges. In the present case, we have $c = 0.5$, which implies an equal concentration of light and heavy atoms, but in a disordered configuration. Hence we should expect a band with distributed spectral weight rather than a weakly dispersive optical branch. Indeed, as figure 3.3 shows, an almost isolated band is seen to emerge as $V \to 1$. The low frequency, in particular $\omega \to 0$, structure of the phonon spectrum is seen to be almost unchanged.

Next, we apply the DCA in two dimensions. A comparison of the phonon DOS from the DCA and ED[167] in two dimensions for a binary mass distribution, impurity
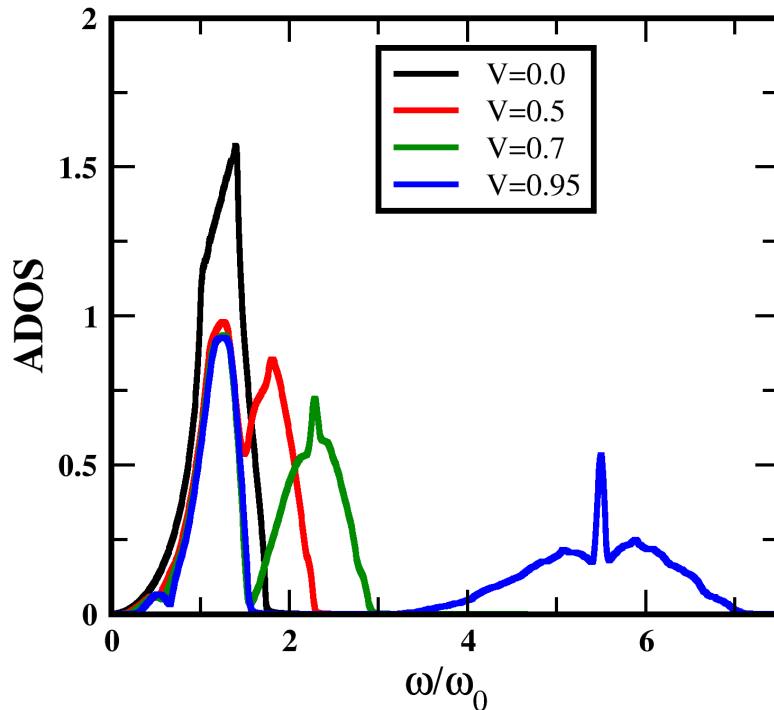


Figure 3.3: Evolution of the average density of states (ADOS) for various values of the disorder potential V with fixed impurity concentration $c = 0.5$ for three-dimensional binary alloy model for a cluster size $N_c = 64$.
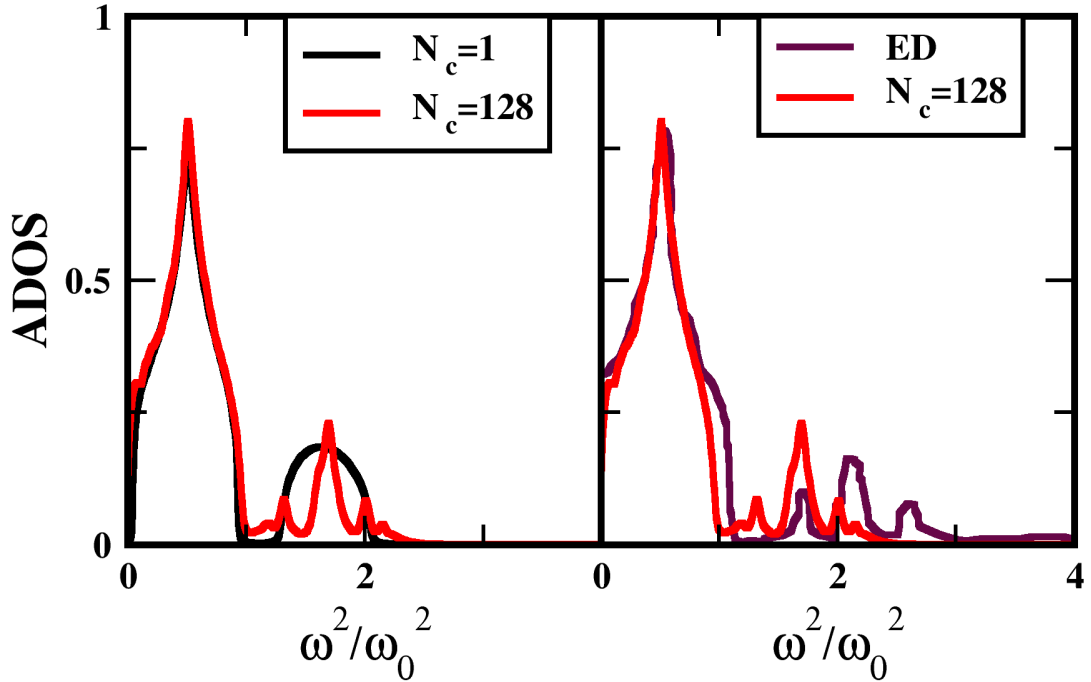
Figure 3.4: Comparison of the density of states obtained from the DCA with exact diagonalization results (taken from Ref [167]) in two dimensions for the binary disorder. The impurity concentration is $c = 0.15$ and disorder potential $V = 0.67$. The left panel shows the evolution of the DOS for cluster sizes $N_c=1$ and $N_c = 128$. Observe that the calculation for $N_c=128$ produces the fine structure of the impurity mode. The right panel shows a good agreement of the density of states obtained from the DCA for cluster size $N_c = 128$ with the exact diagonalization spectrum.

concentration $c = 0.25$, and $V = 0.7$ (implying $M_{imp} = 0.3M_{host}$) is displayed in Fig. 3.4. We find good agreement with ED results in two dimensions as the cluster size increases. Fig. 3.4 shows that the DCA with cluster size $N_c = 128$ successfully reproduces the fine structure and position of the impurity modes as found in ED results.

As a last benchmarking exercise, we look into one-dimensional systems. Since most of the previous studies for disordered lattice vibrations are for one dimension, it gives us a great opportunity to benchmark our DCA results for the one-dimensional system in detail. The comparison between DCA results with a finite cluster size and exact results[166] is displayed in Fig. 3.5. As we anticipate, our DCA results with increasing cluster size $N_c$ due to systematic incorporation of non-local spatial correlation are in
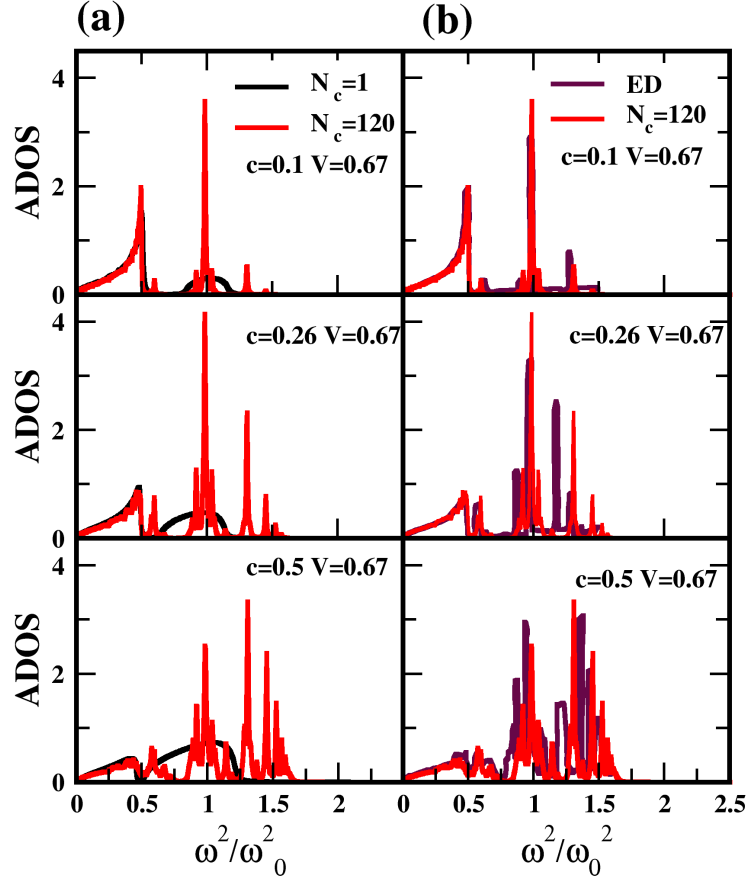
Figure 3.5: A comparison of density of states calculated with DCA and exact diagonalization (ED) method (taken from Ref [166]) at various values of impurity concentration $c$ for disorder potential $V = 0.67$ for a one-dimensional binary alloy system. The left panel shows the variation of density of states with increasing cluster size ($N_c$). The right panel indicates that the DCA with cluster size $N_c = 120$ within computational error systematically reproduces exact results including both the correct position and fine structure feature of the spectra.

good agreement including the correct position and structure of the impurity mode. In addition, our results are in good agreement with the semi-analytical result [177] as shown in Fig. 3.6.

Since the DCA is non-perturbative, it is applicable over the entire alloy regime, $c \in [0, 1]$, which has been a significant limitation of perturbative theories of alloys [159; 155; 154]. A cluster approach developed by Myles and Dow[178] also incorporates non-local correlations. However, this method is limited by a restriction on the combined choice of concentration ($c$) and cluster size ($N_c$), which have to obey the relation,
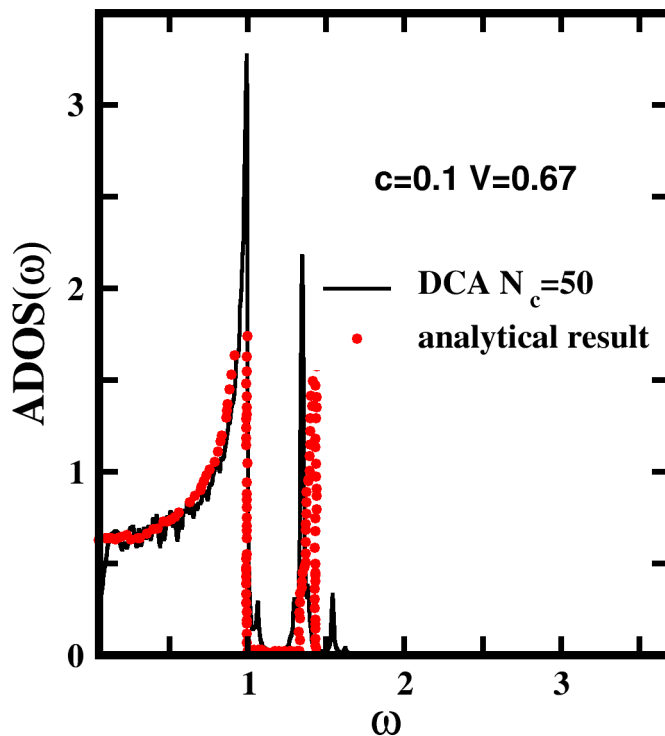
Figure 3.6: A comparison of density of states obtained from the DCA and the semi-analytical method (taken from Ref [177]) at impurity concentration $c = 0.1$ for disorder potential $V = 0.67$ for a one-dimensional binary alloy system.

$cN_c$=integer, akin to supercell-based calculations. The DCA does not suffer from this restriction, which makes it possible to access any impurity concentration for a given cluster size. Another drawback of Myles' cluster method as compared to the DCA is that the effective medium is described within the CPA. As a result, the bandwidth of the local impurity mode obtained from Myles' calculations is too narrow.

The excellent benchmark obtained thus far implies that the DCA scheme for phonons with increasing cluster size ($N_c$) can efficiently predict vibrational spectra for disordered systems. Nevertheless, the DCA is not able to capture Anderson localization[171; 179] of phonons. In order to incorporate the physics of localization, we utilize the TMDCA method, described in section 3.2. The following sub-section describes the validation of the TMDCA through a direct comparison with the transfer matrix method.

## 3.3.2 Typical Medium Dynamical Cluster Approximation

A striking feature of disordered systems in three dimensions is the existence, in the density of states, of a mobility edge [180], which is defined as the energy separating localized and itinerant states. Experimental measurements of the mobility edge are feasible as demonstrated for ultracold atoms in a disordered potential created by laser
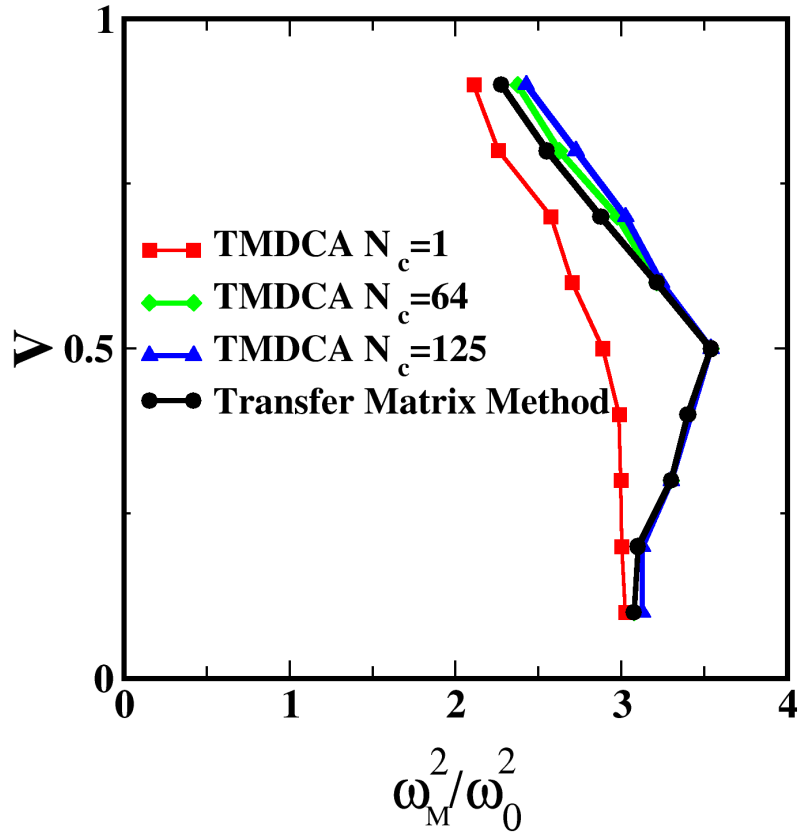


Figure 3.7: A comparison of the mobility edges ($\omega_M$) in the phonon spectrum in three dimensions for a box-distribution, obtained from the transfer matrix method (taken from Ref [168]) against TMDCA. Results from the latter for the larger clusters agree excellently with the TMM results.

speckles [181]. Within the TMDCA, the mobility edge is determined using the band-edges of the typical density of states (TDOS), since the latter is non-zero only for extended states. For a box disorder distribution, defined as $P_V(V_l) = \Theta(V - |V_l|)/2V$ where $V_l = (1 - M_l/M_0)$ and $0 < V \leq 1$, where $l$ is the site index, and $V$ is the width of the distribution that represents the strength of disorder, the mobility edge determined using TMDCA is compared against exact transfer matrix method results in Fig. 3.7. The agreement between results from the TMM (black circles) and the TMDCA for $N_c = 64$ (green diamonds) and 125 (blue triangles) is excellent. Such a result is not surprising, since the TMDCA, for three-dimensional *electronic* disordered systems, agrees very well with the kernel polynomial method and the transfer matrix method[171].

For $V \gtrsim 0.5$, the TMM results and likewise those from TMDCA exhibit a re-entrant transition with increasing disorder, in parallel with the behavior in disordered electronic systems [171]. However, an important difference is that beyond a critical disorder, all the states in the electronic system become localized; while in the phonon case, a finite fraction of the low-frequency states remain extended. In analogy with the electronic case, the re-entrance transition seen in the TMDCA results in Fig. 3.7 has the following explanation: Very low disorder induces states outside the band-edge that merge with the continuum through hybridization. At intermediate levels of disorder, isolated localized modes (analogous to deep trap states) appear beyond the band-edge, which nevertheless hybridize with each other and the extended states on the band-edge, and thus transform into extended states. We note that such a hybridization requires inter-site correlations, that are missing from a single site theory ($N_c = 1$) such as the TMT, and hence a blue shift of the mobility edge (seen in the TMDCA results of Fig. 3.7) is not captured by the single-site theory. However, with increasing disorder, states at the band edges begin to get localized, and hence the mobility edge undergoes a re-entrance crossover.

The failure of single-site theories ($N_c = 1$, red squares in Fig. 3.7), as evidenced by the significant disagreement with TMM results involves two factors: (i) The TMM mobility edge initially blue shifts with increasing disorder, while the $N_c = 1$ result red

shifts monotonically. (ii) The TMM as well as the TMDCA results for higher disorder strengths ($V \gtrsim 0.5$), clearly show a re-entrant transition, which the single-site theory completely misses. Likely, this is due to the fact that the $N_c = 1$ calculation is a single-site theory and hence does not incorporate non-local coherent back-scattering effects; although it does include strong localization effects induced by deep trapped states.

With these results for the DCA and TMDCA, the question 1(a) posed at the end of the introduction is fully answered. Both DCA and TMDCA do yield excellent agreement when compared to exact methods. Now, we move to a discussion of results on the Anderson localization of phonons.

## 3.4   Results from TMDCA

In disordered electronic systems the typical density of states, given by Eq. (3.22), may be used as an order parameter for the Anderson localization transition [174; 171]. While the physical observable is still the *arithmetically* averaged density of states (ADOS($\omega$)), the TDOS($\omega$) yields a mobility edge that separates localized and extended states. Within the TMDCA, the ADOS($\omega$) is computed from $D_{\text{typ}}^{\text{ave}}(\mathbf{K}, \omega)$, which, as explained in Section 3.2, carries information about the typical medium within which the cluster is embedded. The hybridization function connecting the cluster with the host is known [170] to decay as a function of increasing cluster size as $\sim 1/N_c^2$. Hence, the ADOS($\omega$) computed within TMDCA must coincide with the corresponding quantity computed within the DCA in the thermodynamic limit. In practice, we find that even at $N_c = 64$, the two are almost identical. This is shown in Fig. 3.8. We show results for the arithmetically averaged phonon spectra computed within the DCA (black) and TMDCA (red) for a binary, isotopic mass distribution with fixed concentration $c = 0.5$, and various mass ratios ($M_{imp}/M_0$). The main message here is that the physical density of states must not be dependent on the hybridization of the cluster provided that the cluster is large enough. And it is seen clearly in Fig. 3.8 that the ADOS from DCA and TMDCA are identical for all

disorder potentials for larger clusters, i,e $N_c = 64$ and 125. For $N_c = 1$, the two differ significantly at higher disorders, which is expected as mentioned above. However, ADOS is same for low disorder for all the cluster sizes $N_c = 1$, $N_c = 64$ and $N_c = 125$, showing that TMDCA yields the same results as DCA at low disorder. Also, observe that the ADOS is the same for cluster sizes $N_c = 64$ and $N_c = 125$, which ensures
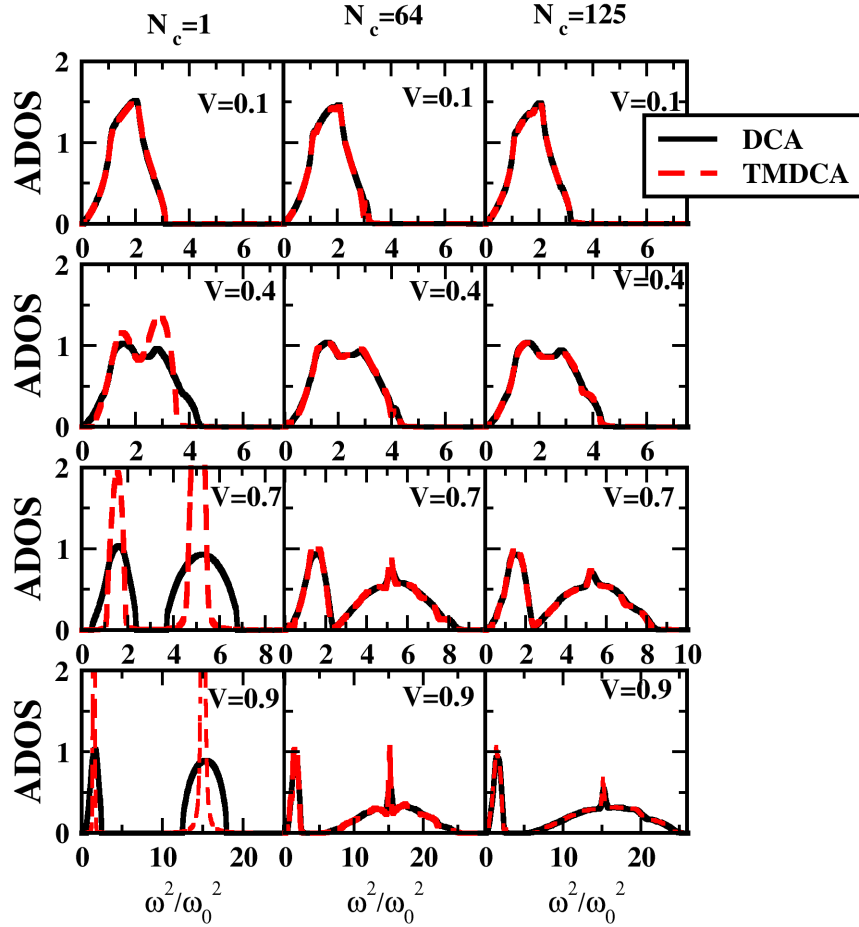


Figure 3.8: The evolution of the ADOS calculated using the DCA (black curves) and TMDCA (red dashed curves) for cluster sizes of $N_c = 1, 64$ and 125 at various values of disorder potential $V$ with fixed impurity concentration $c = 0.5$ for a binary, isotopic distribution of masses in three dimensions. The ADOS obtained from the DCA and TMDCA differ significantly from each other for cluster size $N_c=1$, whereas for higher cluster size ($N_c=64$ and $N_c = 125$), the two are completely identical to each other for all disorder potentials. This result indicates that at higher cluster size, ADOS is independent of hybridization function $\Gamma(\mathbf{K}, \omega)$, and equivalently the disorder averaging procedure.

the convergence of the results as cluster size increases.

In what follows, we will discuss results for the average and the typical density of states, computed through TMDCA for box and binary disorder distributions.
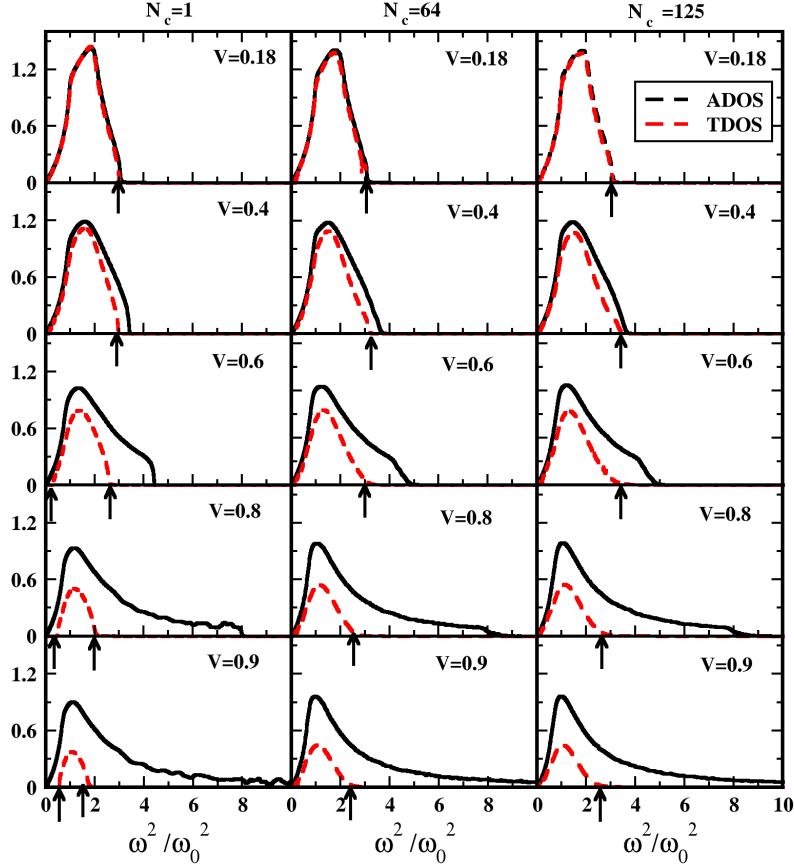


Figure 3.9: The evolution of the ADOS and TDOS, obtained from the TMDCA, as a function of the square of the frequency ($\omega^2$) at various disorder strengths $V$ chosen from a box distribution in three dimensions with cluster sizes $N_c = 1, 64$ and 125. At low disorder ($V$), the shape of the TDOS is similar to ADOS. As $V$ increases, the spectral weight in the TDOS decreases monotonically, while the ADOS, being normalized, develops long, slowly decaying tails that comprise localized phonon modes. The tiny arrows denote mobility edges ($\omega_M$), that have been used for benchmarking against TMM results in Fig. 3.7.

### 3.4.1 Box disorder

We restrict our discussion of TMDCA results to three-dimensional systems and focus first on box disorder. In Fig. 3.9, the ADOS (black) and TDOS (red) are shown for a range of disorder strengths $(V)$ and cluster sizes $N_c = 1, 64$ and $125$ for a *uniform (box)* distribution. As may be expected, the typical DOS is almost the same as the ADOS for low disorder $(V \lesssim 0.4)$. However, for higher $V$, localization sets in at higher frequencies. The ADOS develops long tails, but the TDOS is non-zero over a much smaller frequency interval, indicating that all tail modes are Anderson localized. Moreover, the integrated spectral weight in the TDOS decreases steadily. The TDOS shown in Fig. 3.9 has been used to extract the mobility edges that were compared against TMM results in Fig. 3.7. Note that, for higher $V(\gtrsim 0.8)$ and $N_c = 1$, the spectra exhibit a second mobility edge at low frequencies implying that long wavelength acoustic modes become localized. However, this result is again an artifact of the single-site approximation because higher $N_c$ results show that long wavelength acoustic modes do not localize at all, even when $V \to 1$.

### 3.4.2 Binary isotopic disorder

For a binary, isotopic distribution, the evolution of ADOS and TDOS, obtained within the TMDCA for cluster sizes $N_c = 1$, $N_c = 64$ and $N_c = 125$, with increasing impurity concentration $c$ and fixed disorder potential $V = 0.7$, is shown in Fig. 3.10. Fig. 3.10 displays a transfer of spectral weight from low to high frequencies, and a modest dip in the typical spectral weight around $c = 0.5$.

We find that the ADOS shown in Fig. 3.10 is almost the same than the one found within the DCA (see Fig. 3.2). The main difference is that the ADOS found within the TMDCA is very spiky as compared to the corresponding quantity in the DCA. Interestingly, the *impurity* modes yield a non-zero ADOS beyond the band-edge of the host band, but the TDOS is almost zero for low concentrations $(c \lesssim 0.2)$. The vanishing of the TDOS indicates the localization of the impurity-induced high-frequency modes for such concentrations. As the concentration increases, the low and

high-frequency bands merge, and the TDOS is non-zero over the entire bandwidth. Nevertheless, as the concentration $c \to 1$, the ADOS clearly shows a remnant of the host modes, but the TDOS is quite small in the same frequency range implying that most of those modes are localized. The leftmost panel, for $N_c = 1$, shows that for $c \to 1$, the host modes are completely localized, and a low-frequency mobility edge emerges. However, results for larger cluster sizes of $N_c = 64$ and $125$ show that such a result is an artifact of ignoring non-local dynamical correlations. Far more dramatic changes occur for fixed concentration, $c$, and increasing disorder potential, $V$, as shown in Fig. 3.11. At low $V$ $(\lesssim 0.4)$, the ADOS and TDOS do not differ much, which
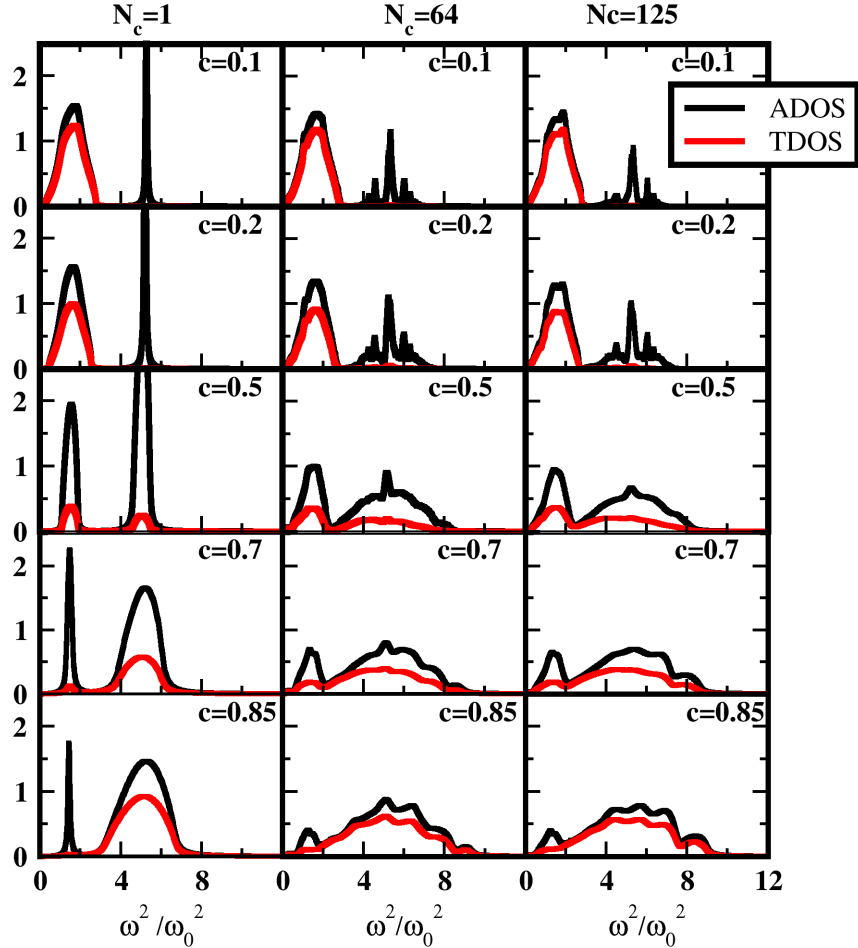


Figure 3.10: The ADOS and TDOS calculated using the TMDCA with cluster sizes $N_c = 1, 64$ and $125$ at various values of impurity concentration $c$ with fixed disorder potential $V = 0.7$ for binary isotopic mass distribution in three dimensions.

57

is expected since the TMDCA reduces to DCA in the low disorder limit [171]. The good agreement between ADOS and TDOS also indicates that most modes remain propagating even if half of the host atoms are replaced with lighter atoms of mass, $M_{imp} \gtrsim 0.6M_0$. However, for higher $V$, the TDOS is sharply suppressed and is seen almost to vanish for $V \to 1$, thus suggesting that almost all modes get localized in this parameter regime. Nevertheless, a complete localization seems to be possible only when $V = 1$, or when $M_{imp} = 0$, which corresponds to vacancies, for which a proper treatment involves the inclusion of spring disorder.

Therefore, localization of the impurity modes in the high-frequency region may be
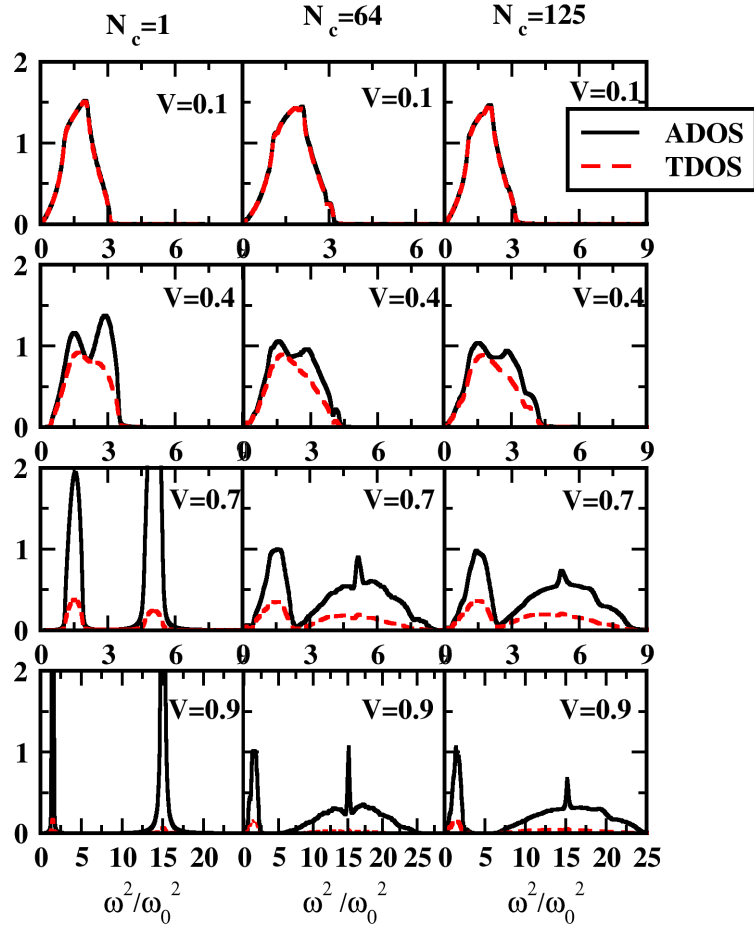


Figure 3.11: The ADOS and TDOS calculated using the TMDCA with cluster sizes $N_c = 1, 64$ and 125 at various values of disorder potential $V$ with impurity concentration $c = 0.5$ for binary, isotopic mass distribution in three dimensions.

achieved with experimentally feasible disorder parameters. However, low-frequency phonons are almost impossible to localize, which is consistent with the argument made in Section 3.2. Howie et al. [182] study Hydrogen-Deuterium mixtures for three concentration ratios, namely $0.6 : 0.4, 0.55 : 0.45$, and $0.5 : 0.5$ using Raman spectroscopy. They observe that the Hydrogen-Deuterium mixture goes into a new phase IV, which may be modeled as an ideal binary isotopic alloy. In this alloy, with a mass-factor of 2 and varying the concentration ratio, they find six localized modes located in the high-frequency region, while four low-frequency modes are found to be delocalized. Our model study using the TMDCA can capture this localization effect qualitatively. It will, naturally, be interesting to explore the phenomenon of acoustic phonon localization using more realistic parameters in the presence of both mass and spring disorder. Such a study is presented in chapter 5.

The results shown in this section allow us to answer the second question posed at the end of the introduction. Although the ADOS shows the physically observable exact spectrum of the disordered phonon system, a clear identification of localized and extended states cannot be made based only on the ADOS. Through a direct comparison of the TDOS with the ADOS, such an identification becomes straightforward. Thus, the TDOS gives great insight into which modes are propagative and which ones are not; that can be further used for developing strategies for e.g decreasing thermal conductivity in thermoelectric materials.

## 3.5 Conclusions

We have developed the DCA and TMDCA formalisms for investigating the effects of disorder on the phonon spectrum. Though the DCA exhibits several advantages over the CPA by including important non-local spatial correlations, it suffers from its inability to capture Anderson localization. Such a failure is due to the arithmetic averaging over disorder configurations. Based on this understanding, we develop the TMDCA, where a typical averaging ansatz replaces the arithmetic averaging step. Using the TMDCA for a binary and a box distribution of mass disorder, we

explore several aspects of Anderson localization in phononic systems. In particular, a comparison of the mobility edge computed through the TMDCA with that from the transfer matrix method yields an excellent agreement including the capture of the re-entrance transition of the mobility edge.

We also find that for a binary isotopic alloy, low concentrations of light impurities introduces high frequency modes, which are Anderson localized. While at high concentrations, the lower frequency modes are localized. Maximum localization over the entire spectrum is observed for equal concentrations of light and heavy atoms. Another finding is that a larger difference between the isotope masses introduces stronger localization effects than the ones due to an increasing in the concentration of impurities.

Addressing the question 1(b) posed at the end of the introduction, the DCA and the TMDCA methods do fulfill several essential characteristics required for a successful cluster theory. They converge systematically to the thermodynamic limit, and with far lower computational expense than exact methods such as ED and TMM. The excellent benchmarks obtained show that not only do the methods work in the full parameter regime, and over all frequencies, the TMDCA is also capable of describing AL of phonons highly accurately.

# Chapter 4

# Effect of short-ranged spatial correlations on the Anderson localization of phonons in mass-disordered systems

In chapter 3, we considered quenched mass disorder chosen to be completely random, and short-range order was totally neglected. The formalism developed in chapter 3 however is not restricted to such a case however. Moreover, real materials cannot be expected to conform to such an ideal choice. The work presented in this chapter aims to demonstrate the application of the TMDCA formalism developed in the previous chapter to investigate the effect of short-range order in the spatial distribution of masses on the AL of phonons. We have organized this chapter as follows. In section 4.1, we present a brief introduction to existing studies that incorporate spatially correlated disorder. In section 4.2, we have described the formalism that we have adopted for generating correlated disorder. In section 4.3, we present results and a discussion. In section 4.4, we give our conclusions.

## 4.1   Introduction

Anderson introduced an ideal theoretical model containing the essential ingredients for studying the nature of one-electron states in disordered systems[1]. The model assumed non-interacting electrons moving in lattice sites and allowed to hop only to

nearest-neighbor sites. Disorder was introduced in the local orbital energies, which were independent quenched random variables distributed according to some specified probability distribution. Anderson predicted that the wave function may become exponentially localized with a characteristic localization length depending on the strength of disorder. Scaling theory[17] propounded Anderson's idea of localization[1] by considering non-interacting electron systems with uncorrelated disorder. It found that all one-electron states are exponentially localized in one and two dimensions even for infinitesimal amount of disorder, with a true metal-insulator transition occurring only in three dimensions (3D) whence the single-particle states may survive as extended states for weak disorder. A series of analytical, numerical and experimental results find strong agreement with one-parameter scaling theory of localization. However, the characteristics of the disorder potential can have a strong impact on Anderson localization. In particular, spatial correlations in the disorder can markedly change the conventional physics of Anderson localization.

Such correlated disorder is relevant to transport properties of binary solids, DNA[183; 184], graphene[185; 186], quantum Hall wires[187], topological insulators[188] and so on. Recently, there has been a growing interest in understanding the effect of spatial correlations on Anderson localization due to tremendous experimental progress. Clement et al.[189] developed a experimental technique for creating correlated disorder through the laser speckle. In this method, one can accurately control the spatial correlation length. A spatial correlation induced localization-delocalization transition has been experimentally observed in GaAs-AlGaAs superlattices[190]. Very recently, a transition between algebraic localization and delocalization in a 1D disordered potential with a bias has been reported[191]. Such experimental observations call for an in-depth theoretical analysis of the effect of short-range correlations on Anderson localization.

We describe briefly the theoretical investigations that have incorporated short-range as well as long-range spatial correlations in the diagonal as well as off-diagonal disorder. A series of one-dimensional versions of the Anderson model have been used to demonstrate a breakdown of Anderson's localization driven by spatial correlations

on the disorder distribution[192; 193; 194; 195; 196]. Also, effort has been made to demonstrate the strong effect of off-diagonal correlated disorder on Anderson localization. For example, a number of studies have employed correlated off-diagonal interactions and found delocalized states[197; 198; 199]. Besides short range correlations, several investigations have been performed considering long range correlations in the disorder distribution. Carpena et al.[200] find a long-range correlation-induced metal–insulator transition using a one-dimensional tight-binding model. Francisco et al. [201] obtain an Anderson-like metal-insulator transition studying a one-dimensional tight-binding model with long-range correlated disorder. All these studies suggest that localization properties are greatly renormalized when some kind of spatial correlation is introduced in the disorder distribution. However, most of the studies are limited to electronic problems and Anderson localization of phonons in the presence of spatially correlated disorder has received scant attention, both theoretically and experimentally.

Being a general wave phenomenon, Anderson localization is ubiquitous. Sajeev John et al [202], using field theoretic techniques, investigated phonon localization in the presence of long range correlated random potential. However, methods like exact diagonalization (ED), transfer matrix method (TMM), multifractal analysis, diagrammatic techniques, itinerant coherent-potential approximation (ICPA) have not been employed for studying phonon localization in the presence of correlated disorder. Most of the mentioned methods have been confined to simple models of lattice vibrations, where the diagonal matrix elements $M(l)$ of the Hamiltonian are independent random variables.

In the previous chapter, we provided a detailed description of a typical medium dynamical cluster approximation (TMDCA), that yields a proper description of the Anderson localization transition in 3D. It adopts the typical density of states (TDOS) as a single particle order parameter for the Anderson localization transition (ALT) which makes it computationally less expensive compared to other numerical methods like ED and TMM. It satisfies all the essential requirements expected of a successful quantum cluster theory. We have also been able to extend the formalism for studying

Anderson localization of phonons in the presence of both diagonal and off-diagonal disorder[203; 204], which forms the subject of the next chapter.

In this chapter, we investigate the nature of the Anderson transition for phonons in the presence of spatially correlated disorder in 3D.

## 4.2 Model and formalism

As before, we consider the following Hamiltonian for the ionic degrees of freedom of a disordered lattice within the harmonic approximation in the momentum ($p$) and displacement($u$) basis, as

$$H = \sum_{\alpha i l} \frac{p_{i\alpha}^2(l)}{2M_i(l)} + \frac{1}{2} \sum_{\alpha\beta ll'ij} \Phi_{ij}^{\alpha\beta}(l, l') u_\alpha^i(l) u_\beta^j(l'), \tag{4.1}$$

where the symbols have their usual meaning (see chapter 3). In this chapter, we again restrict ourselves to a single branch and single basis atom case, hence we drop the indices, $\alpha, \beta, i, j$. The spatial dependence of the ionic masses $M(l)$ is incorporated through a local disorder potential $V$ as

$$\hat{V}_{ll'} = \left[1 - M(l)/M\right]\delta_{l,l'}. \tag{4.2}$$

In the previous chapter, we had considered a uniform box distribution, where the quantity $\left(1 - M(l)/M\right) \in [-V, V]$ can take any value in that interval with equal probability and $0 \le V \le 1$ is the disorder strength. The random $V'$s from site to site were taken to be uncorrelated with each other. As mentioned in the introduction, the objective of this chapter is to investigate the effect of short-range correlations in the mass disorder.

We begin with nearest-neighbour correlations. We first distribute masses randomly on the odd sites and on the even sites, exactly as was done previously, according to a uniform distribution with the same mean and variance. The disorder potential at the odd sites is denoted as $V_1$ and that on the even sites is denoted as

$V_2$. Therefore,

$$\langle V_1^2 \rangle = \sigma^2$$

$$\langle V_2^2 \rangle = \sigma^2$$

$$\langle V_1 V_2 \rangle = 0 \ . \tag{4.3}$$

Now, $V_1$ and $V_2$ are independent, so $\rho_{V_1 V_2} = 0$. From these two uncorrelated random sequences, we want to generate correlations between consecutive sites of the odd and even sequences with a specified correlation coefficient $\rho$. The resulting new sequences for the odd and even sites, denoted as $V_{\text{odd}}$ and $V_{\text{even}}$, should be correlated pairwise. So, the site $2n + 1$ and $2n$ should be correlated.

$$\rho_{V_{\text{odd}} V_{\text{even}}} = \frac{\langle \left( V_{\text{odd}} - \langle V_{\text{odd}} \rangle \right) \left( V_{\text{even}} - \langle V_{\text{even}} \rangle \right) \rangle}{\sigma^2} \ , \tag{4.4}$$

where $\sigma^2$ is the variance. Let us assume that $V_{\text{odd}}$ with $V_1$ and $V_{\text{even}}$ with $V_2$ are related as

$$V_{\text{odd}} = aV_1 + bV_2$$

$$V_{\text{even}} = cV_1 + dV_2 \ . \tag{4.5}$$

So,

$$\langle V_{\text{odd}} V_{\text{even}} \rangle = \langle (aV_1 + bV_2)(cV_1 + dV_2) \rangle$$

$$= ac\langle V_1^2 \rangle + bd\langle V_2^2 \rangle + (ad + bc)\langle V_1 V_2 \rangle \ . \tag{4.6}$$

Using Eq.(4.3) in Eq(4.6), we write

$$\langle V_{\text{odd}} V_{\text{even}} \rangle = (ac + bd)\sigma^2 \ . \tag{4.7}$$

Using Eq.(4.3) in Eq.(4.4), we write

$$\rho_{V_{\text{odd}} V_{\text{even}}} = \frac{\langle V_{\text{odd}} V_{\text{even}} \rangle}{\sigma^2} \ . \tag{4.8}$$

Using Eq. (4.7) in Eq. (4.8), we get

$$\rho_{V_{\text{odd}} V_{\text{even}}} = ac + bd \tag{4.9}$$

65

From Eq(4.5), we write

$$\langle V_{\text{odd}}^2 \rangle = \langle (aV_1 + bV_2)(aV_1 + bV_2) \rangle$$
$$= a^2 \langle V_1^2 \rangle + b^2 \langle V_2^2 \rangle + (ac + bd)\langle V_1 V_2 \rangle . \tag{4.10}$$

Using Eq.(4.3), we get

$$\langle V_{\text{odd}}^2 \rangle = (a^2 + b^2)\sigma^2 . \tag{4.11}$$

Similarly,

$$\langle V_{\text{even}} \rangle = (c^2 + d^2)\sigma^2 . \tag{4.12}$$

We impose the condition

$$\langle V_{\text{odd}}^2 \rangle = \sigma^2 , \tag{4.13}$$

and

$$\langle V_{\text{even}}^2 \rangle = \sigma^2 . \tag{4.14}$$

Comparing Eq.(4.12) with Eq.(4.14) and comparing Eq.(4.11) with Eq.(4.13), we get

$$a^2 + b^2 = c^2 + d^2 = 1 \tag{4.15}$$

So, we can consider the transformation as

$$a = \cos\phi \qquad\qquad b = \sin\phi$$
$$c = \sin\phi \qquad\qquad d = \cos\phi . \tag{4.16}$$

Hence, the expression

$$ac + bd = 2\cos\phi\sin\phi = \sin 2\phi . \tag{4.17}$$

Thus, random $V_{\text{odd}}$ and $V_{\text{even}}$ are correlated with $\rho_{V_{\text{odd}}V_{\text{even}}}$ which is equal to $\sin 2\phi$, where

$$\phi = \frac{1}{2}\sin^{-1}(\rho_{V_{\text{odd}}V_{\text{even}}}) . \tag{4.18}$$

We can verify that this method does induce correlations between the even and the odd sequences. For vanishing correlation, i.e. for $\rho_{V_{\text{odd}} V_{\text{even}}} \to 0$, from Eq. 4.18, $\phi \to 0$ as well. This implies, from Eqs. 4.6 and 4.16, that $a, d \to 1$ and $b, c \to 0$, hence

$$V_{\text{odd}} \to V_1$$

$$V_{\text{even}} \to V_2 \ . \tag{4.19}$$

Since $V_1$ and $V_2$ are anyway uncorrelated, the new sequences, $V_{\text{odd}}$ and $V_{\text{even}}$, in this limit are also uncorrelated. While in the other extreme, namely $\rho_{V_{\text{odd}} V_{\text{even}}} \to 1$, we get $\phi \to \pi/4$, which implies $a, b, c, d \to 1/\sqrt{2}$, and hence $V_{\text{odd}} \simeq V_{\text{even}} \simeq (V_1 + V_2)/\sqrt{2}$. Thus, in this limit, $V_{\text{odd}}$ and $V_{\text{even}}$ become almost equal and are hence fully correlated. We illustrate this in Fig. 4.1, where for four different correlation coefficients, $\rho_{V_{\text{odd}} V_{\text{even}}} = 0.2, 0.5, 0.8$ and $0.99$, the difference of the two sequences, $V_{\text{odd}} - V_{\text{even}}$ is plotted as a function of the site-index. It is seen that for small correlation coefficients, the difference is large, and hence the odd and even sequences are uncorrelated. While for large correlation coefficient ($\gtrsim 0.9$), the difference is very small, and hence the two sequences are strongly correlated.

An algorithm that implements the described formalism for creating correlated disorder potential is stated below:

1. The algorithm for generating correlated disorder potential starts with creating local disorder potential $V_l$, which we initially consider as spatially independent random variables distributed according to uniform (box) distribution as

$$P_v(V_l) = \Theta(V - |V_l|)/2V \ , \tag{4.20}$$

where $V_l$ is the disorder potential defined in Eq.(4.2) and $V$ is the width of the distribution that corresponds to the disorder strength.

2. Identify the $V_l$ at lattice sites $l$ that are labeled by the even number or odd number. We define $V_1(l)$ as the disorder potential at the odd indexed lattice sites and $V_2(l)$ as the disorder potential at the even indexed lattice sites.

3. We set $\rho$ as correlation strength parameter which can be varied from 0 to 1. For a given value of $\rho$, we calculate $\phi$ using Eq.(4.18).

4. The unknown coefficients $a, b, c, d$ are calculated using Eq. 4.16 and the normalization is maintained by imposing the condition given in Eq.(4.15).

5. The spatial correlations among the $V_{\mathrm{odd}}$ and $V_{\mathrm{even}}$ are introduced depending on the strength $\rho$ according the relation given in Eq.(4.5).

The rest of the algorithm is the same as described in chapter 3.

## 4.3   Results and discussions

As we have already discussed, a true delocalization-localization transition occurs in 3D depending on the strength of disorder $(V)$. We investigate this Anderson transition of phonons using the TMDCA in the presence of short range order. In our previous
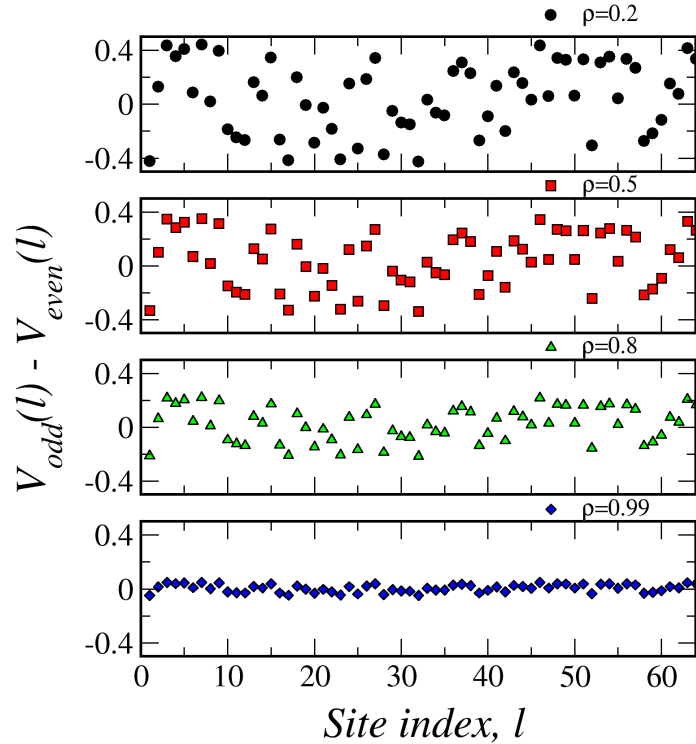


Figure 4.1: A plot of the difference of two correlated random sequences $V_{\mathrm{odd}} - V_{\mathrm{even}}$ for four different values of correlation coefficient $(\rho)$ using cluster size $N_c = 64$. Notice that the two random variables are strongly spatially correlated for $\rho = 0.99$, whereas they are uncorrelated for $\rho = 0.2$.

study, we have already established that the TDOS is a valid order parameter for studying phonon localization. So, we first observe the evolution of the TDOS with increasing disorder strength $V$ for correlated strength $\rho = 0$ (uncorrelated) and $\rho = 0.99$. It is displayed in Fig4.2. As may be expected, the TDOS for $\rho = 0$ is almost the same as the TDOS for $\rho = 0.99$ for low disorder ($V \leq 0.3$). But, for $V > 0.3$, the TDOS for $\rho = 0.99$ starts to deviate strongly from the TDOS for the uncorrelated disorder. We note that the TDOS for $\rho = 0.99$ differs significantly from the TDOS for the uncorrelated disorder at $V = 0.9$. We have already understood that the
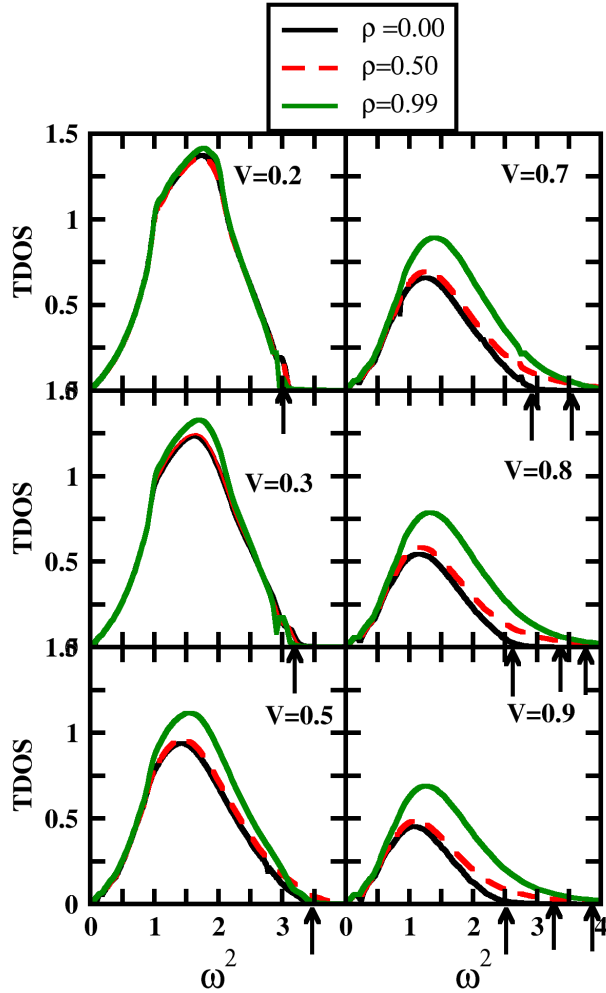


Figure 4.2: The evolution of the TDOS, calculated from the TMDCA, as a function of the square of the frequency ($\omega^2$) with increasing disorder strength ($V$) considering a box distribution in three dimensions using cluster size $N_c = 64$ for the uncorrelated ($\rho = 0.00$) and correlated ($\rho = 0.99$) spatial disorder.

vanishing of the TDOS implies the localization of vibrational modes[203]. Here we reproduce such behavior for $\rho = 0$. The TDOS for $\rho = 0$ decreases with increasing $V$ which indicates that the vibrational modes get localized as disorder increases. This kind of disorder-induced delocalization-localization transition is prevented by the introduction of spatial correlations in the system. Through a direct comparison of the TDOS for $\rho = 0$ with the TDOS for $\rho = 0.99$, such behavior can be easily explained. The TDOS for $\rho = 0.99$ still decreases with increasing $V$. But, the rate is much slower compared to uncorrelated case ($\rho = 0$). To take a more careful look into it, we observe the variation of total spectral weight of the TDOS with increasing $\rho$.

The variation of total spectral weight of the TDOS with increasing correlations is shown in Fig4.3. It clearly shows that the total spectral weight of the TDOS for $\rho = 0.99$ decreases much slower in rate compared to the uncorrelated disorder ($\rho$). Such behavior indicates that the spatial correlations prevent the vibrational modes
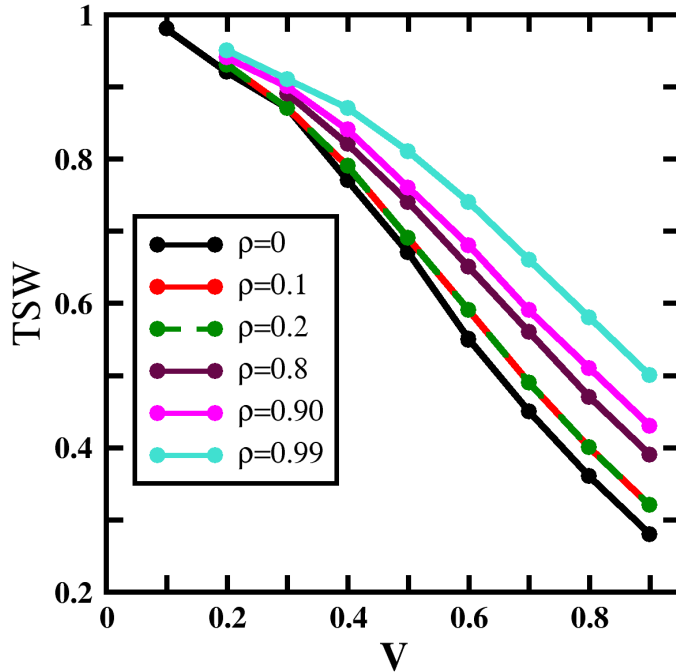


Figure 4.3: Total spectral weight (TSW) of the TDOS as a function of increasing disorder strength ($V$) for correlated strength $\rho = 0.1$ 0.99. We observe that the rate of decrease of the total spectral weight (TSW) of the TDOS decreases with increasing spatial correlation.

to be localized.

Another perspective of spatial correlations is obtained through an investigation of mobility edges which can be extracted from the TDOS presented in Fig4.2. A mobility edge is defined as the energy which separates localized and extended states[205]. The mobility edge has been measured for 3D Anderson localization[206]. The effects of spatial correlations on the mobility edges for Anderson localization of electrons have been studied extensively. However, to best of our knowledge, it has not been yet reported for the Anderson localization of phonons in the correlated disorder case. We define the mobility edge by the boundary of the TDOS and denote by arrows as
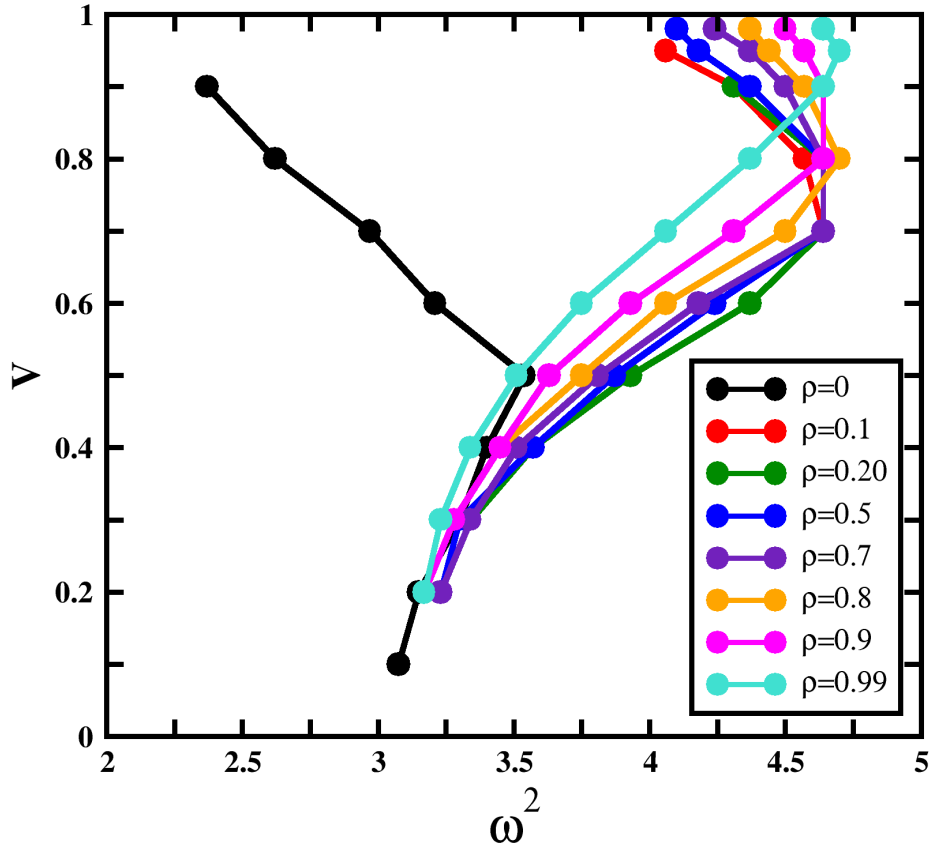


Figure 4.4: Mobility edge trajectory for a box distribution of mass-disordered system in three dimensions. We find that the re-entrance behavior of the mobility edge shifts towards high-frequency region with intermediate correlation strength. Further increase of the correlation strength completely destroys the re-entrance behavior and mobility edges keeps on moving towards high-frequency region indicating a localization-delocalization transition driven by spatial correlations.

indicated in Fig.4.2.

In Fig4.4, we show calculated mobility edges using the TMDCA with $N_c = 64$ for mass disorder. The phase diagram implicates that the spatially correlated diagonal disorder delocalizes the uncorrelated diagonal disorder induced localized vibrational modes. In the phase diagram, we first observe the usual behavior of the mobility edges with increasing $V$ for $\rho = 0$. For small disorder $V < 0.5$, the trajectory of the mobility edges moves outward with increasing $V$. But, it starts moving inward for strong disorder $V \geq 0.5$. Thus, a re-entrance transition with increasing disorder occurs at $V = 0.5$. We explored this behavior of the mobility edges in Ref[203]. The spatially correlated disorder destroys this re-entrant behavior of the mobility edges. As seen in Fig4.4, the trajectory of the mobility edges for $\rho = 0.99$ is almost the same as that for $\rho = 0$ in the presence of small disorder $V \leq 0.5$. However, in contrast to the uncorrelated case, the trajectory of the mobility edges keeps on moving outward with increasing disorder strength $V > 0.5$. It suggests that the spatial correlations drive the system towards delocalization.

## 4.4  Conclusions

We have applied the TMDCA formalism for investigating the effects of short-range spatial correlations on phonon localization in 3D. We have only considered pairwise correlations between the adjacent odd-indexed and even-indexed sites. The correlation strength is varied from 0 to 1. In the weak correlation limit, all the sites have completely random masses, while in the strong correlation limit, the masses of the $(2l-1)^{\text{th}}$ site and the $(2l)^{\text{th}}$ site are the same, but as a function of $l$, the odd/even sequence of masses is still random. Our main conclusion is that correlated disorder with just pairwise correlations can markedly change the localization transition of phonons. Such a conclusion is validated by observing the variation of the TDOS and mobility edges with increasing correlation strength. We show that short-range correlated disorder impedes the localization of the vibrational modes, and eventually, a correlation induced localization-delocalization transition of phonons sets in a 3D

disordered sample. It would certainly be valuable to understand the observed de-localization transition in the presence of long-range correlated disorder. For doing so, an extension of the current framework incorporating long-range correlations is in progress.

# Chapter 5

# Phonon localization in binary alloys with diagonal and off-diagonal disorder: A cluster Green's function approach

In this chapter, we have investigated phonon localization in binary alloys with diagonal and off-diagonal disorder. We have organized this chapter as follows. In section 5.1, we discuss existing studies involving force-constant disorder in binary alloys. In section 5.2, we give the model and formalism that incorporate both mass and force-constant disorder. In section 5.3, we present results and a discussion. In section 5.4, we give conclusions.

## 5.1   Introduction

Most forms of disorder in a crystal structure have two essential consequences, namely a randomness in mass, and a concomitant change in the bond strengths. The phonon spectrum is, naturally, affected strongly by the presence of mass and bond disorder, and can exhibit Anderson localization (AL) [1] depending on the nature and strength of disorder, dimensionality and other factors. Theoretical investigations of spectral dynamics in mass and force constant (FC) disordered systems received a big impetus with the development of mean-field based approaches [207; 208; 209; 210]. However, single-site theories are, by construction, incapable of incorporating the full

non-local nature of force constants. Additionally, some of the Green's function based attempts failed to maintain Herglotz analytic properties [163; 160], which are essential to produce physically acceptable results. Various other extensions of single-site theories[211; 210; 161; 164] have been attempted. Nevertheless, these perturbative methods are plagued by uncontrollable approximations, and hence are unable to treat AL properly.

As a non-perturbative route to understand AL, exact diagonalization (ED) [212] is the most heavily employed method. Although the method does not suffer from approximations, and yields the disorder averaged spectrum, it does have quite a few disadvantages. The state space increases exponentially with system size implying a severe difficulty in simulating large system sizes. The restriction on system sizes, in turn, leads to difficulties in obtaining information of AL[212]. The consideration of three independent force constants namely $\Phi_{AA}, \Phi_{AB}$ and $\Phi_{BB}$ is necessary for a minimal description of FC disorder in a binary alloy system. Such a consideration compounds the computational expense involved in ED calculations. Another important exact method for studying AL of phonons is the transfer matrix method (TMM)[168]. Disorder effects in masses and force constants are intertwined with each other in most of the binary alloys, but the state-of-the-art TMM calculations [168] have, thus far, treated the ionic masses and force constants as uncorrelated variables, which is quite unrealistic. In addition, such an approximation can lead to a violation of sum rules. Thus, despite extensive attempts, a satisfactory, reliable method for studying phonon localization in a strong mass and FC disordered binary alloy is still lacking, which calls for further theoretical development.

In chapter 3, we described the development and application of a typical medium dynamical cluster approximation (TMDCA) for investigating the effect of mass disorder on the AL of phonons. In this chapter, we incorporate the effects of FC disorder into the existing framework, thus taking a step closer to realistic disorder. The present study has two objectives, namely (i) the development of a formalism for mass and FC disordered systems, that is non-perturbative, systematically convergent, causal, computationally feasible, and is well-benchmarked; and (ii) the application of this

formalism to address several open questions (see below). Our first objective has two parts: to develop (a) the DCA to obtain phonon spectra and (b) the TMDCA to investigate phonon localization, in a mass and FC disordered binary alloy. The DCA yields the average density of states (ADOS), which is experimentally observable and is crucial for a basic understanding of disordered lattice vibrations, at a dramatically less computational cost compared to other methods like ED. Concomitantly, the most salient feature of the TMDCA compared to other theories of localization is its ability in predicting localization based on a single-particle order parameter, namely the typical density of states (TDOS). The main development in this work is a cluster adaptation of the Blackman, Esterling and Berk (BEB) formalism [213], which was originally proposed for bond-disordered electronic systems. In this chapter, we adopt a scalar binary alloy model, that consists of a single branch and a single basis atom within the harmonic approximation.

In order to assess the validity of the method, we carry out quantitative benchmarks, and find excellent agreement. Subsequently, through an application of the method, we attempt to address the following questions/issues related to the effects of pure FC disorder and the interplay of mass and FC disorder: (1) Structurally disordered glasses are known to exhibit a low frequency anomaly, known as the Boson peak, in the density of states. Such an anomaly has also been observed in disordered lattice models, though the origin of the Boson peak in the two families of systems might be quite different. It has been argued that a purely FC disordered system can also exhibit such behaviour. We carry out a comprehensive analysis of the deviations from low frequency Debye behaviour, and ask- What are the reasons and conditions for the emergence of a Boson peak in a binary mass and spring disordered system? (2) In a related context, are the modes associated with the Boson peak localized or delocalized? (3) As shown in chapter 3, lighter isotopic impurities lead to strongly localized, short-wavelength phonons in impurity bands. In this chapter, we ask whether the effect of FC disorder is to reinforce or negate the localization induced by mass disorder? (4) And finally, as relevant for improving the figure of merit in thermo-

electrics, we explore the efficacy of vacancies in realizing strong phonon localization over a broad range of frequencies.

## 5.2   Method

As discussed in chapter 3, the Hamiltonian for lattice vibrations involving a single basis atom and a single branch is:

$$H = \sum_l \frac{p^2(l)}{2M(l)} + \frac{1}{2}\sum_{ll'} \Phi(l,l')u(l)u(l') \,, \tag{5.1}$$

where symbols and indices are described in chapter 2. We note that the mass $M(l)$ in Eq.(5.1) can vary randomly from site to site. Since we are considering the Hamiltonian in Eq.(5.1) for a binary alloy, the site $l$ can be occupied by either an A-type atom or a B-type atom, $i.e$ $M(l) \in \{M_A, M_B\}$ with certain probabilities depending on the relative concentrations of the A or B-type atoms. To this end, it is convenient to introduce occupation indices $(x, y)$ for host (A-type atoms) and guest (B-type atoms) as (following Blackman, Ester and Berk (BEB) [213])

$$x_l = 1, y_l = 0, \text{ if } l \in \text{A}$$
$$x_l = 0, y_l = 1, \text{ if } l \in \text{B} \tag{5.2}$$

These occupation indices must obey the following properties:

$$x_l y_l = 0, x_l^2 = x_l$$
$$\langle x_l \rangle = c_\text{A}, \langle y_l \rangle = c_\text{B} \tag{5.3}$$

Note that double occupancy of a given site is prohibited in this formalism. With this assumption, we are ready to express the randomness in the masses as

$$M(l) = \begin{cases} x_l M(l) x_l = M_\text{A} \\ y_l M(l) y_l = M_\text{B} \\ x_l M(l) y_l = M_\text{AB} = 0 \\ y_l M(l) x_l = M_\text{BA} = 0 \end{cases} \tag{5.4}$$

We incorporate such randomness in our formalism by defining a local disorder potential matrix $\hat{V}$, as

$$\left(\hat{V}\right)_{ll'} = (1 - M(l)/M_0)\,\delta_{l,l'} \,. \tag{5.5}$$

The corresponding probability distribution for binary disorder reads as

$$P(V_l) = c_A \delta(V_l - V_A) + c_B \delta(V_l - V_B),\tag{5.6}$$

where $c_A$ and $c_B = 1 - c_A$ are the concentrations of A and B type of atoms respectively.

Mass disorder can be isotopic or non-isotopic. In general, mass disorder will be accompanied by a *corresponding* randomness in the force constants as

$$\Phi(l, l') = \begin{cases} x_l \Phi^{\alpha\beta}(l, l') x_l = \Phi^{\alpha\beta, AA}(l, l') \\ y_l \Phi^{\alpha\beta}(l, l') y_l = \Phi^{\alpha\beta, BB}(l, l') \\ x_l \Phi^{\alpha\beta,}(l, l') y_l = \Phi^{\alpha\beta, AB}(l, l') \\ y_l \Phi^{\alpha\beta}(l, l') x_l = \Phi^{\alpha\beta, BA}(l, l') \end{cases}\tag{5.7}$$

Note that $\Phi(l, l')$ can be decomposed into diagonal $\Phi(l, l)$ and off-diagonal parts

$$\Phi^{\alpha\beta}(l, l') = \delta_{\alpha\beta}(\Phi_D \delta_{l,l'} + \Phi_{nn} \delta_{\mathbf{R}_{l'}, \mathbf{R}_l + \vec{\delta}}),\tag{5.8}$$

where $\Phi_D$ and $\Phi_{nn}$ are the diagonal, and the off-diagonal component of the tensor, respectively, and $\vec{\delta}$ is defined as a vector from a site to its nearest neighbors. Force constant tensor must obey a sum rule, namely $\sum_{l'} \Phi^{\alpha\beta}(l, l') = 0$. For satisfying the sum rule, the formalism has to fulfill two properties: (1) It must incorporate multi-site correlations, because the force-constant tensor is off-diagonal in nature. (2) It must not violate translational invariance. We are satisfying property(1) systematically by increasing $N_c$ and also maintain property(2) by treating force-constant as a coarse-grained quantity.

As shown in chapter 2, we obtain the Dyson equation as

$$M(l)\omega^2 D(l, l', \omega) = \delta_{ll'} + \sum_{l''l'} \Phi(l, l'') D(l'', l', \omega)\tag{5.9}$$

Next, we premultiply and postmultiply the above Eq.(5.9) by $x_l$ and $y_l$, which would generate the four possible configurations of the binary alloy. Combining this with Eqs.(5.3), (5.4) and (5.7) yields four self-consistent equations for the Green's functions

as given below:

$$D_{\mathrm{AA}}(l,l') = \delta_{ll'} + d_{\mathrm{A}}(l) \sum_{l'' \neq l} \Phi^{\mathrm{AA}}(l,l'') D_{\mathrm{AA}}(l'',l')$$

$$+ d_{\mathrm{A}}(l) \sum_{l'' \neq l} \Phi^{\mathrm{AB}}(l,l'') D_{\mathrm{BA}}(l'',l') \tag{5.10}$$

$$D_{\mathrm{AB}}(l,l') = d_{\mathrm{A}}(l) \sum_{l'' \neq l} \Phi^{\mathrm{AA}}(l,l'') D_{\mathrm{AB}}(l'',l')$$

$$+ d_{\mathrm{A}}(l) \sum_{l'' \neq l} \Phi^{\mathrm{AB}}(l,l'') D_{\mathrm{BB}}(l'',l') \tag{5.11}$$

$$D_{\mathrm{BA}}(l,l') = d_{\mathrm{B}}(l) \sum_{l'' \neq l} \Phi^{\mathrm{BA}}(l,l'') D_{\mathrm{AA}}(l'',l')$$

$$+ d_{\mathrm{B}}(l) \sum_{l'' \neq l} \Phi^{\mathrm{BB}}(l,l'') D_{\mathrm{BA}}(l'',l') \tag{5.12}$$

$$D_{\mathrm{BB}}(l,l') = \delta_{ll'} + d_{\mathrm{B}}(l) \sum_{l'' \neq l} \Phi^{\mathrm{BA}}(l,l'') D_{\mathrm{AB}}(l'',l')$$

$$+ d_{\mathrm{B}}(l) \sum_{l'' \neq l} \Phi^{\mathrm{BB}}(l,l'') D_{\mathrm{BB}}(l'',l') \tag{5.13}$$

where the four configuration-dependent Green's function are defined as

$$x_l D(l,l') x_{l'} = D_{\mathrm{AA}}(l,l')$$

$$x_l D(l,l') y_{l'} = D_{\mathrm{AB}}(l,l')$$

$$y_l D(l,l') x_{l'} = D_{\mathrm{BA}}(l,l')$$

$$y_l D(l,l') y_{l'} = D_{\mathrm{BB}}(l,l') \tag{5.14}$$

and the bare locators, $d_{\mathrm{A}}$ and $d_{\mathrm{B}}$ are given by

$$x_l d(l) x_l = d_{\mathrm{A}}(l) = \frac{1}{[M_{\mathrm{A}}\omega^2 - \Phi^{\mathrm{AA}}(l,l)]} \tag{5.15}$$

$$y_l d(l) y_l = d_{\mathrm{B}}(l) = \frac{1}{[M_{\mathrm{B}}\omega^2 - \Phi^{\mathrm{BB}}(l,l)]} \tag{5.16}$$

The four self-consistent equations, Eqs.(5.10)-Eqs.(5.13) may be combined in a convenient $2 \times 2$ matrix form as

$$\begin{pmatrix} D_{\mathrm{AA}} & D_{\mathrm{AB}} \\ D_{\mathrm{BA}} & D_{\mathrm{BB}} \end{pmatrix}_{ll'} = \begin{pmatrix} d_{\mathrm{A}} & 0 \\ 0 & d_{\mathrm{B}} \end{pmatrix}_l \delta_{ll'} +$$

$$\begin{pmatrix} d_{\mathrm{A}} & 0 \\ 0 & d_{\mathrm{B}} \end{pmatrix}_l \sum_{l'' \neq l} \begin{pmatrix} \Phi^{\mathrm{AA}} & \Phi^{\mathrm{AB}} \\ \Phi^{\mathrm{BA}} & \Phi^{\mathrm{BB}} \end{pmatrix}_{ll''} \begin{pmatrix} D_{\mathrm{AA}} & D_{\mathrm{AB}} \\ D_{\mathrm{BA}} & D_{\mathrm{BB}} \end{pmatrix}_{l''l'}$$

And finally, even this matrix equation can be compactified to get

$$\underline{D} = \underline{d} + \underline{d} \times \underline{\Phi} \times \underline{D} \tag{5.17}$$

Here $\underline{D}$ is a $2N_c \times 2N_c$ matrix, whereas matrix size of $\underline{d}$ is $N_c \times N_c$.

Thus, we have obtained an equation which has a structure similar to the one obtained in the BEB formalism for the electronic problem. It is interesting to note that there is no randomness associated with $\Phi$ matrices. All the randomness is absorbed in the $d$ matrices, and the origin of this randomness lies in the mass term. The $\Phi$ matrices will take the values depending on the random values associated with the mass term. Hence, diagonal mass disorder and off-diagonal spring disorder are dependent on each other. The other point to note is that we can consider three different spring constants, which has been a computational limitation for some theoretical approaches [214; 215]. In order to solve these equations, we have adopted the dynamical cluster approximation. The formalism is similar to the one presented in chapter 3, but there are certain steps that are unique to the force-constant disorder case. In the next section, we provide the details of the formalism.

## 5.2.1 Dynamical Cluster Approximation (DCA)

The DCA algorithm that we have implemented is derived using the formalism described in chapter3 and is discussed below:

1. We start with an initial guess of the hybridization function as

$$\underline{\Delta(\mathbf{K}, \omega)} = \begin{pmatrix} \Delta^{\mathrm{AA}}(\mathbf{K}, \omega) & \Delta^{\mathrm{AB}}(\mathbf{K}, \omega) \\ \Delta^{\mathrm{BA}}(\mathbf{K}, \omega) & \Delta^{\mathrm{BB}}(\mathbf{K}, \omega) \end{pmatrix}$$

This guess may be obtained through a coarse graining of the non-disordered Green's function, or from a previously converged calculation.

2. As a first step for solving the cluster problem, we generate random configurations of the disorder potential V. The disorder potentials $V_A$ and $V_B$ are assigned depending on whether the site is occupied by an A- or B- type atom. We generate

some random number and if it is less than a given impurity concentration $c_A$, we assign a given site as A-type, else it is assigned as B-type.

3. We define $\Phi'$ as configuration dependent force-constants which can be obtained by configuration dependent Fourier transform as shown below

$$\Phi'(l,l') = \begin{cases} \sum_{\mathbf{K}} \left(\underline{\omega^2_{\mathbf{K}}}\right)^{\mathrm{AA}} e^{i\mathbf{K}\cdot(\vec{R}_l - \vec{R}_{l'})}, & \text{if } l \in \mathrm{A},\, l' \in \mathrm{A} \\ \sum_{\mathbf{K}} \left(\underline{\omega^2_{\mathbf{K}}}\right)^{\mathrm{AB}} e^{i\mathbf{K}\cdot(\vec{R}_l - \vec{R}_{l'})}, & \text{if } l \in \mathrm{A},\, l' \in \mathrm{B} \,. \\ \sum_{\mathbf{K}} \left(\underline{\omega^2_{\mathbf{K}}}\right)^{\mathrm{BA}} e^{i\mathbf{K}\cdot(\vec{R}_l - \vec{R}_{l'})}, & \text{if } l \in \mathrm{B},\, l' \in \mathrm{A} \,. \\ \sum_{\mathbf{K}} \left(\underline{\omega^2_{\mathbf{K}}}\right)^{\mathrm{BB}} e^{i\mathbf{K}\cdot(\vec{R}_l - \vec{R}_{l'})}, & \text{if } l \in \mathrm{B},\, l' \in \mathrm{B} \,. \end{cases}$$

where the 2×2 dispersion matrix is given by

$$\underline{\omega^2_{\mathbf{K}}} = \begin{pmatrix} \Phi^{\mathrm{AA}} & \Phi^{\mathrm{AB}} \\ \Phi^{\mathrm{BA}} & \Phi^{\mathrm{BB}} \end{pmatrix} \bar{\omega}^2_{\mathbf{K}}$$

and the coarse-grained dispersion is given by

$$\bar{\omega}^2_{\mathbf{K}} = \frac{N_c}{N} \sum_{\tilde{k}} \left[ \sin^2\left(\frac{(K_x + \tilde{k}_x)a}{2}\right) \right. $$
$$\left. + \sin^2\left(\frac{(K_y + \tilde{k}_y)a}{2}\right) + \sin^2\left(\frac{(K_z + \tilde{k}_z)a}{2}\right) \right]$$

The real space hybridization function $\Delta'$ is obtained from the configuration dependent Fourier transform as below:

$$\Delta'(l,l') = \begin{cases} \sum_{\mathbf{K}}[\Delta^{\mathrm{AA}}(\mathbf{K},\omega)] e^{i\mathbf{K}.(R_l - R_{l'})}, & \text{if } l \in \mathrm{A},\, l' \in \mathrm{A} \\ \sum_{\mathbf{K}}[\Delta^{\mathrm{AB}}(\mathbf{K},\omega)] e^{i\mathbf{K}.(R_l - R_{l'})}, & \text{if } l \in \mathrm{A},\, l' \in \mathrm{B} \,. \\ \sum_{\mathbf{K}}[\Delta^{\mathrm{BA}}(\mathbf{K},\omega)] e^{i\mathbf{K}.(R_l - R_{l'})}, & \text{if } l \in \mathrm{B},\, l' \in \mathrm{A} \,. \\ \sum_{\mathbf{K}}[\Delta^{\mathrm{BB}}(\mathbf{K},\omega)] e^{i\mathbf{K}.(R_l - R_{l'})}, & \text{if } l \in \mathrm{B},\, l' \in \mathrm{B} \,. \end{cases}$$

After constructing $\Phi'$, $\Delta'$ and $V$, we compute the corresponding cluster Green function through the mass-weighted Dyson's equation [203] as

$$D^c(l,l',\omega,V) = \sqrt{1 - (\hat{V})_l}\,(\omega^2 I - \underline{\Phi}' - \underline{\Delta}' - \underline{\hat{V}})^{-1}_{ll'} \sqrt{1 - (\hat{V})_{l'}}\,. \qquad (5.18)$$

4. The next step is disorder averaging over disorder configurations denoted by $\langle (...) \rangle$. These disorder averaged Green's functions correspond to a translationally invariant

system, and are denoted by the DCA subscript:

$$\left(D^c_{\text{DCA}}\right)_{\text{AA}} = \left\langle D^c(l, l', \omega) \right\rangle, \qquad\qquad \text{if } l \in \text{A}, \, l \in \text{A}$$

$$\left(D^c_{\text{DCA}}\right)_{\text{AB}} = \left\langle D^c(l, l', \omega) \right\rangle, \qquad\qquad \text{if } l \in \text{A}, \, l \in \text{B}$$

$$\left(D^c_{\text{DCA}}\right)_{\text{BA}} = \left\langle D^c(l, l', \omega) \right\rangle, \qquad\qquad \text{if } l \in \text{B}, \, l \in \text{A}$$

$$\left(D^c_{\text{DCA}}\right)_{\text{BB}} = \left\langle D^c(l, l', \omega) \right\rangle, \qquad\qquad \text{if } l \in \text{B}, \, l \in \text{B}$$

$$(5.19)$$

Next, we construct a matrix of the cluster Green function by re-expanding the Green function to a $2N_c \times 2N_c$ matrix. It can be represented as

$$\underline{D^c_{DCA}} = \begin{pmatrix} \left(D^c_{\text{DCA}}\right)_{\text{AA}} & \left(D^c_{\text{DCA}}\right)_{\text{AB}} \\ \left(D^c_{\text{DCA}}\right)_{\text{BA}} & \left(D^c_{\text{DCA}}\right)_{\text{BB}} \end{pmatrix}$$

5. As mentioned above, after disorder averaging, the translation symmetry is restored and we can perform Fourier transform for each component to get disorder averaged $\mathbf{K}$ dependent cluster Green function as

$$\underline{D^c(\mathbf{K}, \omega)} = \begin{pmatrix} D^c_{\text{AA}}(\mathbf{K}, \omega) & D^c_{\text{AB}}(\mathbf{K}, \omega) \\ D^c_{\text{BA}}(\mathbf{K}, \omega) & D^c_{\text{BB}}(\mathbf{K}, \omega) \end{pmatrix}$$

6. Once the cluster problem is solved, we calculate the coarse-grained lattice Green function as

$$\underline{D^{\text{CG}}(\mathbf{K}, \omega)} = \frac{N_c}{N} \sum_{\tilde{k}} \left[ \underline{D^c(\mathbf{K}, \omega)}^{-1} + \underline{\Delta(\mathbf{K}, \omega)} - \underline{\omega^2_k} + \underline{\bar{\omega}^2(\mathbf{K})} \right] \qquad (5.20)$$

which in explicit matrix form is given by,

$$\underline{D^{\text{CG}}(\mathbf{K}, \omega)} = \begin{pmatrix} D^{\text{CG}}_{\text{AA}}(\mathbf{K}, \omega) & D^{\text{CG}}_{\text{AB}}(\mathbf{K}, \omega) \\ D^{\text{CG}}_{\text{BA}}(\mathbf{K}, \omega) & D^{\text{CG}}_{\text{BB}}(\mathbf{K}, \omega) \end{pmatrix}$$

7. The DCA self consistency condition requires that the disorder averaged cluster Green function equal the coarse-grained lattice Green's function

$$\underline{D^c(\mathbf{K}, \omega)} = \underline{D^{\text{CG}}(\mathbf{K}, \omega)} \qquad\qquad\qquad (5.21)$$

8. The self consistency condition is used for updating the hybridization function for each component

$$\Delta_n^{AA}(\mathbf{K}, \omega) = \Delta_o^{AA}(\mathbf{K}, \omega)$$
$$+ \xi \left[ \left( D_{AA}^c(\mathbf{K}, \omega) \right)^{-1} - \left( D_{AA}^{CG}(\mathbf{K}, \omega) \right)^{-1} \right] \qquad (5.22)$$

$$\Delta_n^{BB}(\mathbf{K}, \omega) = \Delta_o^{BB}(\mathbf{K}, \omega)$$
$$+ \xi \left[ \left( D_{BB}^c(\mathbf{K}, \omega) \right)^{-1} - \left( D_{BB}^{CG}(\mathbf{K}, \omega) \right)^{-1} \right] \qquad (5.23)$$

$$\Delta_n^{AB}(\mathbf{K}, \omega) = \Delta_o^{AB}(\mathbf{K}, \omega)$$
$$+ \xi \left[ \left( D_{AB}^c(\mathbf{K}, \omega) \right)^{-1} - \left( D_{AB}^{CG}(\mathbf{K}, \omega) \right)^{-1} \right] \qquad (5.24)$$

$$\Delta_n^{BA}(\mathbf{K}, \omega) = \Delta_o^{BA}(\mathbf{K}, \omega)$$
$$+ \xi \left[ \left( D_{BA}^c(\mathbf{K}, \omega) \right)^{-1} - \left( D_{BA}^{CG}(\mathbf{K}, \omega) \right)^{-1} \right] \qquad (5.25)$$

In the above equations, the $\xi$ is a mixing parameter that determines the fraction of the updated hybridization that should be mixed with the existing one, thus ensuring smooth convergence of the DCA iterations.

As is well known, the Anderson localization of phonons requires us to go beyond DCA. The arithmetic averaging procedure needs to be modified, and a typical averaging ansatz needs to be evolved. Such an ansatz has been worked out in the electronic case, and has been benchmarked against known results [172]. We have adopted the same ansatz in the phonon case, and have found that it yields the same level of benchmarks as the electronic case. The formalism that employs this typical averaging ansatz is called the typical medium DCA or the TMDCA, and is detailed in the next section.

## 5.2.2 Typical Medium Dynamical Cluster Approximation (TMDCA)

As mentioned in chapter 3, the effective medium is constructed via algebraic averaging in the DCA, while the TMDCA utilizes geometric averaging to construct the effective medium. We employ the same ansatz for evaluating the typical density of states as

in the electronic case [172], as:

$$
\underline{\rho_{typ}^c}(\mathbf{K}, \omega) = \exp\left(\frac{1}{N_c}\sum_{i=1}^{N_c}\langle\ln\rho_{\mathrm{ii}}(\omega)\rangle\right)\times
$$

$$
\begin{pmatrix} \left\langle \dfrac{-\frac{1}{\pi}\mathrm{ImD}_{\mathrm{AA}}^{\mathrm{c}}(\mathbf{K},\omega)}{\frac{1}{N_c}\sum_{i=1}^{N_c}\left(-\frac{1}{\pi}\mathrm{ImD}_{\mathrm{ii}}^{\mathrm{c}}(\omega)\right)} \right\rangle & \left\langle \dfrac{-\frac{1}{\pi}\mathrm{ImD}_{\mathrm{AB}}^{\mathrm{c}}(\mathbf{K},\omega)}{\frac{1}{N_c}\sum_{i=1}^{N_c}\left(-\frac{1}{\pi}\mathrm{ImD}_{\mathrm{ii}}^{\mathrm{c}}(\omega)\right)} \right\rangle \\[4mm] \left\langle \dfrac{-\frac{1}{\pi}\mathrm{ImD}_{\mathrm{BA}}^{\mathrm{c}}(\mathbf{K},\omega)}{\frac{1}{N_c}\sum_{i=1}^{N_c}\left(-\frac{1}{\pi}\mathrm{ImD}_{\mathrm{ii}}^{\mathrm{c}}(\omega)\right)} \right\rangle & \left\langle \dfrac{-\frac{1}{\pi}\mathrm{ImD}_{\mathrm{BB}}^{\mathrm{c}}(\mathbf{K},\omega)}{\frac{1}{N_c}\sum_{i=1}^{N_c}\left(-\frac{1}{\pi}\mathrm{ImD}_{\mathrm{ii}}^{\mathrm{c}}(\omega)\right)} \right\rangle \end{pmatrix}, \quad (5.26)
$$

where $D_{ii}^c$ is defined as

$$
D_{ii}^c(\omega) = \sum_{\mathbf{K}}\left(D_{\mathrm{AA}}^c(\mathbf{K},\omega) + D_{\mathrm{BB}}^c(\mathbf{K},\omega) + \mathbf{D}_{\mathrm{AB}}^{\mathbf{c}}(\mathbf{K},\omega) + \mathbf{D}_{\mathrm{BA}}^{\mathbf{c}}(\mathbf{K},\omega)\right), \quad (5.27)
$$

and the local spectral function is given by

$$
\rho_{ii}(\omega) = -\frac{1}{\pi}\left[D_{ii}^c(\omega)\right]. \quad (5.28)
$$

Next, we calculate the cluster-averaged typical Green function which is also a $2\times 2$ matrix

$$
\underline{D_{\mathrm{typ}}^c} = \begin{pmatrix} \left(D_{\mathrm{typ}}^c\right)_{\mathrm{AA}} & \left(D_{\mathrm{typ}}^c\right)_{\mathrm{AB}} \\[3mm] \left(D_{\mathrm{typ}}^c\right)_{\mathrm{BA}} & \left(D_{\mathrm{typ}}^c\right)_{\mathrm{BB}} \end{pmatrix} \quad (5.29)
$$

We compute each component of the cluster-averaged typical Green's function from the corresponding component of the typical density of states (5.26) using the Hilbert transform,

$$
\left(D_{\mathrm{typ}}^c\right)_{\mathrm{AA}} = \mathcal{P}\int d\omega' \frac{\rho_{typ}^{\mathrm{AA}}(\mathbf{K},\omega')}{\omega^2 - \omega'^2} - i\frac{\pi}{2\omega}\rho_{typ}^{\mathrm{AA}}
$$

$$
\left(D_{\mathrm{typ}}^c\right)_{\mathrm{AB}} = \mathcal{P}\int d\omega' \frac{\rho_{typ}^{\mathrm{AB}}(\mathbf{K},\omega')}{\omega^2 - \omega'^2} - i\frac{\pi}{2\omega}\rho_{typ}^{\mathrm{AB}}
$$

$$
\left(D_{\mathrm{typ}}^c\right)_{\mathrm{BA}} = \mathcal{P}\int d\omega' \frac{\rho_{typ}^{\mathrm{BA}}(\mathbf{K},\omega')}{\omega^2 - \omega'^2} - i\frac{\pi}{2\omega}\rho_{typ}^{\mathrm{BA}}
$$

$$
\left(D_{\mathrm{typ}}^c\right)_{\mathrm{BB}} = \mathcal{P}\int d\omega' \frac{\rho_{typ}^{\mathrm{BB}}(\mathbf{K},\omega')}{\omega^2 - \omega'^2} - i\frac{\pi}{2\omega}\rho_{typ}^{\mathrm{BB}} \quad (5.30)
$$

Once the disorder-averaged cluster Green function is calculated using (5.30), the self-consistency follows the same steps as in the DCA presented in previous section. The coarse-grained lattice Green's function is then calculated using (5.20), which is utilized to update the hybridization function in (5.25).

Using DCA and TMDCA, we can calculate the arithmetically averaged density of states (ADOS) and typical density of states (TDOS) respectively as follows:

$$\text{ADOS}(\omega^2) = -\frac{2\omega}{N_c\pi}\text{Im}\sum_{\mathbf{K},\sigma_l\sigma_{l'}}\left(D^c_{\text{DCA}}(\mathbf{K},\omega)\right)_{\sigma_l\sigma_{l'}} \tag{5.31}$$

$$\text{TDOS}(\omega^2) = -\frac{2\omega}{N_c\pi}\text{Im}\sum_{\mathbf{K},\sigma_l\sigma_{l'}}\left(D^c_{\text{typ}}(\mathbf{K},\omega)\right)_{\sigma_l\sigma_{l'}}, \tag{5.32}$$

where $\sigma_l\sigma_{l'} = A/B$. The formalism described above has been implemented, and we present results and a discussion in the following section.

## 5.3  Results and discussions

We begin our discussion with a validation of the method. To that end we compute the ADOS via exact diagonalization (ED) of a large number of phonon models of large sized disordered supercells. Within the supercells the impurities are randomly distributed and beyond the supercell boundaries the impurity distributions periodically repeat. Specifically for each set of model parameters we derive the force constant matrices of 100 supercells each with 60 impurities and roughly 400 sites on average. The dynamical matrix of each supercell is then evaluated and diagonalized on a $10 \times 10 \times 10$ supercell momentum space grid. We note that not only the impurity distributions but also the shapes of the supercells are randomized under the following constraints. The supercell volumes vary within 375 and 430 sites and the angles between the vectors that span the supercells vary between 75 and 105 degrees.

The left panels of figure 5.1 show DCA results (red solid lines) and ED results (black solid lines) for a binary alloy ($c = 0.15; V = 0.67$) with three different spring constant combinations. A good agreement is seen over all scales thus validating the formalism. We also note that the DCA can access detailed information of the ADOS with relatively small cluster sizes, i.e $N_c = 64$ which shows that the DCA is dramatically less expensive compared to ED while being numerically exact. To check the sensitivity of the DCA results on the choice of cluster size $N_c$, we present the ADOS for different $N_c$ in the right panel of Fig.5.1. We find that the ADOS for

$N_c = 64$ and $N_c = 125$ are almost identical which implies a rapid convergence of our calculations with respect to increasing $N_c$. In contrast to the results for $N_c = 64$ and $N_c = 125$, the single-site ($N_c = 1$) calculations (solid blue lines) are unable to capture non-local fluctuations and disagree significantly with the converged spectra.

The result presented above, namely a comparison of DCA with ED, lends strong
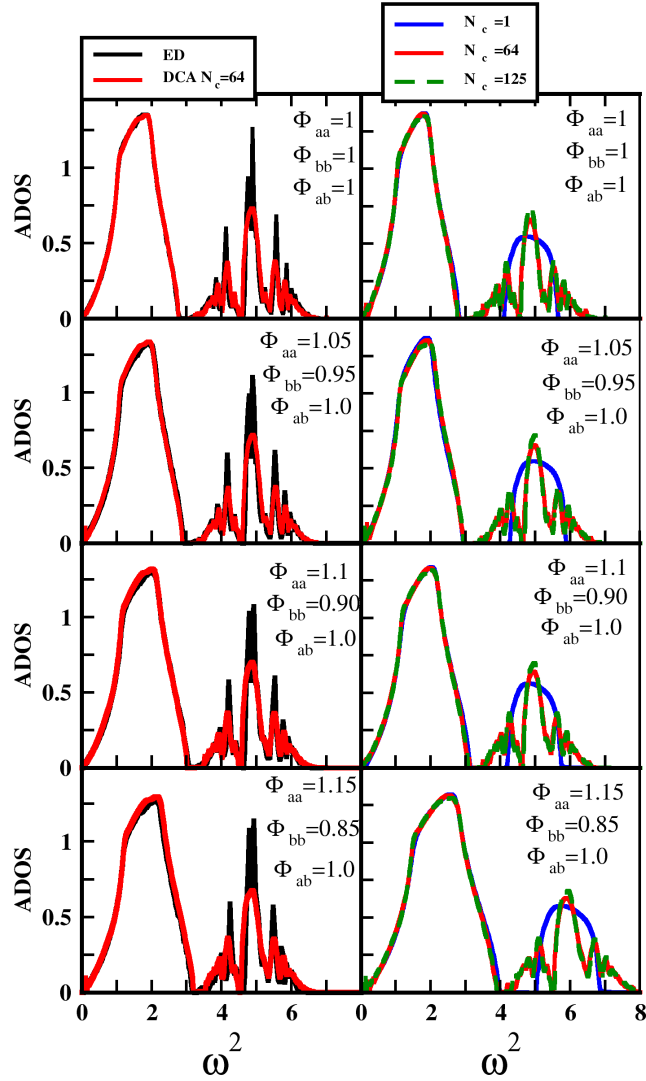


Figure 5.1: Validation and the convergence of the results using DCA. Left panel:The comparison of the arithmetic density of states (ADOS) obtained from the DCA using $N_c$=64 and ED for various values of $\Phi_{aa}$, $\Phi_{bb}$ and impurity concentration $c$ keeping fixed values of $\Phi_{ab} = \frac{\Phi_{aa}+\Phi_{bb}}{2}$ and disorder potential $V = 0.67$ for the three-dimensional binary alloy model. We find a good agreement between the DCA and ED results. Right panel: The evolution of the ADOS for $N_c = 1, 64, 125$ for the same parameter values. Results are converged for $N_c = 64$.

credence to results from DCA. Hence, we employ DCA, and subsequently TMDCA to investigate the interplay of spring and mass disorder on phonon spectra and on AL of phonons. We begin with an investigation of the effect of pure force-constant disorder on phonon spectra.

The upper panel in figure 5.2 shows the average DOS for pure spring disorder (i.e. $V \to 0$) with spring constant values $\Phi_{AA} = 1.0, \Phi_{BB} = 0.1$ and $\Phi_{AB} = 0.3$ for various impurity concentrations ($c_B$) ranging from 0.95 to 0.05. The parameters have been chosen to mimic the values obtained in a recent experiment [216] on crystals of binary hard-soft microgel particles with three distinct interparticle potentials. The spring constant values imply that A are hard particles, while B are soft. Hence, $c_B = 0.95$ corresponds to B-particle concentration of 95% which implies hard sphere concentration of 5%. As expected, the spectrum for a higher concentration of hard particles (stiffer springs, $c_B = 0.05, c_A = 0.95, \Phi_{AA}/\Phi_{BB} = 10$) has almost entire spectral weight at higher frequencies, and as $c_B$ varies from 0.05 to 0.95, spectral weight is transferred to lower frequencies. The DOS at 20% to 40% soft particles ($c_B = 0.2 - 0.4$) shows a clear excess density of states around a frequency, that occurs far below the van Hove singularities of the pure hard particle system. Such behavior is strongly reminiscent of disordered systems, where the origin of such an excess of DOS, termed a Boson peak, has generated a lot of debate. It has been shown theoretically [124], that a strongly disordered three-dimensional system of coupled harmonic oscillators with a *continuous* force constant distribution exhibits an excess low-frequency DOS (boson peak) as a generic feature. Specifically, if the system is proximal to the borderline of stability, a low-frequency peak (i.e the Boson peak) appears in the quantity $g(\omega)/\omega^2$ as a precursor of the instability. Our results have been obtained for a binary alloy with three values of force-constants, and we see that a Boson peak appears in a regime of lower soft particle concentration. Experimental measurements [217] of normal modes and the DOS in a disordered colloidal crystal showed Debye-like behavior at low energies and an excess of modes, or Boson peak, at higher energies. The normal modes took the form of plane waves, that hybridized with localized short wavelength features in the Debye regime but lost both

87

longitudinal and transverse plane-wave character at a common energy near the Boson peak. More recently, experiments[216] on deformable microgel colloidal particles with random stiffness appear to contradict the theoretical results of Ref[124]. The authors create crystals of binary hard-soft microgel particles with three distinct inter-particle potentials distributed randomly on a two-dimensional triangular lattice. The nearest-neighbor bonds are either very stiff ($\Phi_{AA}$), very soft ($\Phi_{BB}$), or of intermediate stiffness ($\Phi_{AB}$). Subsequently, they obtain, experimentally, the phonon modes in crystals with bond strength disorder as a function of increasing dopant concentration. The interesting feature of the microgel crystal is that although the bonds are randomly distributed, the masses are nearly identical, hence the disorder is purely off-diagonal. The results show the absence of a boson peak, although an excess in the density of states as compared to conventional Debye behaviour was observed. In the
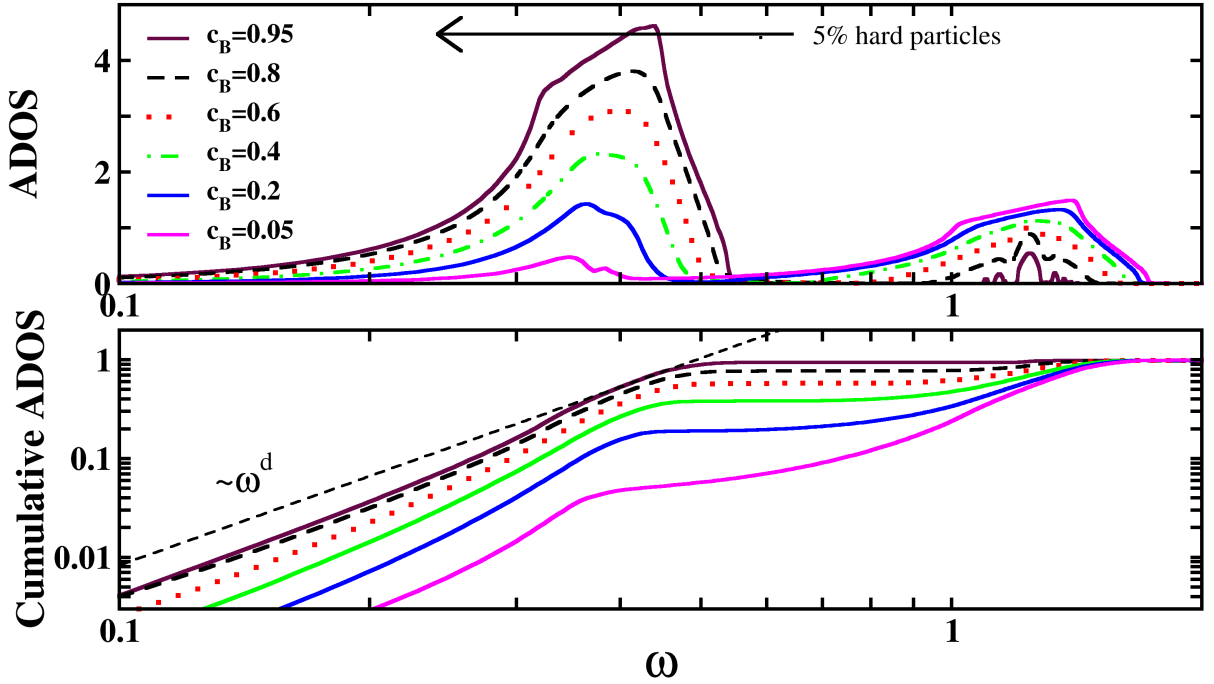


Figure 5.2: Boson peak appearance at intermediate concentrations – For pure spring disorder with $V = 0.01, \Phi_{AA} = 1.0, \Phi_{BB} = 0.1, \Phi_{AB} = 0.3$, the disorder averaged phonon spectra (top panel) and the corresponding cumulative spectra (bottom panel) are shown for a range of soft particle concentrations ($c_B = 0.05 - 0.95$). A feature, reminiscent of the Boson peak, appears for $c_B \sim 0.2 - 0.4$.

lower panel of figure 5.2, we present integrated DOS as a function of frequency. The results indicate conventional Debye behaviour ($\sim \omega^d$) at lowest frequencies followed by a deviation, and finally a convergence to the normalization value of one at the highest frequencies. In the experiment, the hard particle concentration has been varied from 0 to about 21%. A comparison to figure 3 of Yodh *et. al*[216] shows that our results concur well with the experiments. An absence of Boson peak, as concluded in the experiments, is natural since a clear Boson peak occurs only in the opposite limit of lower soft particle concentration. To summarize, within the framework of DCA, we find (see figure 5.2), for a binary alloy, that a transfer of spectral weight to lower frequencies results in the Boson peak, which emerges as a crossover feature between a pure host system and a pure guest system.

A question that has been much debated in the literature is about the nature of states within the boson peak - Are they localized or delocalized? This question can be effectively answered through the evaluation of the typical DOS, since the typical spectral weight is a measure of the proximity to Anderson localization. A subtle issue about the interpretation of the typical density of states must be mentioned here. A non-zero typical DOS signifies the presence of extended states. According to Mott, a degeneracy of localized and extended states should lead to their hybridization, and hence an eventual delocalization of the localized states. The average DOS and the typical DOS, being different at a given energy, is thus immaterial regarding the identification of the states being extended or localized. If the typical DOS is non-zero, the states at that energy should be interpreted as being extended. Concomitantly, a large difference between the average and typical DOS does indicate a proximity to the Anderson localization transition (ALT).

In figure 5.3, we show, for the same parameters as figure 5.2, a series of average (black solid lines) and the corresponding typical spectra (red dashed lines).

The boson peak is seen to have numerically negligible typical spectral weight (TSW) until $c_B \sim 0.4$, beyond which the low frequency peak acquires finite and significant TSW. Thus, the states in the BP exhibit a kind of crossover from being almost localized (proximal to ALT) to being delocalized (relatively smaller difference

between average and typical DOS) with increasing $c_B$. The overall typical spectral weight, shown in the bottom left panel, is non-monotonic, and shows a minimum at $c_B \sim 0.5$, showing that the overall system is closest to the ALT when the ratio of the concentrations of the two species is roughly equal to one.

In order to understand the interplay of mass and spring disorder, we consider two protocols. In the first, we keep the mass ratio parameter, $V = 0.67$ and the impurity concentration $c = 0.5$ as constants, and increase the spring disorder systematically by varying $\Phi_{AA}/\Phi_{BB}$ (with $\Phi_{BB} = 1$, and $\Phi_{AB} = (\Phi_{AA} + \Phi_{BB})/2$) from 0.2 to 2.0, representing a change of host spring constants from very soft to very stiff. The resulting spectra (ADOS as solid black lines and TDOS as dashed red lines) are shown in figure 5.4, while the inset shows the integrated typical spectral weight (TSW, solid blue circles) as a function of $\Phi_{AA}$. For soft A-springs, the characteristic frequencies of the system must be lower than a pure B-type system, and as the $\phi_{AA}$ is increased,
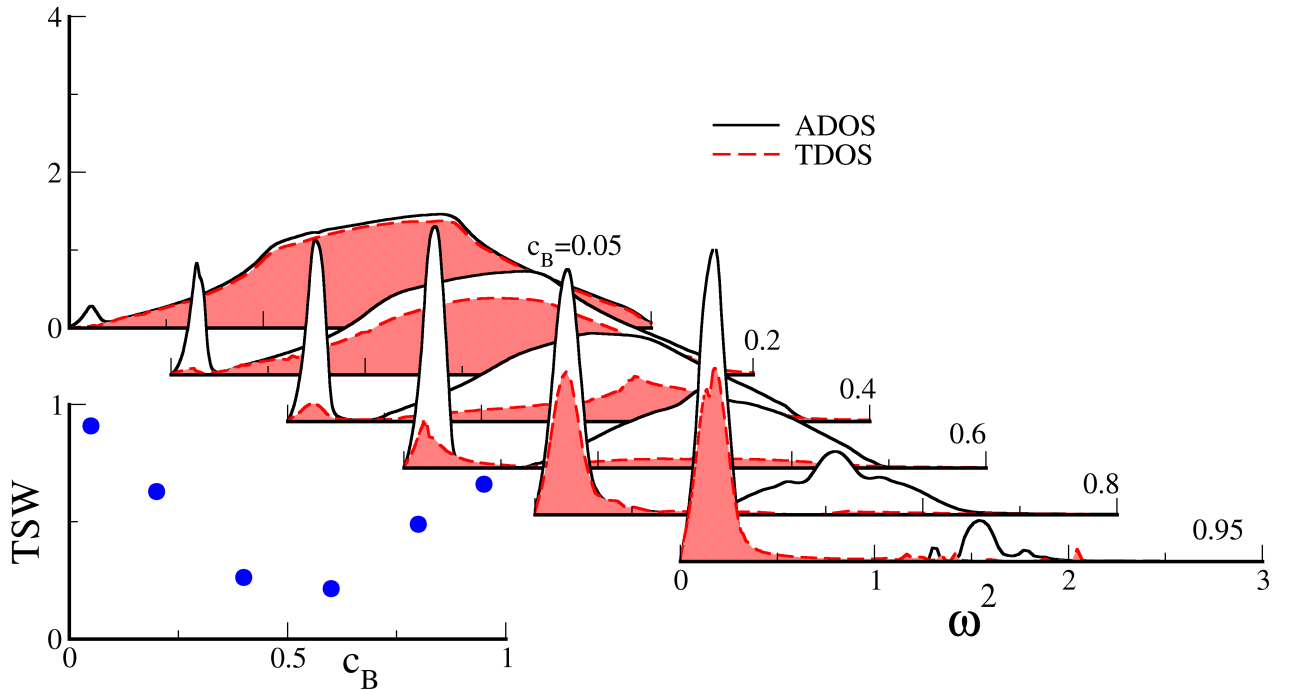


Figure 5.3: Boson peak – localized or delocalized? - For the same parameters as figure 5.2, the ADOS (solid black line) and TDOS (dashed red line) are shown for concentrations $c_B$ from 0.05 to 0.95. The bottom left panel shows the integrated spectral weight of the typical density of states $vs$ $c_B$ as solid blue circles.

spectral weight in the second, high frequency peak increases, as also the bandwidth of the system. So, nominally, it appears that the system is getting delocalized, as the host springs are made stiffer for a fixed mass disorder. However, the inset shows a decrease in TSW with increasing stiffness of $\Phi_{AA}$, which implies that the order parameter for AL is decreasing, and hence the system is moving closer to localization. If we focus on a fixed frequency, say $\omega^2 = 5.0$, then we see that for $\Phi_{AA} = 0.2$, the ADOS and TDOS are zero, while for $\Phi_{AA} = 2.0$, both the average and typical DOS are non-zero, suggesting the interpretation that spring disorder is of a delocalizing nature and counters the localization produced by mass disorder alone. However, the order parameter for AL, namely the TSW, decreases sharply. Thus the interplay of mass and spring disorder is quite subtle, and an interpretation of the results need to be done carefully. It must be emphasized here, that the subtlety of this interplay has been uncovered through the application of TMDCA, which is able to produce, simultaneously, the typical and the average DOS.

The second protocol is to vary the mass ratio parameter, $V = 1 - M_{imp}/M_{host}$,
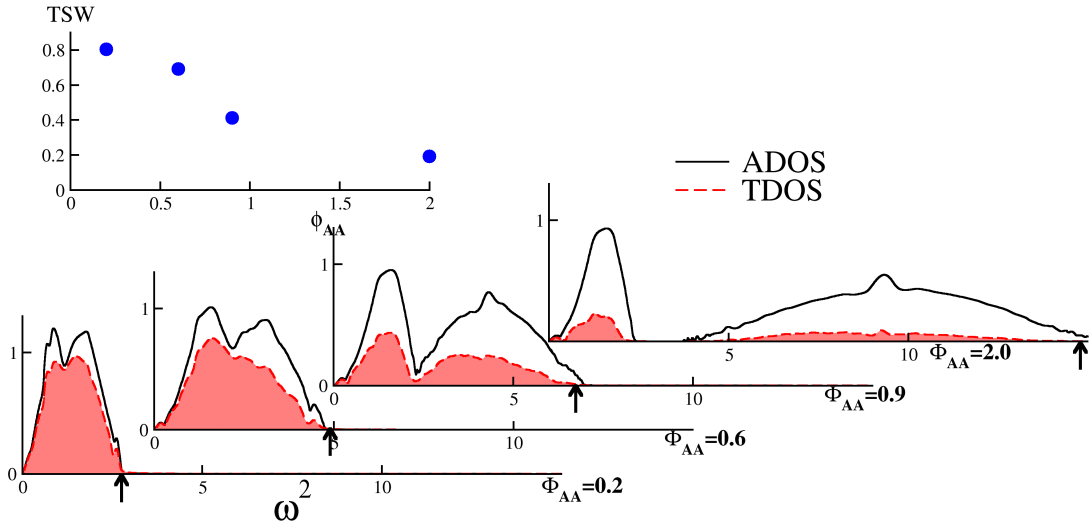


Figure 5.4: The Average DOS(solid black line) and Typical DOS(dashed red line) for different values of $\Phi_{AA}$ is shown. The arrows mark the upper mobility edge. The evolution of the mobility edge and typical spectral weight with increasing values of $\Phi_{AA}$ is noticeable: The parameters, $\Phi_{BB} = 1.0$, $V = 0.67$ and $c = 0.5$ are fixed, while $\Phi_{AB} = 0.5(\Phi_{AA} + \Phi_{BB})$ changes correspondingly. The inset shows the decrease of the integrated typical spectral weight (blue solid circles) with increasing $\Phi_{AA}$.

keeping the relative concentrations as well the spring constants fixed. The ADOS and TDOS are shown in figure 5.5 for $V = 0.01$ to 0.9, implying a systematic decrease in the B-site ionic mass. Again, lighter impurities imply transfer of spectral weight to higher frequencies, and the B-site band appears as a separate feature, which blue shifts significantly with increasing $V$. In parallel with the results of the first protocol, this result lends itself to an interpretation of delocalization of modes at higher frequencies, but the vanishing of the typical density of states shows that the high frequency modes for $V \to 1$ are almost localized. The inset shows that the TSW (solid blue circles) decreases sharply with increasing $V$, and this also implies that increasing mass disorder in the presence of fixed spring disorder pushes the system closer to the AL transition.

The insight we gain from the study of the interplay of mass and spring disorder is that an inference of localization/delocalization of specific modes cannot be made on
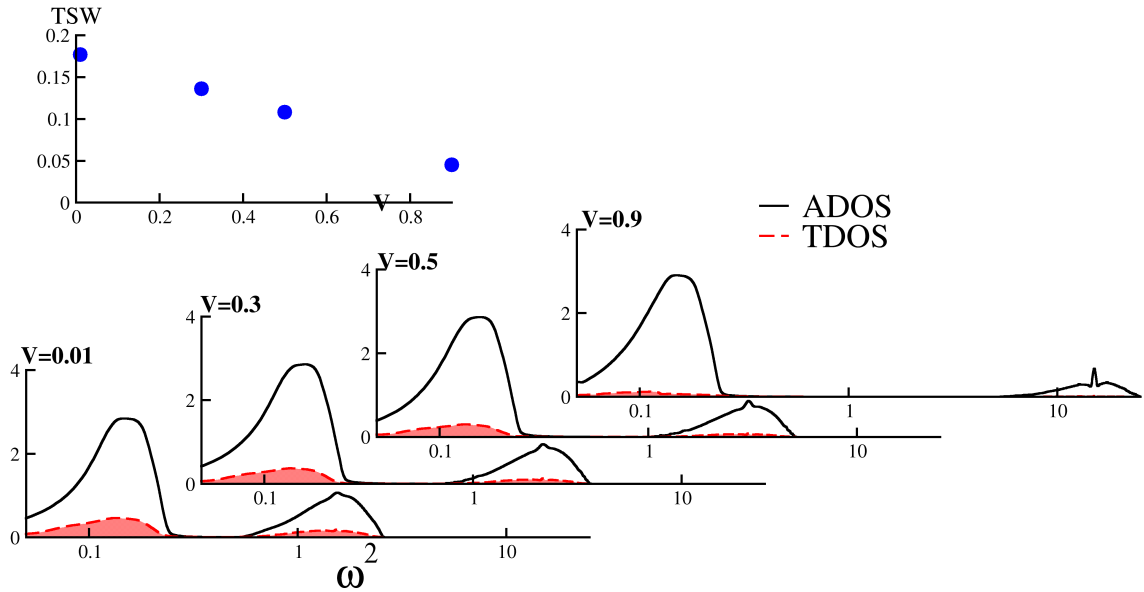


Figure 5.5: The Average DOS(solid black line) and Typical DOS(dashed red line) for increasing values of $V$ is displayed. The influence of $V$ on the mobility edges and the typical spectral weight is demonstrated: The parameters, $\Phi_{AA} = 1, \Phi_{BB} = 0.1, \Phi_{AB} = 0.3$ and $c = 0.5$ are fixed, and the mass ratio of B to A type sites is varied from $\sim 1$ to 0.1, which corresponds to changing $V$ from 0.01 to 0.9. The inset shows the decrease of the integrated typical spectral weight (blue solid circles) with increasing $V$.

the basis of ADOS alone, and the TDOS must be concomitantly examined.

Vacancies, even at low concentrations, can lead to strong localization of phonons. Within the present theoretical framework, we model vacancies as weakly bonded sites with vanishing mass. So, we choose $M_{imp} = M_{host}/20$, which is equivalent to $V = 0.95$, and spring constants as $\phi_{AA} = 1, \phi_{BB} = 0.15, \phi_{AB} = 0.15$. For these parameters, in figure 5.6, we show the average DOS (upper panel) and typical DOS
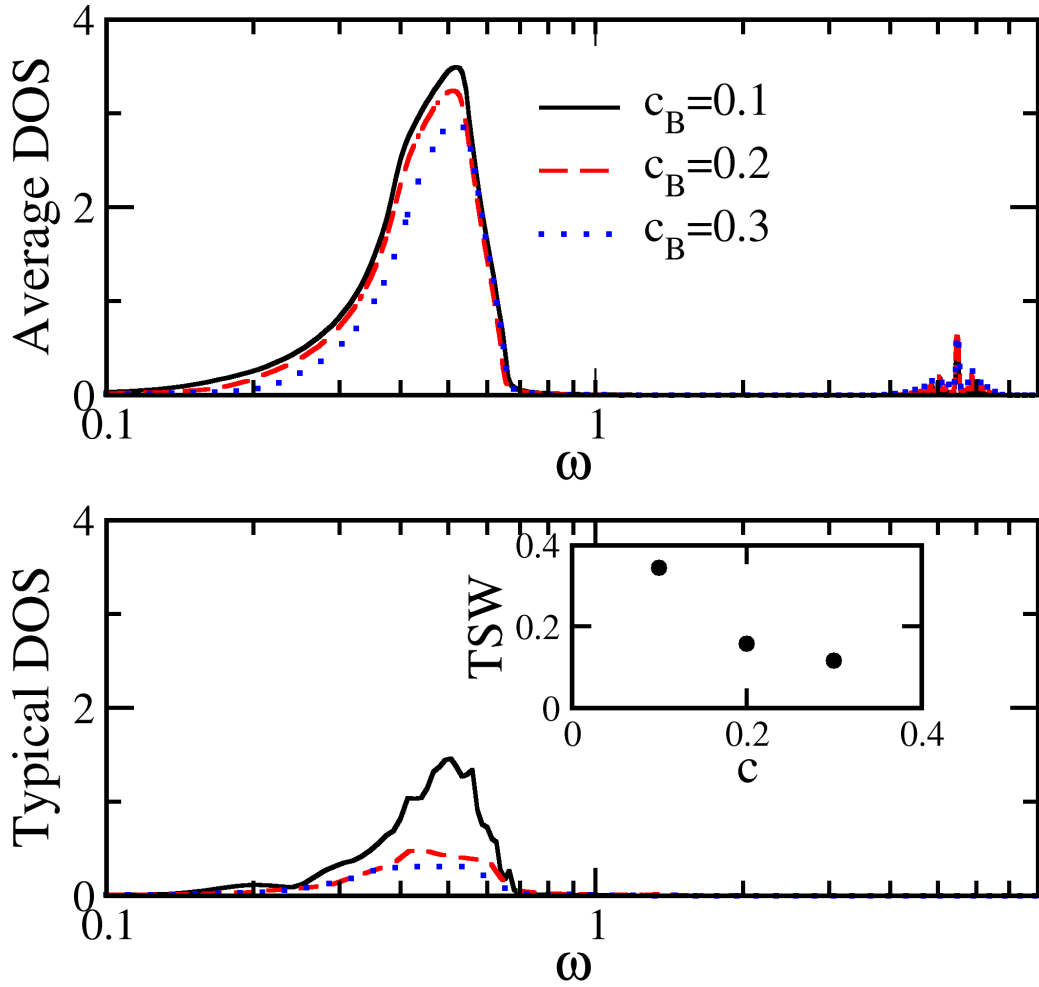


Figure 5.6: Modeling Vacancies: The spring constants, $\phi_{AA} = 1, \phi_{BB} = 0.15, \phi_{AB} = 0.15$ and the mass ratio, $V = 0.95$ are fixed, and three different guest concentrations are considered, namely $c = 0.1$(solid black), $c = 0.2$(dashed red), and $c = 0.3$(dotted blue). The upper panel shows the average DOS, while the lower panel shows the typical DOS. The inset in the lower panel shows the rapid decrease of the integrated typical spectral weight (blue solid circles) with increasing concentration, $c$.

(lower panel) for three different guest concentrations, namely $c = 0.1$(solid black), $c = 0.2$(dashed red), and $c = 0.3$(dotted blue). The upper panel shows that the average DOS hardly changes with increasing concentration, while the corresponding typical DOS (lower panel) undergoes significant changes. The inset in the lower panel shows the rapid decrease of the integrated typical spectral weight (blue solid circles) with increasing concentration, $c$. Modeling real vacancies is quite challenging, but the present analysis with a very crude model for vacancies is already indicative of their strong localization effects. The figure of merit for thermoelectrics is inversely proportional to the thermal conductivity, and directly proportional to electrical conductivity. So, in order to maximize the figure of merit, the vacancy concentration, $c$ should be tuned to an optimal value such that it is less than, but not too close to the percolation limit, implying that the electrical conductivity is not too significantly affected, but the thermal conductivity due to phonons gets drastically reduced due to the strong localization of acoustic phonons in a large part of the spectrum.

Finally, we attempt a qualitative comparison with experiments. It has been argued for a $Ni_xPt_{1-x}$ alloy, that $x = 0.65$ constitutes weak force-constant disorder, while $x = 0.5$ constitutes strong mass and force-constant disorder. Ghosh *et. al.*[164] demonstrate that for $x = 0.5$, a CPA-level consideration of inter-atomic force-constants leads to a split-band spectrum. The authors show that a proper treatment of force-constant disorder using itinerant CPA leads to a closure of the gap. Our calculations are in full qualitative agreement with these conclusions as argued below. Figure 5.7 shows ADOS for a binary alloy with $M_{imp}=M_{host}/3$ as appropriate for Ni impurities in Pt host. The left panel is for $N_c = 1$, equivalent to a CPA calculation, while the right panel is for $N_c = 64$, which is equivalent to the thermodynamic limit. The impurity concentration used is $c = 0.5$, which implies strong mass disorder; and the spectra corresponding to three distinct force-constant combinations are shown. The black solid line corresponds to pure mass-disorder, which at the CPA-level shows a split-band (left panel), while at the DCA-level (right panel), the spectrum has a two peak structure with a soft-gap between the peaks. The red and green lines correspond to weak and strong force-constant disorder respectively. Again, the CPA results are
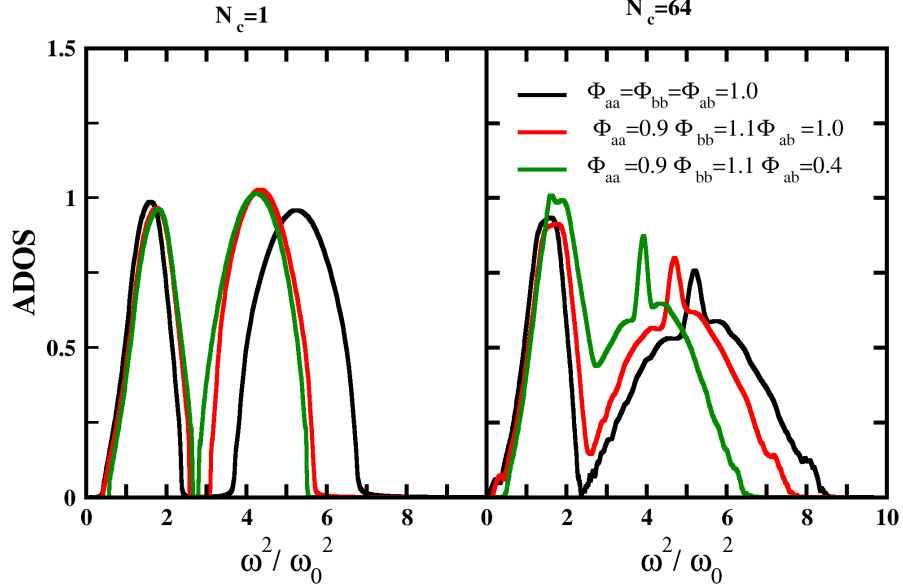
Figure 5.7: Validation against experiments on NiPt alloy and ICPA. Left panel: ADOS obtained from the DCA method for a three-dimensional binary alloy model at various values of force constants $\Phi_{aa}$, $\Phi_{bb}$ and $\Phi_{ab}$ for fixed impurity concentration $c = 0.5$, disorder potential $V = 0.67$. Right panel: The corresponding results are shown using same parameter values for $N_c = 64$. In the presence of strong spring disorder, the gap in the ADOS obtained from $N_c = 64$ reduces which is consistent with neutron scattering data as well as previous ICPA results.

hardly affected by an increase in disorder, while the DCA results for $N_c = 64$ show that increasing force-constant disorder leads to significant spectral weight transfer, especially a filling-up of the soft-gap. Since the force constant combination represented by the green line most closely corresponds to the $Ni_{0.5}Pt_{0.5}$ alloy, we conclude that our results agree qualitatively with the ICPA results as well as experimental neutron scattering data for $Ni_{0.5}Pt_{0.5}$ [218].

## 5.4 Conclusions

The incorporation of the BEB formalism for off-diagonal disorder into the TMDCA yields a reliable, and computationally feasible approach for investigating binary mass and force-constant-disordered alloys. Such a conclusion is supported by the bench-

marking studies discussed in the initial part of the results section. For a fixed mass ratio, and fixed force-constants ($\Phi_{AA}, \Phi_{BB}$ and $\Phi_{AB}$) increasing the soft particle concentration leads to an excess density of states below the first van Hove singularity of the host hard particle system. In the present context, it may be identified as the Boson peak, commonly observed in structurally disordered glasses as well as disordered lattice systems, albeit with different origins. We conclude that the origin of the Boson peak in the disordered binary alloy system is a transfer of spectral weight from the guest to the host system, with a necessary condition being the presence of off-diagonal disorder. We emphasize that with pure mass disorder, even though spectral weight transfer does occur, such a BP does not emerge. Additionally, we find that at very low soft particle concentrations, the states in the BP are completely localized, but some of the states crossover to being extended as their concentration is increased. The BP eventually ceases to be an anomaly, as the soft particle system becomes the host, and the hard particles assume the role of impurities. The interplay of mass and spring disorder is found to be quite subtle. The overall typical spectral weight decreases upon increasing either of the types of disorder, which indicates that there is a co-operative interplay. However, an added clause is that the interpretation of a co-operative or competitive interplay is also frequency selective, since different parts of the spectrum can transform from being localized to delocalized or vice-versa, depending on the protocol. With a crude modeling of vacancies, we suggest that tuning the concentration of vacancies to an optimal level, which is below but not close to the percolation limit, should be an optimal route to maximizing the figure of merit of thermoelectric materials. All the above results finally culminate in an attempt to understand experiments on $Ni_x Pt_{1-x}$ alloys, where, in agreement with ICPA results, we show that $x = 0.65$ constitutes weak force-constant disorder, while $x = 0.5$ represents a system with strong mass and force-constant disorder. Of course, such a conclusion is qualitative at best, because the real system has a non-trivial structure with multiple branches and spring-constant disorder, while the present implementation is restricted to a scalar approximation and force-constant disorder.

# Chapter 6

# A dynamical cluster approximation for studying vibrational excitations in mass-disordered systems with multiple branches

The model we have studied so far involves single branch phonons, which neglects the off-diagonal components of the force-constant tensor. In this chapter, we go beyond such a scalar approximation and incorporate the vectorial nature of phonons within the DCA formalism. We have organized this chapter as follows. In section 6.1, we briefly discuss the current literature involving vector phonons. In section 6.2, we have described the DCA formalism developed for multi-branch lattice vibrations. In section 6.3, we present and discuss the validation of our method, and the results. In section 6.4, we conclude the chapter with a brief discussion of future directions and possible improvements.

## 6.1   Introduction

As discussed in chapter 1, there have been many reports of the direct observation of Anderson localization of phonons in many technologically important materials. For example, Manley et al.[219] have found ferroelectric phonon localization in relaxor ferroelectric PMN-30%PT using neutron scattering. Howie et al.[182] have observed phonon localization in dense hydrogen-deuterium binary alloys. Faez et al.[220]

have experimentally revealed the criticality at the Anderson localization transition for phonons. Phonon localization has been observed in a random three-dimensional elastic network[115]. All these experimental observations have motivated theorists to investigate phonon localization in a realistic model involving complex degrees of freedom.

The development of efficient methods for studying phonon localization in real materials has been a daunting challenge. The two core aspects of such methods are (1) constructing material-specific many-body models and (2) solving them for predicting Anderson localization. The absence of lattice translational symmetry in disordered solids and the corresponding breakdown of the Bloch theorem is one of the biggest obstacles in step(1). In addition, the vector character of lattice vibrational waves is an essential ingredient for a realistic model. Step(2) poses more challenges. Approximate mean-field based calculations can not yield localization because the latter manifests in two-particle transport quantities. Therefore, we can expect that a finite size scaling study of two particle properties can provide important insights into Anderson localization. However, such calculations are numerically expensive especially for a given realistic model including multiple branches of lattice vibrations. A successful theory must be able to fulfill the above mentioned two requirements, and naturally, must be computationally feasible and inexpensive.

Many methods have been explored to investigate phonon localization. These include continuum field theory[116], diagrammatic techniques[117], exact diagonalization [167; 169], multifractal analysis[126] and transfer matrix method[221]. These methods have used a simple and extensively employed model of lattice vibrations to investigate Anderson localization of phonons in three dimensions by neglecting the vector character of vibrations. An itinerant coherent-potential approximation (ICPA)[164] was developed and applied to random binary alloys with mass and force-constant disorder taking into account the vector nature of vibrations. But this method in its present form is not able to explore the physics of phonon localization.

Recently, the importance of direction of propagation in Anderson localization has been appreciated. It has been shown that the vector nature of light may suppress

Anderson localization of light in a point-scatterer model [222]. Anderson transition for elastic waves in three dimensions has been demonstrated in the resonant and non-resonant scattering models of elastic-wave scattering including three-dimensional wave propagation [223]. Disorder is introduced in the force-constants which couples three directions of the atomic vibrations, whereas the resonant model considers point-like resonant scatterers placed in a homogeneous and isotropic elastic medium. Though the resonant model is applicable to artificially constructed elastic networks[115] in which phonon localization has been directly observed, it is not ideally pertinent to the realistic mass-disordered alloys which do show phonon localization with practical disorder strength[182]. In addition, the non-resonant model falls short of introducing mass disorder in the medium. The universality class and criticality of the Anderson transition for elastic waves have been explored in this thorough study[223]. The reported values of the critical exponent $\nu$ are $1.564 \pm 0.009$ and $1.554 \pm 0.085$ for the two models which are in good agreement with the $\nu \approx 1.57$ in 3D orthogonal university class. Therefore, the Anderson transition of elastic waves can be classified to be in the same orthogonal universality class as the electrons without vector character.

Despite the in-depth understanding achieved over the past several decades on the nature of Anderson transition for classical waves including their vector character as discussed above, an understanding of phonon localization in lattice vibrational systems with multiple branches is still wanting.

In this chapter, we study a well-known lattice vibrational model in three dimensions with a monoatomic basis, thus including three branches in the presence of mass disorder. The DCA, established in chapter 3, for investigating phonons in mass-disordered systems was limited to a single branch. In this work, we have extended the DCA formalism by incorporating multiple non-degenerate branches. The multi-branch DCA that we develop in this chapter is a general formalism valid for any disorder distribution. Although a binary disorder is more realistic, considering binary alloy systems, in this work, we have considered uniform distribution of mass disorder. So, the DCA formalism developed in this work should be able to incorporate material specific force-constants matrix in the lattice vibrational model and

solve it with dramatically less computational expense than the other state-of-the-art methods. Thus, the present work will further enrich our understanding of the spectral dynamics of vector phonons as well as provides a good starting point for studying Anderson localization of phonons in real materials.

## 6.2 Model and Formalism

The Hamiltonian of lattice vibrations within the harmonic approximation in terms of momentum ($p$) and displacement ($u$) basis reads as

$$H = \sum_{\alpha il} \frac{p_{i\alpha}^2(l)}{2M_i(l)} + \frac{1}{2} \sum_{\alpha\beta ll'ij} \Phi_{ij}^{\alpha\beta}(l, l') u_\alpha^i(l) u_\beta^j(l'),\qquad(6.1)$$

where $p_{i\alpha}(l)$ and $u_\alpha^i(l)$ represent, respectively, the momentum and the displacement of site $i$ belonging to the unit cell $l$ along the Cartesian coordinate $\alpha = (x, y, z)$ direction. The index $i$ runs from 1 to $N_{\text{cell}}$ where the latter denotes the number of atoms in the basis. The force-constant tensor, $\Phi$, is a function of $[\mathbf{R}_i(l) - \mathbf{R}_j(l')]$, where $\mathbf{R}_i(l)$ is the position of ion $i$ in unit cell $l$.

The Hamiltonian given in Eq.6.1 yields an equation of motion for the displacement-displacement Green's function involving multiple branches which reads as

$$M_i(l)\omega^2 D_{\alpha\beta}^{ij}(l, l', \omega) = \delta_{\alpha\beta}\delta_{ll'}\delta_{ij} + \sum_{\gamma, l''j'} \Phi_{ij'}^{\alpha\gamma}(l, l'') D_{\gamma\beta}^{j'j}(l'', l', \omega).\qquad(6.2)$$

To proceed further, let us investigate Eq.6.2 in the zero disorder limit ($M_i(l) = M_0 \ \forall \ (i, l)$).

$$M_0\omega^2 D_{\alpha\beta}(l, l', \omega) = \delta_{\alpha\beta}\delta_{ll'} + \sum_{\gamma, l''j'} \Phi^{\alpha\gamma}(l, l'') D_{\gamma\beta}(l'', l', \omega).\qquad(6.3)$$

In the absence of disorder, the system is translationally invariant. The Fourier transform and inverse Fourier transform are defined as

$$D_{\alpha\beta}(\mathbf{k}, \omega) = \sum_{ll'} D_{\alpha\beta}(l, l', \omega) \exp(i\mathbf{k}.(\mathbf{R_l} - \mathbf{R_{l'}}))$$
$$D_{\alpha\beta}(l, l', \omega) = \sum_{\mathbf{k}} D_{\alpha\beta}(\mathbf{k}, \omega) \exp(-\mathbf{k}.(\mathbf{R_l} - \mathbf{R_{l'}}))\qquad(6.4)$$

which when used in Eq.6.3, we get

$$M_0\omega^2 D_{\alpha\beta}(\mathbf{k},\omega) = \delta_{\alpha\beta} + \sum_{\gamma}(F(\mathbf{k}))^{\alpha\gamma}D_{\gamma\beta}(\mathbf{k},\omega) \tag{6.5}$$

where $F(\mathbf{k})$ is defined as

$$(F(\mathbf{k}))_{\alpha\beta} = \sum_{l'}\frac{\Phi_{\alpha\beta}(l,l')}{M_0}e^{i\mathbf{k}\cdot(\mathbf{R}_l-\mathbf{R}_{l'})} \ . \tag{6.6}$$

We note that for each $\mathbf{k}$, $F$ is an $N_b \times N_b$ matrix, where $N_b$ is the number of phonon branches. The matrix form $\hat{F}(\mathbf{k})$ can be expressed as

$$(\hat{F}(\mathbf{k})) = \hat{\Phi}\omega_k^2 \ .$$

where we have absorbed the force-constant information in $\hat{\Phi}$ as (for three branches) ,

$$\hat{\Phi} = \begin{pmatrix} \Phi_{xx} & \Phi_{xy} & \Phi_{xz} \\ \Phi_{yx} & \Phi_{yy} & \Phi_{yz} \\ \Phi_{zx} & \Phi_{zy} & \Phi_{zz} \end{pmatrix} \tag{6.7}$$

Any lattice anisotropy is incorporated through $\hat{\Phi}$. We also note that the elements of the $\Phi$ tensor are fixed and may be chosen independently, without of course, violating symmetry constraints and sum rules. Another factor in $\hat{\Phi}$ is $\omega_k^2$, the bare dispersion, assumed to be identical for all the branches, which is equivalent to assuming that the ratio of the diagonal to off-diagonal values of each of the force-constants is identical. This assumption can definitely be relaxed, in which case the dispersion cannot be pulled out of the $\hat{F}(\mathbf{k})$ matrix, and the momentum summations cannot be carried out through a partial density of states integration. Hence the calculations will be much more involved, but the formalism can be easily adapted to such cases.

Thus, from Eq.6.5, we can write the expression of the bare Green's function as

$$\hat{D}^{(0)}(\mathbf{k},\omega) = \left[\omega^2\mathbb{1} - \hat{F}(\mathbf{k})\right]^{-1} \tag{6.8}$$

So far, we have described our Green's function formalism for the model given in Eq.6.1 and explored it in the clean limit. Now, we can modify the mass-disordered TMDCA algorithm (as we described in chapter 3) to incorporate multiple branches. The details of the algorithm are given below:

## Algorithm

*Starting with the lattice quantities*

**Step 1:** *Hybridization Function*

Our algorithm starts with an initial guess of the hybridization function $\Gamma_{\text{old}}(\mathbf{K}, \omega)$. This hybridization function can also be taken from previous calculations or through a coarse-graining of non-disordered Green's function.

$$\hat{\Gamma}_{\text{old}}(\mathbf{K}, \omega) = \omega^2 \mathbb{1} - \hat{F}(\mathbf{K}) - \left[ \hat{D}^{(o)}(\mathbf{K}, \omega) \right]^{-1}, \tag{6.9}$$

where $\hat{F}(\mathbf{K})$ is defined as

$$\hat{F}(\mathbf{K}) = \hat{\Phi}\omega^2(\mathbf{K}).$$

We construct $\hat{D}^{(0)}(\mathbf{K}, \omega)$ as :

$$\hat{D}^{(0)}(\mathbf{K}, \omega) = \sum_{\mathbf{K}+\tilde{k}} \left[ \omega^2 \mathbb{1} - \hat{F}_{\mathbf{K}+\tilde{k}} \right]^{-1}$$

$$= \int d\epsilon \, \text{PDOS}(\mathbf{K}, \epsilon) [\omega^2 \mathbb{1} - \hat{\Phi}\epsilon]^{-1},$$

where $\hat{F}_{\mathbf{K}+\tilde{k}} = \bar{\hat{\Phi}}\omega^2_{\mathbf{K}+\tilde{k}}$.

**Step 2:** *Cluster excluded Green's function*

With the hybridization function as defined in Eq.(6.9), we calculate the cluster-excluded Green's function

$$\hat{\mathcal{D}}(\mathbf{K}, \omega) = \left[ \omega^2 \mathbb{1} - \hat{F}(\mathbf{K}) - \hat{\Gamma}_{\text{old}}(\mathbf{K}, \omega) \right]^{-1} \tag{6.10}$$

For each $\mathbf{K}$, $\hat{\mathcal{D}}$ is an $N_b \times N_b$ matrix.

**Step 3:** *Momentum space to real space*

The cluster excluded Green's function defined in Eq.(6.10), is then transformed from momentum space to real space via Fourier transform as

$$\hat{\mathcal{D}}(l, l', \omega) = \sum_{\mathbf{K}} \hat{\mathcal{D}}(\mathbf{K}, \omega) \exp\left[ i\mathbf{K}.(\mathbf{R_l} - \mathbf{R_{l'}}) \right] \tag{6.11}$$

Note that the cluster excluded Green's function is an $N_b \times N_b$ matrix for each combination of $(l, l')$.

However, for incorporating disorder through the Dyson's equation, we need a single matrix that incorporates the branch structure, and well as the real space indices. Hence we create a composite index by combining the branch index $(\alpha/\beta)$ and the real space index $(l/l')$, and rewrite the cluster excluded Dyson's equation as a single matrix in this composite index space. However, we observe that there is an inherent ambiguity in the sense that we could write $N_b \times N_b$ matrices for each real space index pair $(l, l')$ or for each branch index pair $(\alpha, \beta)$, we could write an $N_c \times N_c$ matrix. Both of these procedures have been tested for electronic multi-orbital systems[224; 173]. The second procedure has been found to yield better benchmarks against exact methods. Thus, in the multi-branch phonon case, we also adopt the same.

In the representation where the branch and the real space site indices are distinct, the cluster excluded Green's function, $\hat{\mathcal{D}}$ appears (in three dimensions, for a monoatomic lattice) as

$$
\hat{\mathcal{D}} = 
\begin{array}{c}
\\
\alpha = x \\
\\
\\
\\
\alpha = y \\
\\
\\
\\
\alpha = z \\
\\
\end{array}
\begin{pmatrix}
\overset{\beta = x}{} & & & \overset{\beta = y}{} & & & \overset{\beta = z}{} & & \\
D_{11} & \dots & D_{1N_c} & D_{11} & \dots & D_{1N_c} & D_{11} & \dots & D_{1N_c} \\
\vdots & & \vdots & \vdots & & \vdots & \vdots & & \vdots \\
D_{N_c1} & \dots & D_{N_cN_c} & D_{N_c1} & \dots & D_{N_cN_c} & D_{N_c1} & \dots & D_{N_cN_c} \\
\\
D_{11} & \dots & D_{1N_c} & D_{11} & \dots & D_{1N_c} & D_{11} & \dots & D_{1N_c} \\
\vdots & \vdots & & \vdots & & \vdots & \vdots & & \vdots \\
D_{N_c1} & \dots & D_{N_cN_c} & D_{N_c1} & \dots & D_{N_cN_c} & D_{11} & \dots & D_{1N_c} \\
\\
D_{11} & \dots & D_{1N_c} & D_{11} & \dots & D_{1N_c} & D_{11} & \dots & D_{1N_c} \\
\vdots & & \vdots & \vdots & & \vdots & \vdots & & \vdots \\
D_{N_c1} & \dots & D_{N_cN_c} & D_{N_c1} & \dots & D_{N_cN_c} & D_{1N_c} & \dots & D_{N_cN_c}
\end{pmatrix}
$$

(6.12)

**Step-4:** *Modeling mass disorder*

We generate the disorder potential V with a box distribution as

$$P(V_l) = \frac{1}{2W}\Theta(W - V_l),\tag{6.13}$$

where $V_l = 1 - M(l)/M_{\text{host}}$. This set of $V_l$ values are then placed in an $N_b N_c \times N_b N_c$ matrix in exactly the same way as the cluster excluded Green's function shown in the previous step, keeping in view that the matrix has only diagonal values, which have no branch dependence.

$$
\hat{\hat{V}} =
\begin{array}{c}
\begin{array}{cc} \beta = x & \beta = y & \beta = z \end{array} \\
\begin{array}{c} \alpha = x \\ \\ \\ \alpha = y \\ \\ \\ \alpha = z \\ \\ \\ \end{array}
\left(
\begin{array}{ccccccccc}
V_{11} & \dots & 0 & 0 & \dots & 0 & 0 & \dots & 0 \\
\vdots & & \vdots & \vdots & & \vdots & \vdots & & \vdots \\
0 & \dots & V_{N_c N_c} & 0 & \dots & 0 & 0 & \dots & 0 \\
0 & \dots & 0 & V_{11} & \dots & 0 & 0 & \dots & 0 \\
\vdots & & \vdots & \vdots & & \vdots & \vdots & & \vdots \\
0 & \dots & 0 & 0 & \dots & V_{N_c N_c} & 0 & \dots & 0 \\
0 & \dots & 0 & 0 & \dots & 0 & 0 & \dots & 0 \\
\vdots & & \vdots & \vdots & & \vdots & \vdots & & \vdots \\
0 & \dots & 0 & 0 & \dots & 0 & 0 & \dots & V_{N_c N_c}
\end{array}
\right)
\end{array}
\tag{6.14}
$$

*Going to cluster quantity from lattice quantity*

**Step-5:** *Cluster Green's function*

With the knowledge of cluster excluded Green's function given in Eq.(6.11) and the desired modeling of disorder as done in step-5, we calculate the mass-weighted cluster Green's function using the Dyson equation as

$$\hat{D}^c_{\alpha\beta}(l, l', \omega) = \sqrt{1 - V_l}\left[[\hat{\mathcal{D}}(\omega)]^{-1} - \omega^2 \hat{V}\right]^{-1}_{\alpha\beta, ll'} \sqrt{1 - V_{l'}}.\tag{6.15}$$

104

Since the cluster excluded Green's function, $\hat{\mathcal{D}}$ is an $N_b N_c \times N_b N_c$ matrix, the cluster Green's function, $\hat{D}^c$ is also an $N_b N_c \times N_b N_c$ matrix.

## Step-6: *Disorder averaging*

After getting the cluster Green's function in Eq.(6.15), we perform arithmetic averaging over all disorder realizations. This is the defining step of the dynamical cluster approximation (DCA). In all the previous chapters, we had carried out typical averaging for investigating Anderson localization. For the multi-branch phonon case, the ansatz that yields the typical density of states, needs to be worked out in parallel to the multi-orbital electronic case. In the absence of such an ansatz, the results obtained in this chapter pertain to the DCA (rather than the TMDCA), and hence phonon localization will not be a consideration in our results. The main aim of this chapter is to establish a quantitatively accurate method to get the disorder averaged phonon spectrum and to reveal the additional features of a multi-branch system as compared to single-branch systems considered in the previous chapters.

$$\hat{D}^c_{\alpha\beta,\mathrm{DCA}}(l, l'; \omega) = \left\langle \hat{D}^c_{\alpha\beta}(l, l', \omega) \right\rangle \tag{6.16}$$

Here, the disorder averaged Green's function, $\hat{D}^c_{DCA}$ is an $N_b N_c \times N_b N_c$ matrix.

## step-7: *Lattice Green's function*

We note that disorder averaging restores translational invariance, hence the averaged cluster Green's function obtained in Eq.(6.16) may be Fourier transformed from real space to momentum space and employed to calculate the coarse-grained lattice Green's function.

$$\hat{D}^{CG}(\mathbf{K}, \omega) = \sum_{\tilde{\mathbf{k}}} \left[ \left( \hat{D}^c_{\mathrm{DCA}}(\mathbf{K}, \omega) \right)^{-1} + \hat{\Gamma}_{\mathrm{old}}(\mathbf{K}, \omega) - \hat{F}(\mathbf{K} + \tilde{\mathbf{k}}) + \overline{\hat{F}(\mathbf{K})} \right]^{-1}$$

$$= \int d\epsilon \frac{\mathrm{PDOS}(\mathbf{K}, \epsilon)}{\left[ \left( \hat{D}^c_{\mathrm{DCA}}(\mathbf{K}, \omega) \right)^{-1} + \hat{\Gamma}_{\mathrm{old}}(\mathbf{K}, \omega) - \hat{\Phi}\epsilon + \overline{\hat{F}(\mathbf{K})} \right]} . \tag{6.17}$$

where $\overline{\hat{F}(\mathbf{K})}$ consist of $\hat{\Phi}$ and coarse-grained bare dispersion $\omega^2(\mathbf{K})$ and the $\hat{D}^{CG}$ is an $N_b \times N_b$ matrix for each $\mathbf{K}$.

**Step-8:** *Self consistency*

The coarse-grained lattice Green's function calculated using Eq.(6.17) and cluster Green's functions in Eq.(6.15) are inverted to get the new hybridization function as

$$\hat{\Gamma}_{\text{new}}(\mathbf{K},\omega) = \hat{\Gamma}_{\text{old}}(\mathbf{K},\omega) + \xi\left[\left(\hat{D}^{CG}(\mathbf{K},\omega)\right)^{-1} - \left(\hat{D}^{c}_{\text{DCA}}(\mathbf{K},\omega)\right)^{-1}\right], \qquad (6.18)$$

where the $N_b \times N_b$ matrix $\Gamma_{\text{old}}(\mathbf{K},\omega)$ is the hybridization function at the beginning of the DCA iteration as defined in Eq.(6.9). Naturally, the new hybridization function is also $\Gamma_{\text{new}}$ is also $N_b \times N_b$ matrix.

We carry out the DCA calculations for a simple cubic lattice using cluster sizes $N_c = 8, 27$ considering $600 - 6000$ disorder realizations.

## 6.3 Results and discussions

Before we begin the discussion of our results, we emphasize that this work considers pure isotopic mass disorder. The values in the force constant tensor are deterministic (not stochastic) and can be chosen freely, respecting the sum rules and constraints mentioned in the methods section. Our first result considers an isotropic force-constant tensor, implying that the force-constants belonging to the three branches are chosen to be of equal strength. Hence, the ADOS for the three branches are identical to each other, and for clarity, we present a single ADOS.

In Fig.6.1, we show a direct comparison of the arithmetically averaged density of states (ADOS) obtained from the DCA with results from exact diagonalization (ED) for a three dimensional mass disordered system with the random masses chosen from a box distribution at various values of the disorder potential $(V)$.

The ED results are derived from 50 randomly shaped supercells with approximately 100 sites on average for a simple cubic lattice. These ED calculations have been carried out by Dr. Tom Berlijn from Oak Ridge National Laboratory, USA. We find excellent agreement between the ED and DCA over the entire spectrum. The evolution of the ADOS at various values of $V$ and $\Phi$ are also corroborated by the ED
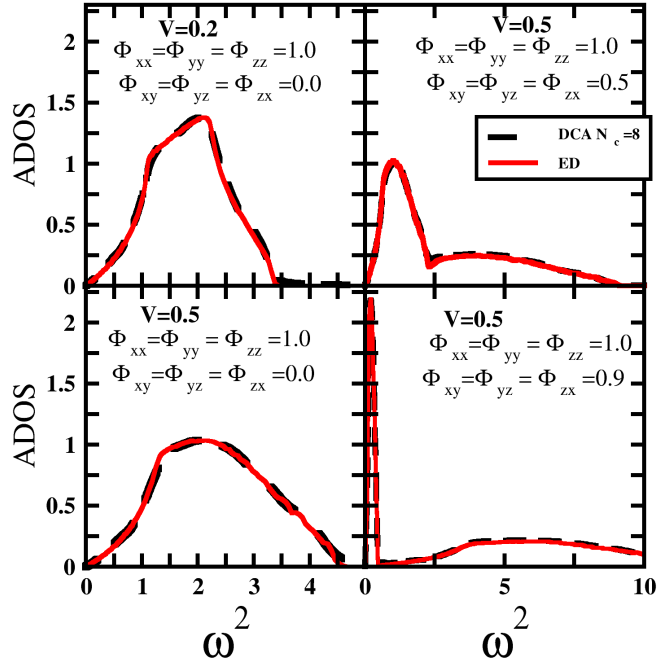
Figure 6.1: A comparison of the arithmetic density of states (ADOS) obtained from the DCA using $N_c = 8$ and the same from exact diagonalization (ED) for various values of force-constants between different branches. We see that the results obtained from the DCA are in good agreement with those from ED.

calculations. We note that the formalism yields such exact results using a relatively small cluster size of $N_c = 8$, which clearly demonstrates the high computational efficiency of the DCA for multiple branches compared to other methods like ED. Such an agreement validates the DCA developed in this chapter for disordered multi-branch phonon systems.

Our next result exhibits the rapid convergence of the DCA with increasing cluster sizes. The ADOS obtained from the DCA for various cluster sizes ($N_c$) are shown in Fig6.2 for two values of mass disorder, namely $V = 0.2$ and $0.5$. As is well known, the DCA when applied to a single-site cluster ($N_c = 1$) is equivalent to a coherent potential approximation (CPA) which, as shown in the previous chapters, fails quantitatively, and even qualitatively. The DCA incorporates systematic and causal corrections to the CPA by incorporating non-local fluctuations with increasing cluster size. Although the results obtained from $N_c = 1$ and $N_c > 1$ calculations are
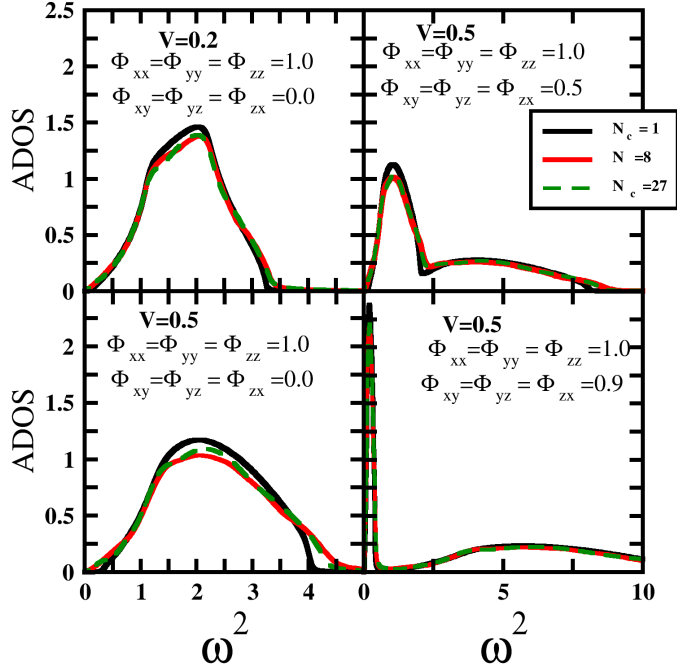
Figure 6.2: This figure shows the rapid convergence of the method with increasing cluster size. The arithmetically averaged density of states (ADOS) obtained from the DCA using cluster size, $N_c = 1, 8, 27$ are shown for two values of $V$, namely 0.2 and 0.5. We note that the results are converged for $N_c = 8$.

seen to not differ much for low disorder ($V = 0.2$), the differences emerge and show up significantly for $V = 0.5$. The low-frequency and high-frequency edge of the ADOS for $N_c = 8$ acquire tails as disorder increases. Also, the ADOS for $N_c = 8$ does not show a gap in the low-frequency region. The CPA ($N_c = 1$) is not able to capture these features due to the neglect of non-local dynamical fluctuations. To test the convergence of DCA with respect to cluster size, we compare the ADOS for $N_c = 8$ with the ADOS for higher $N_c = 27$. Fig.6.2 clearly shows that results obtained from $N_c = 8$ resembles the $N_c = 27$ result very closely, which confirms the convergence of our calculations with respect to cluster size at $N_c = 8$. Henceforth, we will show the results obtained from the DCA for $N_c = 8$. With this, we understand the effect of diagonal mass disorder ($V$) in the lattice vibrational system of three branches($x, y, z$) which are connected by the force-constants ($\Phi_{xy}, \Phi_{yz}, \Phi_{zx}$).

In our published work[203], described in chapter-3 of the thesis, we have ex-

plored the effects of the diagonal mass-disorder in a single-branch phonon system. We demonstrated that phonon localization sets in from the higher frequency region of the spectrum in the presence of strong mass disorder. In our present work, we have chosen a three branch system where the branches are inter-connected by the force-constants ($\Phi_{xy}, \Phi_{yz}, \Phi_{zx}$). In Fig6.3, we present the evolution of the ADOS (solid black line) with increasing $V$ for fixed inter-branch force-constants. As expected, the ADOS is almost the same as the DOS for the clean system at low disorder ($V \leq 0.2$). But, with increasing $V$, there is a significant transfer of spectral weight in the ADOS from low to high frequencies. We also present the ADOS (denoted by solid red line) for the independent branches ($\Phi_{xy} = \Phi_{yz} = \Phi_{zx} = 0.0$). A comparison between the ADOS (denoted by solid black line) for the interacting branches and the ADOS for
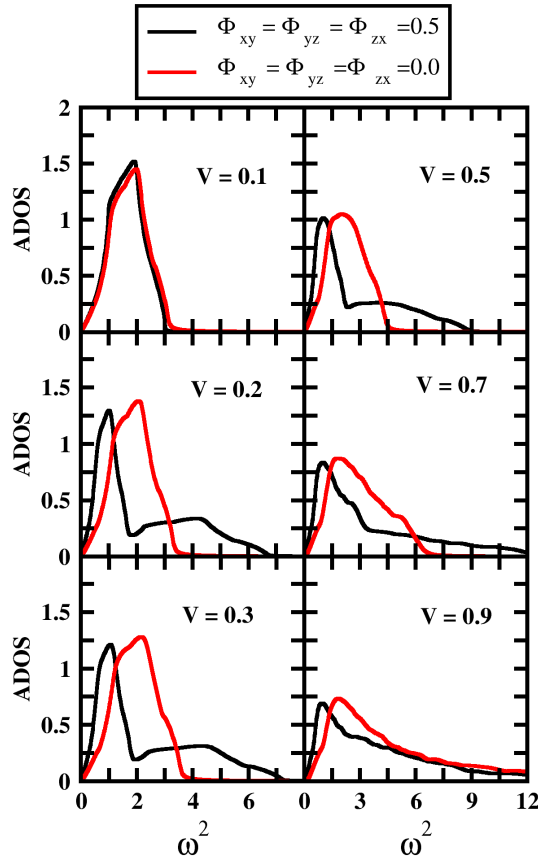


Figure 6.3: The evolution of average DOS with increasing values of $V$ for a fixed $\Phi_{xy} = \Phi_{yz} = \Phi_{zx} = 0.5$ is shown.

the independent branches (denoted by solid red line) clearly shows that the correlation between different branches increases spectral weight at higher frequencies, which are easier to localize, and hence may play a significant role in localization. Though the ADOS can describe such precursor effects of localization, it is not critical at the Anderson transition. Hence, localization can only be explored through the evaluation of the typical DOS (TDOS) and these calculations are underway.

To understand the effect of the inter-branch force-constants in a detailed manner, we display the variation of the ADOS for various values of the inter-branch force-constants at fixed $V$ in fig6.4. As we have already observed in Fig6.3, the spectral weight of ADOS undergoes a blueshift with increasing $V$. The effect of increasing inter-branch force constants turns out to be similar. The spectral weight of the ADOS is transferred from the low-frequency region to the high-frequency region with increasing inter-branch force constants which yields an impurity band at the high-
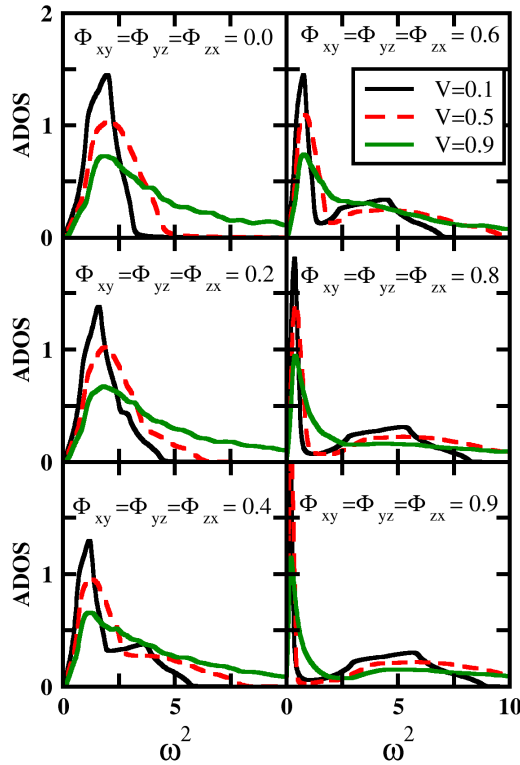


Figure 6.4: The average DOS for increasing values of $V$ is displayed. For a given $V$, the parameters $\Phi_{xy}$, $\Phi_{yz}$ and $\Phi_{zx}$ are varied, while $\Phi_{xx}$, $\Phi_{yy}$ and $\Phi$ are fixed to 1.

frequency region. As shown in 6.4, the impurity mode starts to form at $\Phi_{xy} = \Phi_{yz} = \Phi_{zx} = 0.5$. Further increase of inter-branch force-constants from 0.5 to 0.9 leads to broadening of the high-frequency impurity mode. These observations support our expectation that the combination of lighter impurities and stiffer inter-branch force-constants is highly effective in localizing vibrational modes, especially at the high-frequency region. It would be interesting to look at the typical density of states in this parameter regime, which is left for future studies.

Until now, we have considered all of the off-diagonal components of the force constant to be identical, but different from the diagonal components. In the final part, we introduce inhomogeneity in the inter-branch force-constants. The intra-branch force-constants $\Phi_{xx}$, $\Phi_{yy}$ have been fixed at unity, while the intra-branch force-constant $\Phi_{zz}$ and inter-branch force-constants $\Phi_{xy}$, $\Phi_{yz}$, and $\Phi_{zx}$ are varied from
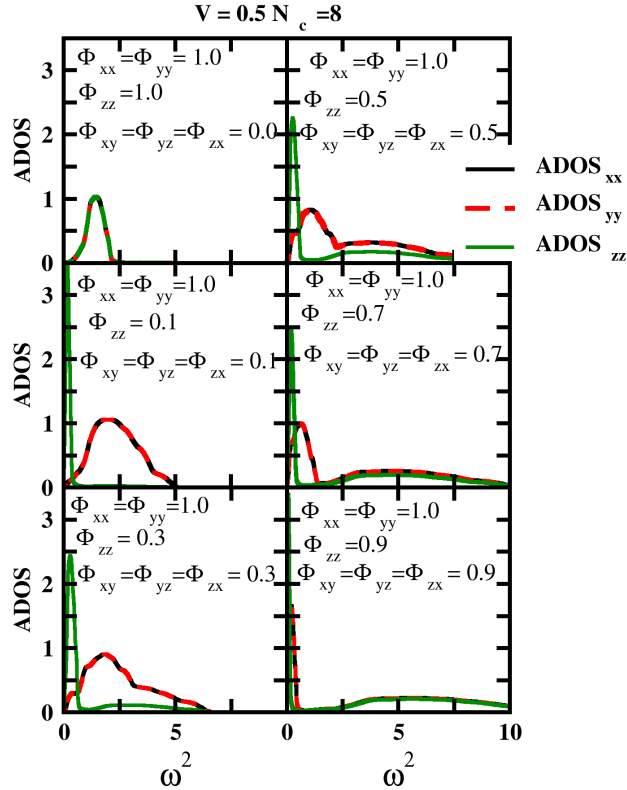


Figure 6.5: The average DOS corresponding to $x$ ($\mathrm{ADOS}_{xx}$), $y$ ($\mathrm{ADOS}_{yy}$) and $z$ ($\mathrm{ADOS}_{zz}$) directions of propagation are displayed. The parameters $\phi_{xx} = 1$, $\Phi_{yy} = 1$, $V = 0.5$ are fixed, while $\Phi_{zz}$, $\Phi_{xy}$, $\Phi_{yz}$, $\Phi_{zx}$ are varied from 1 to 0.1.

111

0 to 0.9. We show the ADOS at these parameter values in Fig6.5. We observe that the ADOS corresponding to $x$, $y$ and $z$ direction of propagation differ significantly from each other, which is as expected. As shown in Fig6.5, the $\text{ADOS}_{zz}$ differs significantly from the $\text{ADOS}_{yy}$ and $\text{ADOS}_{zz}$ when $\Phi_{zz}$ is varied from 1 to 0.1 fixing $\Phi_{xx}$ and $\Phi_{yy}$ to 1. It would be interesting to search for a *branch selective Anderson localization of phonons*, since that would imply propagation in selective directions. Such investigations are in progress.

## 6.4 Conclusions

We have extended the dynamical cluster approximation to treat multibranch disordered phononic systems. We have shown that this formalism fulfills all of the features of a successful cluster approximation when applied to a multi-branch lattice vibrational systems. The results obtained from the multi-branch DCA for vector phonons (a) are shown to be fully causal; (b) reduce to the single-site coherent potential approximation as cluster size goes to one and (c) become exact in the thermodynamic limit. Our method is able to capture sharp features and band tailing of three vibrational spectra corresponding to three different directions. We have displayed a direct comparison of results using the DCA with ED results and found an excellent agreement between the DCA and ED. In addition, the DCA is shown to converge rapidly to the exact, thermodynamic limit result for cluster sizes as small as $N_c = 8$. Thus, we have validated the DCA for multibranch disordered phonon systems. Using the same method, we have also investigated the precursor effects of phonon localization. This work offers a natural starting point for studying phonon localization in real materials.

# Chapter 7

# Conclusions

This thesis is a study of Anderson localization of phonons in three dimensions. A new computational approach for studying the Anderson localization of phonons has been developed, and the intriguing physics of phonon localization caused by quenched disorder in the masses and force constants has been explored.

Disordered phononic systems exhibit all the rich features of the Anderson localization transition. Moreover, phonon localization has been directly observed in experiments. Also, it can be useful in designing high-performance thermoelectric materials. With these as the motivation, we have investigated phonon localization in this thesis.

For investigating disordered phononic systems, two Green's function based quantum cluster methods have been introduced. One is based on the dynamical cluster approximation (DCA), and the other is its typical medium extension, named as typical medium dynamical cluster approximation (TMDCA). These methods have been validated and established for disordered electronic systems. In this thesis, we have introduced them for the first time for disordered phononic systems. We have shown that both the methods satisfy all the requirements of a successful cluster theory for the phonon case. The DCA is presented as a systematic extension of the coherent potential approximation (CPA) for disordered phononic systems. We have shown that the results obtained from the DCA using a single-site cluster agree well with the existing CPA results for disordered phononic systems. Unlike the CPA, we reveal that the DCA yields accurate vibrational spectra which carries all the dynamical informa-

tion of interest, and is an experimental observable. Despite such an advantage of the DCA over the CPA, we find that the DCA fails to capture phonon localization. In particular, we know that the globally averaged vibrational spectra is not critical at the Anderson transition of phonons. To capture phonon localization, the TMDCA has been developed wherein we adopt an ansatz for typical averaging that was originally proposed for electronic systems. Using this ansatz, we demonstrate that the typical density of states (TDOS) serves as an apposite order parameter for phononic systems, too. We have checked various features of the TMDCA ansatz for phonons. The vibrational TDOS at small disorder strength for phonons obtained from the TMDCA reduces to the globally averaged vibrational spectra that are obtained from the DCA. Most importantly, at high disorder values, the vibrational TDOS is shown to be critical at the Anderson transition and the TMDCA provides a correct description of phonon localization. As found in the electronic case, we confirm that the TMDCA is capable of treating the different energy scales such that the characteristic re-entrant behavior of the mobility edge is captured correctly. We also confirm that the local typical medium theory(TMT) fails to give correct behavior of mobility edges for the Anderson transition of phonons. Our findings are corroborated by the existing exact methods like exact diagonalization (ED) and transfer matrix (TMM). We have achieved a systematic convergence of our results to the thermodynamic limit with far lower computational expense than exact methods such as ED and TMM. Overall, this thesis establishes the DCA and TMDCA for disordered phononic systems.

Besides the establishment of the methods, we have extensively applied the DCA and TMDCA for various kinds of disorders, including diagonal mass disorder, diagonal short-range spatially correlated mass disorder, and off-diagonal force-constant disorder. The DCA formalism for the mass disorder has been extended to multi-branch phononic systems.

By applying the TMDCA, we provide insight into the physics of phonon localization. We find that the high-frequency modes are localized with the introduction of lighter impurities considering a uniform distribution of mass disorder. We suggest that

the disorder-induced delocalization-localization transition of vibrational modes is similar to that of electronic systems. Naturally, there are some differences, too. One such noticeable difference is that all the states in the electronic system become localized beyond a critical disorder strength, while in the phonon case, low-frequency vibrational modes survive as delocalized states even in the presence of strong mass disorder. However, the physics of Anderson localization changes significantly if short range order is introduced, or equivalently the disorder is not completely random, but correlated. By considering pairwise correlations between the adjacent odd-indexed and even-indexed sites, we found that correlated disorder prevents the localization of the vibrational modes, and eventually, a correlation induced localization-delocalization transition of phonons occurs in a 3D disordered sample.

Phonon localization in binary alloys is another theme of investigation in the thesis. We find that for a binary *isotopic* alloy in the presence of mass disorder (without force-constant disorder), high-frequency vibrational modes are Anderson localized at a relatively low concentration of lighter impurities. Although at high concentration, the lower-frequency modes are indeed affected, nevertheless most of them survive as delocalized states. Our findings indicate that phonon localization over the entire spectrum is hard to achieve. We suggest that maximum localization over the entire spectrum can be observed for equal concentrations of light and heavy atoms in a binary alloy, provided the force constants are equal. Otherwise, the minimum in the typical spectral weight (which indicates maximum localization) can occur at a different ratio (than 1:1). In such a binary alloy, there is always a concomitant change in the bond strength with a randomness in mass. So, we have also studied phonon localization in the binary alloy considering both mass and force-constant disorder on equal footing. We have predicted that the interplay of force-constant and mass disorder is highly frequency-dependent. For a certain range of frequencies, the force constant disorder and mass disorder can be competitive or co-operative in localizing vibrational modes, in the sense that the typical density of states can vanish or appear respectively with increasing disorder. However, the integrated typical spectral weight always decreases with increasing disorder, hence in this sense, mass disorder

and force constant disorder can be considered to be cooperative in leading to phonon localization. The inclusion of the force-constant disorder in our formalism enables us to model vacancies, which we define as weakly bonded sites with vanishing mass. We have demonstrated that strong phonon localization over the entire spectrum can be achieved by tuning the concentration of vacancies. This finding is very significant for controlling thermal transport, especially in maximizing the figure of merit of ther-moelectric materials. Another intriguing and well-debated issue that this thesis deals with is the Boson peak in the spectrum. In particular, we have revealed the origin of the boson peak by considering force constant disorder. We demonstrate that the boson peak appears as a narrow resonance noticeably below the van Hove singular-ity for low soft particle concentrations. Also, we show that the vibrational modes associated with the boson peak cross over from being completely localized to being extended with increasing soft particle concentration. We note that the force constant disorder plays a major role in controlling the phonon dynamics, especially for strong force-constant disorder binary alloy. As a test case, we have considered $Ni_xPt_{1-x}$ al-loy. We have successfully explained the experimental results in a qualitative way for this material by incorporating force constant disorder in our formalism. However, we do need to consider a material-specific realistic model to get quantitative agreement and gain insight into phonon localization in real materials.

To treat realistic multibranch phononic systems, we have extended the DCA for-malism. We have validated the multibranch DCA formalism and shown that it fulfills all the requirements of a successful cluster theory. We have reserved the develop-ment of its typical medium extension for future studies. However, the present work brings the TMDCA one step closer to becoming an effective tool for studying phonon localization in real materials. As we have shown comprehensively, this method is com-putationally relatively inexpensive compared to other existing exact methods which should enable us to incorporate material-specific information by combining with first-principles approaches for phonons. Besides, the TMDCA holds many more promises. Since the current formulation adopts the Green's function approach, it can be easily

extended to layered geometries (DCA in two dimensions), thus allowing for investigations of phonon engineering in superlattice structures, heterostructures, thin films, and interfaces. In principle, it can also be applied to investigate Anderson localization of other elementary excitations like photons, and magnons. Incorporating diagrammatic perturbation theory into the cluster solver gives us access to phenomena like Umklapp scattering, electron-phonon interactions etc, which should eventually lead to a single framework for investigating the effect of disorder on electrical and thermal transport.

# Appendix A

## A.1 Derivation of force-constants sum rule

Let's consider $F_r^\gamma(m)$ is the force in $\gamma^{th}$ direction for the $r^{th}$ atom in the $m^{th}$ unit cell. We can calculate this force from the Hamiltonian (as defined in chapter 2) as

$$F_r^\gamma(m) = -\frac{\partial H}{\partial u_r^\gamma(m)}$$
$$= -\frac{1}{2}\sum_{\beta,j,l'}\Phi_{\gamma\beta}^{rj}(m,l')u_\beta^j(l') - \frac{1}{2}\sum_{\alpha il}\Phi_{\alpha\gamma}^{ir}(l,m)u_\alpha^i(l) \ . \qquad (A.1)$$

Changing dummy indices $\beta$ to $\alpha$, $j$ to $i$ and $l'$ to $l$ in first term, we can write

$$F_r^\gamma(m) = -\frac{1}{2}\sum_{\alpha il}\Phi_{\gamma\alpha}^{ri}(m,l')u_\alpha^i(l) - \frac{1}{2}\sum_{\alpha il}\Phi_{\alpha\gamma}^{ir}(l,m)u_\alpha^i(l)$$
$$= -\frac{1}{2}\sum_{\alpha il}[\Phi_{\gamma\alpha}^{ri}(m,l') + \Phi_{\alpha\gamma}^{ir}(l,m)]u_\alpha^i(l) \ . \qquad (A.2)$$

Using the property as given in Eq. (2.6), we write

$$F_\gamma^r(m) = \sum_{\alpha il}\Phi_{\alpha\beta}^{ir}(l,m)u_\alpha^i(l) \ . \qquad (A.3)$$

Now total force will be zero in the $\gamma^{th}$ direction. i.e $\sum_{r,m}F_\gamma^r(m) = 0$. Hence,

$$\sum_{r,m}\sum_{\alpha il}\Phi_{\gamma\alpha}^{ri}(m,l)u_\alpha^i(l) = 0$$

$$\sum_{\alpha il}u_\alpha^i(l)\sum_{r,m}\Phi_{\gamma\alpha}^{ri}(m,l) = 0 \ .$$

There are no net displacements in the $\alpha$ direction i.e $\sum_{il}M_iu_i^\alpha(l) = 0$. Assuming $u_i^\alpha(l)$ are independent, we find

$$\sum_{r,m}\Phi_{\gamma\alpha}^{ri}(m,l) = 0 \ . \qquad (A.4)$$

Eq.(A.4) can be re-written as

$$\Phi^{ii}_{\beta\alpha} = - \sum_{j,j\neq i,l',l'\neq l} \Phi^{j,i}_{\beta\alpha}(l',l) \, .$$

(A.5)

## A.2  Calculations of the commutator $[u^i_\alpha(l,t), H]$

$$[u^i_\alpha(l,t), H] = [u^i_\alpha(l,t), \sum_{\gamma i' l'} \frac{p^2_{i'\gamma}(l')}{2M_{i'}(l')}]$$

$$= \sum_{\gamma i' l'} \frac{1}{2M_{i'}(l')}[u^i_\alpha(l), p_{i'\gamma}(l')]p_{i'\gamma}(l') + \sum_{\gamma i' l'} \frac{1}{2M_{i'}(l')}p_{i'\gamma}(l')[u^i_\alpha(l), p_{i'\gamma}(l')]$$

$$= \sum_{\gamma i' l'} \frac{1}{2M_{i'}(l')}i\delta_{\alpha\gamma}\delta_{ii'}\delta(l,l')p_{i'\gamma}(l') + \sum_{\gamma i' l'} \frac{1}{2M_{i'}(l')}i\delta_{\alpha\gamma}\delta_{ii'}\delta(l,l')p_{i'\gamma}(l')$$

$$= i\frac{1}{2M_i(l)}p_{i\alpha}(l) + i\frac{1}{2M_i(l)}p_{i\alpha}(l)$$

$$= i\frac{p_{i\alpha}}{M_i(l)}.$$

Thus,

$$[u^i_\alpha(l,t), H] = i\frac{p_{i\alpha}}{M_i(l)}$$

(A.6)

## A.3 Calculations of the commutator $\frac{1}{M_i(l)}[p_{i\alpha}(l,t), H]$

$$\frac{1}{M_i(l)}[p_{i\alpha}(l,t), H] = \frac{1}{M_i(l)}[p_{i\alpha}(l,t), \frac{1}{2}\sum_{i'j'\gamma\gamma'l'l''}\Phi^{\gamma\gamma'}_{i'j'}(l',l'')u^{i'}_\gamma(l')u^{j'}_{\gamma'}(l'')]$$

$$= \frac{1}{2M_i(l)}\sum_{i'j'\gamma\gamma'l'l''}\Phi^{\gamma\gamma'}_{i'j'}(l',l'')[p_{i\alpha}(l,t), u^{i'}_\gamma(l')]u^{j'}_{\gamma'}(l'')$$

$$+ \frac{1}{2M_i(l)}\sum_{\gamma\gamma'l'l''}^{i'j'}\Phi^{\gamma\gamma'}_{i'j'}(l',l'')u^{i'}_\gamma(l')[p_{i\alpha}(l,t), u^{j'}_{\gamma'}(l'')]$$

$$= \frac{-i}{2M_i(l)}\sum_{i'j'\gamma\gamma'l'l''}\Phi^{\gamma\gamma'}_{i'j'}(l',l'')\delta_{ii'}\delta_{\alpha\gamma}\delta(l,l')u^{j'}_{\gamma'}(l'')$$

$$+ \frac{-i}{2M_i(l)}\sum_{i'j'\gamma\gamma'l'l''}\Phi^{\gamma\gamma'}_{i'j'}(l',l'')\delta_{ij'}\delta_{\alpha\gamma'}u^{i'}_\gamma(l')\delta(l,l'')$$

$$= \frac{-i}{2M_i(l)}\sum_{j'\gamma'l''}\Phi^{\alpha\gamma'}_{ij'}(l,l'')u^{j'}_{\gamma'}(l'') + \frac{-i}{2M_i(l)}\sum_{i'\gamma l'}\Phi^{\gamma\alpha}_{i'i}(l,l'')u^{i'}_\gamma(l').$$

$$(A.7)$$

Changing the dummy indices in the second term, we can write

$$\frac{1}{M_i(l)}[p_{i\alpha}(l,t), H] = \frac{-i}{2M_i(l)}\sum_{j'\gamma'l''}\Phi^{\alpha\gamma'}_{ij'}(l,l'')u^{j'}_{\gamma'}(l'') + \frac{-i}{2M_i(l)}\sum_{j'\gamma'}\Phi^{\gamma'\alpha}_{j'i}(l'',l)u^{j'}_{\gamma'}(l'').$$

Recalling the symmetry property of the force-constant as given in Eq. (2.6),we obtain

$$\frac{1}{M_i(l)}[p_{i\alpha}(l,t), H] = \frac{-i}{M_i(l)}\sum_{j'\gamma'l''}\Phi^{\alpha\gamma'}_{ij'}(l,l'')u^{j'}_{\gamma'}(l''). \qquad (A.8)$$

## A.4 Hermiticity of the Dynamical matrix

$$D^{ji}_{\text{mat},\beta\alpha}(\mathbf{k}) = \frac{1}{\sqrt{M^iM^j}}\sum_{l'}\Phi^{ji}_{\beta\alpha}(l',l)\exp\left(-i\mathbf{k}.(\mathbf{R}_l - \mathbf{R}_{l'})\right)$$

$$= \frac{1}{\sqrt{M^iM^j}}\sum_{l'}\Phi^{ij}_{\alpha\beta}(l,l')\exp\left(-i\mathbf{k}.(\mathbf{R}'_l - \mathbf{R}_l)\right)$$

$$= \frac{1}{\sqrt{M^iM^j}}\sum_{l'}\Phi^{ij}_{\alpha\beta}(l,l')\exp\left(i\mathbf{k}.(\mathbf{R}_l - \mathbf{R}_{l'})\right)$$

$$= \left(D^{ij}_{\text{mat},\alpha\beta}\right)^*(\mathbf{k}) . \qquad (A.9)$$

Eq.(A.9) shows that the dynamical matrix is Hermitian.

## A.5 Commutation relation between $b_s$ and $b_{s'}$

$$b_s = \sum_{l\alpha} B_\alpha^s(l) \frac{1}{\sqrt{2M(l)\omega_s}} \Big( M(l)\omega_s u_\alpha(l) + ip_\alpha(l) \Big) \tag{A.10}$$

$$b_s^\dagger = \sum_{l\alpha} B_\alpha^s(l) \frac{1}{\sqrt{2M(l)\omega_s}} \Big( M(l)\omega_s u_\alpha(l) - ip_\alpha(l) \Big) . \tag{A.11}$$

$$
\begin{aligned}
b_s b_{s'}^\dagger &= \sum_{l\alpha} B_\alpha^s(l) \frac{1}{\sqrt{2M(l)\omega_s}} \Big( M(l)\omega_s u_\alpha(l) + ip_\alpha(l) \Big) \\
&\quad \sum_{l'\alpha'} B_{\alpha'}^{s'}(l') \frac{1}{\sqrt{2M(l')\omega_{s'}}} \Big( M(l')\omega_{s'} u_{\alpha'}(l') - ip_{\alpha'}(l') \Big) \\
&= \sum_{ll'\alpha\alpha'} B_\alpha^s(l) B_{\alpha'}^{s'}(l') \frac{1}{2\omega_s} \frac{1}{\sqrt{M(l)M(l')}} \Big( M(l)M(l')\omega_s^2 u(l)u(l') \\
&\quad - iM(l)\omega_{s'} u(l)p(l') + i\omega_{s'} M(l')p(l)u(l') + p(l)p(l') \Big) \\
b_s b_{s'}^\dagger &= \sum_{ll'\alpha\alpha'} B^s(l) B^{s'}(l') \frac{1}{2\omega_s} \frac{1}{\sqrt{M(l)M_{\alpha'}(l')}} M(l)M(l')\omega_s^2 u(l)u(l') \\
&\quad + \sum_{ll'\alpha\alpha'} B^s(l) B^{s'}(l') \frac{1}{2\omega_{s'}} \frac{1}{\sqrt{M(l)M(l')}} p(l)p(l') \\
&\quad - \sum_{ll'\alpha\alpha'} B^s(l) B^s(l') \frac{1}{2\omega_{s'}} \frac{1}{\sqrt{M(l)M(l')}} i\omega_s M(l) u_\alpha(l)p_{\alpha'}(l') \\
&\quad + \sum_{ll'\alpha\alpha'} B^s(l) B^s(l') \frac{1}{2\omega_{s'}} \frac{1}{\sqrt{M(l)M_{\alpha'}(l')}} i\omega_s M(l') p_\alpha(l)u_{\alpha'}(l') ,
\end{aligned}
\tag{A.12}
$$

and

$$
\begin{aligned}
b_{s'}^\dagger b_s &= \sum_{l'\alpha'} B_{\alpha'}^{s'}(l') \frac{1}{\sqrt{2M(l')\omega_{s'}}} \Big( M(l')\omega_s u_{\alpha'}(l') - ip_{\alpha'}(l') \Big) \\
&\quad \sum_{l\alpha} B_\alpha^s(l) \frac{1}{\sqrt{2M_\alpha(l)\omega_s}} \Big( M(l)\omega_s u(l) + ip(l) \Big) \\
&= \sum_{ll'\alpha\alpha'} B_{\alpha'}^{s'}(l') B_\alpha^s(l) \frac{1}{2\omega_s} \frac{1}{\sqrt{M(l)M(l')}} \omega_s\omega_{s'} M_{\alpha'}(l')M(l) u_{\alpha'}(l')u_\alpha(l) \\
&\quad + \sum_{ll'\alpha\alpha'} B_{\alpha'}^s(l') B_\alpha^s(l) \frac{1}{2\omega_s} \frac{1}{\sqrt{M(l)M(l')}} \omega_s\omega_{s'} M(l')M(l) u_{\alpha'}(l')u_\alpha(l) \\
&\quad + \sum_{ll'\alpha\alpha'} B_{\alpha'}^{s'}(l') B_\alpha^s(l) i\omega_s \frac{1}{2\omega_s} \frac{1}{\sqrt{M(l)M_{\alpha'}(l')}} u_{\alpha'}(l')p_\alpha(l) \\
&\quad - \sum_{ll'\alpha\alpha'} B_{\alpha'}^{s'}(l') B_\alpha^s(l) i\omega_s \frac{1}{2\sqrt{\omega_s\omega_{s'}}} \frac{1}{\sqrt{M(l)M(l')}} p_{\alpha'}(l')u_\alpha(l) .
\end{aligned}
\tag{A.13}
$$

Using Eq.(A.12) and Eq.(A.13), we evaluate the commutator $[b_s b_{s'}^\dagger]$ as

$$
\begin{aligned}
[b_s, b_{s'}^\dagger] &= \sum_{ll'\alpha\alpha'} B_{\alpha'}^s(l') B_{\alpha}^s(l) \frac{1}{2\omega_s} \frac{1}{\sqrt{M_\alpha(l)M_{\alpha'}(l')}} \omega_s^2 M_{\alpha'}(l') M_\alpha(l)[u_\alpha(l), u_{\alpha'}(l')] \\
&+ \sum_{ll'\alpha\alpha'} B_{\alpha'}^s(l') B_{\alpha}^s(l) \frac{1}{2\omega_s} \frac{1}{\sqrt{M_\alpha(l)M_{\alpha'}(l')}} \omega_s^2 M_{\alpha'}(l') M_\alpha(l)[p_\alpha(l), p_{\alpha'}(l')] \\
&- \sum_{ll'\alpha\alpha'} B_{\alpha'}^s(l') B_{\alpha}^s(l) \frac{1}{2\sqrt{\omega_s\omega_{s'}}} i\omega_s \frac{1}{\sqrt{M_\alpha(l)M_{\alpha'}(l')}} M_\alpha(l)[u_\alpha(l), p_{\alpha'}(l')] \\
&+ \sum_{ll'\alpha\alpha'} B_{\alpha'}^s(l') B_{\alpha}^s(l) \frac{1}{2\sqrt{\omega_s\omega_{s'}}} \frac{1}{\sqrt{M_\alpha(l)M_{\alpha'}(l')}} M_{\alpha'}(l')[p_{\alpha'}(l'), u_\alpha(l)] \\
&= - \sum_{ll'\alpha\alpha'} B_{\alpha'}^s(l') B_{\alpha}^s(l) \frac{1}{2\sqrt{\omega_s\omega_{s'}}} i\omega_s \frac{1}{\sqrt{M_\alpha(l)M_{\alpha'}(l')}} M_\alpha(l)[u_\alpha(l), p_{\alpha'}(l')] \\
&+ \sum_{ll'\alpha\alpha'} B_{\alpha'}^s(l') B_{\alpha}^s(l) \frac{1}{2\sqrt{\omega_s\omega_{s'}}} \frac{1}{\sqrt{M_\alpha(l)M_{\alpha'}(l')}} i\omega_{s'} M_{\alpha'}(l')[p_{\alpha'}(l'), u_\alpha(l)] . \quad \text{(A.14)}
\end{aligned}
$$

Using the orthonormality property in Eq .(2.25), we get

$$
[b_s, b_{s'}^\dagger] = \frac{1}{2\sqrt{\omega_s\omega_{s'}}} \omega_s \delta_{ss'} + \frac{1}{2\sqrt{\omega_s\omega_{s'}}} \omega_{s'} \delta_{ss'}
$$

$$
[b_s, b_{s'}^\dagger] = \delta_{ss'} \tag{A.15}
$$

Thus we show that the creation and annihilation operator satisfy general boson algebra.

## A.6 Displacement-displacement Green's function in mass-disordered systems

To derive the displacement-displacement Green's function in mass-disordered systems, let us first recall our required displacement-displacement correlation function. Using

Eq.(2.24), we evaluate the correlation function $\langle u(l,t)u(l',0)\rangle$ as

$$\langle u_\alpha(l,t); u_\beta(l',0)\rangle = \frac{1}{2}\frac{1}{\sqrt{M(l)M(l')}}\sum_{ss'}B^s(l)B^{s'}(l')\frac{1}{\sqrt{\omega_s\omega_{s'}}}$$

$$\left\langle \left(b_s\exp(-i\omega_st) + b_s^\dagger\exp(i\omega_st)\right)\left(b_{s'} + b_{s'}^\dagger\right)\right\rangle$$

$$= \frac{1}{\sqrt{M(l)M(l')}}\sum_{ss'}B^{(s)}(l)B^{s'}(l')\frac{1}{2\sqrt{\omega_s\omega_{s'}}}$$

$$\left\langle b_sb_{s'}\exp(-i\omega_st) + b_sb_{s'}^\dagger\exp(-i\omega_st) + b_s^\dagger b_{s'}\exp(i\omega_st) + b_s^\dagger b_{s'}^\dagger\exp(i\omega_st)\right\rangle$$

$$= \sum_{ss'}A_{\alpha\beta}^{ss'}(l,l')\left\langle b_sb_{s'}\exp(-i\omega_st) + b_sb_{s'}^\dagger\exp(-i\omega_st)\right.$$

$$\left. + b_s^\dagger b_{s'}\exp(i\omega_st) + b_s^\dagger b_{s'}^\dagger\exp(i\omega_st)\right\rangle, \tag{A.16}$$

where

$$A_{\alpha\beta}^{ss'}(l,l') = \frac{1}{\sqrt{M(l)M(l')}}B_\alpha^s(l)B_\beta^{s'}(l')\frac{1}{2\sqrt{\omega_s\omega_{s'}}} \tag{A.17}$$

Hence,

$$\left\langle u(l,t); u(l',0)\right\rangle = \sum_{ss'}A^{ss'}(l,l')$$

$$\left[b_sb_{s'}\exp(-i\omega_st) + b_sb_{s'}^\dagger\exp(-i\omega_st) + b_s^\dagger b_{s'}\exp(i\omega_st) + b_s^\dagger b_{s'}^\dagger\exp(i\omega_st)\right].$$
$$\tag{A.18}$$

We can translate this result for another correlation function $\langle u(l',0); u(l,t)\rangle$ by changing the dummy indices. So, we write

$$\left\langle u(l',0); u(l,t)\right\rangle = \sum_{ss'}A^{s's}(l',l)\left\langle \left(b_{s'} + b_{s'}^\dagger\right)\left(b_s\exp(-i\omega_st) + b_s^\dagger\exp(i\omega_st)\right)\right\rangle$$

$$= \sum_{ss'}A^{s's}(l',l)\left\langle b_{s'}b_s\exp(-i\omega_st) + b_{s'}b_s^\dagger\exp(i\omega_st)\right.$$

$$\left. + b_{s'}b_s\exp(i\omega_st) + b_{s'}^\dagger b_s^\dagger\exp(i\omega_st)\right\rangle$$

$$= \sum_{ss'}A^{s's}(l',l)\left\langle b_{s'}b_s\exp(-i\omega_st) + b_{s'}b_s^\dagger\exp(i\omega_st)\right.$$

$$\left. + b_{s'}b_s\exp(i\omega_st) + b_{s'}^\dagger b_s^\dagger\exp(i\omega_st)\right\rangle. \tag{A.19}$$

Therefore, the displacement-displacement Green's function can be written as

$$iD(l, l', t) = \Theta(t) \sum_{ss'} A^{ss'}(l, l') \Big\langle b_s b_{s'} \exp(-i\omega_s t) + b_s b_{s'}^\dagger \exp(-i\omega_s t)$$

$$+ b_s^\dagger b_{s'} \exp(i\omega_s t) + b_s^\dagger b_{s'}^\dagger \exp(i\omega_s t) \Big\rangle$$

$$+ \Theta(-t) \sum_{ss'} A^{s's}(l', l) \Big\langle b_{s'} b_s \exp(-i\omega_s t)$$

$$+ b_{s'} b_s^\dagger \exp(i\omega_s t) + b_{s'} b_s \exp(i\omega_s t) + b_{s'}^\dagger b_s^\dagger \exp(i\omega_s t) \Big\rangle$$

$$= \Big\langle \sum_{ss'} D^>(l, l', t) + \sum_{ss'} D^<(l, l', t) \Big\rangle . \tag{A.20}$$

Where

$$D^>(l, l', t) = \Theta(t) \exp(-i\omega_s t) A^{ss'}(l, l') \Big[ b_s b_{s'} + b_s b_{s'}^\dagger \Big]$$

$$+ \Theta(t) \exp(i\omega_s t) A^{ss'}(l, l') \Big[ b_s^\dagger b_{s'} + b_s^\dagger b_{s'}^\dagger \Big]$$

$$= D_1^>(l, l', 0) \Theta(t) \exp(-i\omega_s t) + D_2^>(l, l', 0) \Theta(t) \exp(i\omega_s t) , \tag{A.21}$$

considering

$$D_1^>(l, l', 0) = A^{ss'}(l, l') \Big[ b_s b_{s'} + b_s b_{s'}^\dagger \Big] + D_2^>(l, l', 0)$$

$$= A^{ss'}(l, l') \Big[ b_s^\dagger b_{s'} + b_s^\dagger b_{s'}^\dagger \Big] , \tag{A.22}$$

$$D^<(l, l', t) = \Theta(-t) \exp(-i\omega_s t) A^{s's}(l'l) \Big[ b_{s'} b_s + b_{s'}^\dagger b_s \Big]$$

$$+ \Theta(-t) \exp(i\omega_s t) A^{s's}(l'l) \Big[ b_{s'} b_s^\dagger + b_{s'}^\dagger b_s^\dagger \Big]$$

$$= D_1^<(l, l', 0) \Theta(-t) \exp(-i\omega_s t) + D_2^<(l, l', 0) \Theta(-t) \exp(i\omega_s t) , \tag{A.23}$$

considering

$$D_1^<(l, l', 0) = A^{s's}(l'l) \Big[ b_{s'} b_s + b_{s'}^\dagger b_s \Big]$$

$$D_2^<(l, l', 0) = A^{s's}(l'l) \Big[ b_{s'} b_s^\dagger + b_{s'}^\dagger b_s^\dagger \Big] . \tag{A.24}$$

To write down the Green's function in frequency ($\omega$) space, we consider Fourier transform from time (t) to frequency ($\omega$) as

$$D(l, l', \omega) = \int_{-\infty}^{\infty} dt D(l, l', t) \exp(i\omega t)$$

$$D(l, l', t) = \frac{1}{2\pi} \int_{-\infty}^{\infty} d\omega D(l, l', \omega) \exp(-i\omega t) . \tag{A.25}$$

We note down useful identities as

$$\frac{1}{2\pi}\int_{-\infty}^{\infty}d\omega\frac{i\exp(-i\omega t)}{\omega-\omega_s+i\eta}=+\exp(-i\omega_s t)\Theta(+t)$$

$$\frac{1}{2\pi}\int_{-\infty}^{\infty}d\omega\frac{i\exp(-i\omega t)}{\omega-\omega_s-i\eta}=-\exp(-i\omega_s t)\Theta(-t)$$

$$\int_{-\infty}^{\infty}dt\exp(i\omega t)\exp(-i\omega_s t)\Theta(+t)=+\frac{i}{\omega-\omega_s+i\eta}$$

$$\int_{-\infty}^{\infty}dt\exp(i\omega t)\exp(-i\omega_s t)\Theta(-t)=-\frac{i}{\omega-\omega_s-i\eta}\;. \tag{A.26}$$

Now, we write the Green's function in frequency space as

$$D(l,l',\omega)=\int_{-\infty}^{\infty}dtD(l,l',t)\exp(i\omega t)$$

$$=\int_{-\infty}^{\infty}dt[D^>(l,l',t)+D^<(l,l',t)]\exp(i\omega t) \tag{A.27}$$

Let us evaluate the first term in right hand side of the above equation Eq.(A.27) as

$$\int_{-\infty}^{\infty}dtD^>(l,l',t)\exp(i\omega t)$$

$$=D_1^>(l,l',0)\int_{-\infty}^{\infty}dt\exp(i\omega t)\exp(-i\omega_s t)\Theta(t)+D_2^>(l,l',0)$$

$$\int_{-\infty}^{\infty}dt\exp(i\omega t)\exp(i\omega_s t)\Theta(t)$$

$$=D_1^>(l,l',0)\frac{i}{\omega-\omega_s+i\eta}+D_2^>(l,l',0)\frac{i}{\omega+\omega_s+i\eta}\;, \tag{A.28}$$

whereas second term can be evaluated as

$$\int_{-\infty}^{\infty}dtD^<(l,l',t)\exp(i\omega t)$$

$$=D_1^<(l,l',0)\int_{-\infty}^{\infty}dt\exp(i\omega t)\exp(-i\omega_s t)\Theta(-t)+D_2^<(l,l',0)\int_{-\infty}^{\infty}dt\exp(i\omega t)\exp(i\omega_s t)\Theta(-t)$$

$$=D_1^<(l,l',0)\frac{-i}{\omega-\omega_s-i\eta}+D_2^<(l,l',0)\frac{-i}{\omega+\omega_s-i\eta}\;. \tag{A.29}$$

Using Eq(A.28) and Eq(A.29) in Eq(A.27), we obtain

$$
\begin{aligned}
&D(l, l', \omega) \\
&= \int_{-\infty}^{\infty} dt D(l, l', t) \exp(i\omega t) \\
&= D_1^>(l, l', 0)\frac{i}{\omega + i\eta - \omega_s} + D_2^>(l, l', 0)\frac{i}{\omega + i\eta + \omega_s} \\
&+ D_1^<(l, l', 0)\frac{-i}{\omega - i\eta - \omega_s} + D_2^<(l, l', 0)\frac{-i}{\omega - i\eta + \omega_s} \\
&= D_1^>(l, l', 0)\frac{i}{\omega + i\eta sgn(\omega) - \omega_s} \\
&+ D_2^>(l, l', 0)\frac{i}{\omega + i\eta sgn(\omega) + \omega_s} \\
&+ D_1^<(l, l', 0)\frac{-i}{\omega + i\eta sgn(\omega) - \omega_s} \\
&+ D_2^<(l, l', 0)\frac{-i}{\omega + i\eta sgn(\omega) + \omega_s} \\
&= \frac{i}{\omega^+ - \omega_s}\Big(D_1^>(l, l', 0) - D_1^<(l, l', 0)\Big) \\
&+ \frac{i}{\omega^+ + \omega_s}\Big(D_2^>(l, l', 0) - D_2^<(l, l', 0)\Big) \\
&= \frac{i}{\omega^+ - \omega_s}\Big(\sum_{ss'} A^{ss'}(l, l')\Big[b_s b_{s'} + b_s b_{s'}^\dagger\Big] \\
&- \sum_{ss'} A^{s's}(l'l)\Big[b_{s'} b_s + b_{s'}^\dagger b_s\Big]\Big) \\
&- \sum_{ss'} A^{s's}(l'l)\Big[b_{s'} b_s + b_{s'}^\dagger b_s\Big]\Big) \\
&+ \frac{i}{\omega^+ + \omega_s}\Big(\sum_{ss'} A^{ss'}(l, l')\Big[b_s^\dagger b_{s'} + b_s^\dagger b_{s'}^\dagger\Big] \\
&- \sum_{ss'} A^{s's}(l'l)\Big[b_{s'} b_s^\dagger + b_{s'}^\dagger b_s^\dagger\Big]\Big) \\
&= i\sum_{ss'} A^{ss'}\frac{1}{\omega^+ + -\omega_s}\Big([b_s b_{s'}] + [b_s b_{s'}^\dagger]\Big) \\
&+ i\sum_{ss'} A^{ss'}\frac{1}{\omega^+ + \omega_s}\Big([b_s^\dagger b_{s'}] + [b_s^\dagger b_{s'}^\dagger]\Big) \\
&= i\sum_{ss'} A^{ss'}\frac{1}{\omega^+ - \omega_s}\delta_{ss'} - \sum_{ss'} A^{ss'}\frac{1}{\omega^+ + \omega_s}\delta_{ss'} \\
&= i\sum_{s} A^{s}\frac{1}{\omega^+ - \omega_s} - i\sum_{s} A^{s}\frac{1}{\omega^+ + \omega_s}
\end{aligned}
\tag{A.30}
$$

Using Eq(A.28) and Eq(A.29) in Eq(A.27), we obtain

$$
D(l, l', \omega)
$$

$$
= \int_{-\infty}^{\infty} dt D(l, l', t) \exp(i\omega t)
$$

$$
= D_1^>(l, l', 0)\frac{i}{\omega + i\eta - \omega_s} + D_2^>(l, l', 0)\frac{i}{\omega + i\eta + \omega_s}
$$

$$
+ D_1^<(l, l', 0)\frac{-i}{\omega - i\eta - \omega_s} + D_2^<(l, l', 0)\frac{-i}{\omega - i\eta + \omega_s}
$$

$$
= D_1^>(l, l', 0)\frac{i}{\omega + i\eta \, sgn(\omega) - \omega_s} + D_2^>(l, l', 0)\frac{i}{\omega + i\eta \, sgn(\omega) + \omega_s}
$$

$$
+ D_1^<(l, l', 0)\frac{-i}{\omega + i\eta \, sgn(\omega) - \omega_s} + D_2^<(l, l', 0)\frac{-i}{\omega + i\eta \, sgn(\omega) + \omega_s}
$$

$$
= \frac{i}{\omega^+ - \omega_s}\left( D_1^>(l, l', 0) - D_1^<(l, l', 0) \right)
$$

$$
+ \frac{i}{\omega^+ + \omega_s}\left( D_2^>(l, l', 0) - D_2^<(l, l', 0) \right)
$$

$$
= \frac{i}{\omega^+ - \omega_s}\left( \sum_{ss'} A^{ss'}(l, l')\left[ b_s b_{s'} + b_s b_{s'}^\dagger \right] \right.
$$

$$
- \sum_{ss'} A^{s's}(l'l)\left[ b_{s'} b_s + b_{s'}^\dagger b_s \right] \Bigg)
$$

$$
+ \frac{i}{\omega^+ + \omega_s}\left( \sum_{ss'} A^{ss'}(l, l')\left[ b_s^\dagger b_{s'} + b_s^\dagger b_{s'}^\dagger \right] \right.
$$

$$
- \sum_{ss'} A^{s's}(l'l)\left[ b_{s'} b_s^\dagger + b_{s'}^\dagger b_s^\dagger \right] \Bigg)
$$

$$
= i\sum_{ss'} A^{ss'}\frac{1}{\omega^+ + -\omega_s}\left( [b_s b_{s'}] + [b_s b_{s'}^\dagger] \right) + i\sum_{ss'} A^{ss'}\frac{1}{\omega^+ + \omega_s}\left( [b_s^\dagger b_{s'}] + [b_s^\dagger b_{s'}^\dagger] \right)
$$

$$
= i\sum_{ss'} A^{ss'}\frac{1}{\omega^+ - \omega_s}\delta_{ss'} - \sum_{ss'} A^{ss'}\frac{1}{\omega^+ + \omega_s}\delta_{ss'}
$$

$$
= i\sum_{s} A^s\frac{1}{\omega^+ - \omega_s} - i\sum_{s} A^s\frac{1}{\omega^+ + \omega_s}
$$

$$
= i\sum_{s} A^s\left( \frac{1}{\omega^+ - \omega_s} - \frac{1}{\omega^+ + \omega_s} \right)
$$

$$
= i\sum_{s} A^s\frac{2\omega_s}{(\omega^+)^2 - \omega_s^2}
$$

$$
= i\sum_{s} \frac{1}{\sqrt{M(l)M(l')}}B^s(l)B^s(l')\frac{1}{2\sqrt{\omega_s\omega_s}}2\omega_s\frac{1}{(\omega^+)^2 - \omega_s^2}
$$

$$
= i\frac{1}{\sqrt{M(l)M(l')}}\sum_{s} B^s(l)B^s(l')\frac{1}{(\omega^+)^2 - \omega_s^2} \ . \tag{A.31}
$$

This way, we obtain displacement-displacement retarded Green's function in frequency ($\omega$) space as

$$iD(l,l',\omega) = i\frac{1}{\sqrt{M(l)M(l')}}\sum_s B^s(l)B^s(l')\frac{1}{(\omega^+)^2 - \omega_s^2} \; . \qquad (A.32)$$

Now, we define normalized density of states from this Green's function. From Eq.(A.32), we find

$$iD(l,l',\omega) = \frac{i}{\sqrt{M(l)M(l')}}\sum_s B^s(l)B^s(l')\frac{1}{(\omega^+)^2 - \omega_s^2} \qquad (A.33)$$

Multiplying $2\omega^+$ in numerator and denominator of the right hand side of the above equation, we find

$$
\begin{aligned}
iD(l,l',\omega^2) &= \frac{i}{\sqrt{M(l)M(l')}}\sum_s B^s(l)B^s(l')\frac{1}{2\omega^+}\frac{2\omega^+}{(\omega^+)^2 - \omega_s^2} \\
&= \frac{i}{\sqrt{M(l)M(l')}}\sum_s B^s(l)B^s(l')\frac{1}{2\omega^+}\left[\frac{1}{\omega^+ - \omega_s} + \frac{1}{\omega^+ + \omega_s}\right] \qquad (A.34)
\end{aligned}
$$

Here we define density of states (DOS) as

$$\text{DOS}(\omega^2) = -\frac{Im}{\pi}\int_0^\infty d\omega\, 2\omega^+ \sqrt{M(l)}D(l,l',\omega^2)\sqrt{M(l')} \; , \qquad (A.35)$$

which is normalized as shown below:

$$
\begin{aligned}
-\frac{Im}{\pi}\int_0^\infty &d\omega\, 2\omega^+ \sqrt{M(l)}D(l,l',\omega)\sqrt{M(l')} \\
&= \sum_s B^s(l)B^s(l')[\delta(\omega - \omega_s) + \delta(\omega + \omega_s)] \\
&= \sum_s B^s(l)B^s(l') \\
&= \delta_{ll'} \; . \qquad (A.36)
\end{aligned}
$$

Thus, normalized phonon density of states in the disordered systems reads as

$$\text{DOS}(\omega^2) = -\frac{Im}{\pi}\int_0^\infty d\omega\, 2\omega^+ \sqrt{M(l)}D(l,l',\omega^2)\sqrt{M(l')} = \delta_{ll'} \; . \qquad (A.37)$$

# Bibliography

[1] P. W. Anderson. Absence of diffusion in certain random lattices. *Phys. Rev.*, 109:1492–1505, 1958.

[2] Patrick A. Lee and T. V. Ramakrishnan. Disordered electronic systems. *Rev. Mod. Phys.*, 57:287–337, Apr 1985. doi: 10.1103/RevModPhys.57.287. URL https://link.aps.org/doi/10.1103/RevModPhys.57.287.

[3] P Phillips. Anderson localization and the exceptions. *Annual Review of Physical Chemistry*, 44(1):115–144, 1993. doi: 10.1146/annurev.pc.44.100193.000555. URL https://doi.org/10.1146/annurev.pc.44.100193.000555.

[4] Ferdinand Evers and Alexander D. Mirlin. Anderson transitions. *Rev. Mod. Phys.*, 80:1355–1417, Oct 2008. doi: 10.1103/RevModPhys.80.1355. URL https://link.aps.org/doi/10.1103/RevModPhys.80.1355.

[5] Daniel Steck. Paralysed by disorder. *Nature*, 453:866, 2008.

[6] A. lagendijk, B. Tiggelen, and S. Wiersma. Fifty years of anderson localization. *Physics Today*, 62:24–29, 2009.

[7] Elihu Abrahams. *50 Years of Anderson Localization.* WORLD SCIENTIFIC, 2010. doi: 10.1142/7663. URL https://www.worldscientific.com/doi/abs/10.1142/7663.

[8] N. Bloembergen. On the interaction of nuclear spins in a crystalline lattice. *Physica*, 15:386–426, 1958.

[9] A.M Portis. Spectral diffusion in magnetic resonance. *Phys. Rev*, 104:584, 1956.

[10] G. Feher and E.A Gere. Electron spin resonance experiments on donors in silicon. ii. electron spin relaxation effects. *Phys. Rev*, 114:1245, 1959.

[11] Jean Philibert. One and a half century of diffusion: Fick, einstein, before and beyond. *Diffusion Fundamentals*, 2, 11 2004.

[12] D J Thouless. Anderson's theory of localized states. *Journal of Physics C: Solid State Physics*, 3(7):1559, 1970. URL `http://stacks.iop.org/0022-3719/3/i=7/a=012`.

[13] R Abou-Chacra, D J Thouless, and P W Anderson. A selfconsistent theory of localization. *Journal of Physics C: Solid State Physics*, 6(10):1734, 1973. URL `http://stacks.iop.org/0022-3719/6/i=10/a=009`.

[14] D J Thouless. Anderson's theory of localized states. *Journal of Physics C: Solid State Physics*, 3(7):1559, 1970. URL `http://stacks.iop.org/0022-3719/3/i=7/a=012`.

[15] D.J. Thouless. Electrons in disordered systems and the theory of localization. *Physics Reports*, 13(3):93 – 142, 1974. ISSN 0370-1573. doi: https://doi.org/10.1016/0370-1573(74)90029-5. URL `http://www.sciencedirect.com/science/article/pii/0370157374900295`.

[16] Franz J. Wegner. Electrons in disordered systems. scaling near the mobility edge. *Zeitschrift für Physik B Condensed Matter*, 25(4):327–337, Dec 1976. ISSN 1431-584X. doi: 10.1007/BF01315248. URL `https://doi.org/10.1007/BF01315248`.

[17] E. Abrahams, P. W. Anderson, D. C. Licciardello, and T. V. Ramakrishnan. Scaling theory of localization: Absence of quantum diffusion in two dimensions. *Phys. Rev. Lett.*, 42:673–676, 1979.

[18] J T Edwards and D J Thouless. Numerical studies of localization in disordered systems. *Journal of Physics C: Solid State Physics*, 5(8):807, 1972. URL `http://stacks.iop.org/0022-3719/5/i=8/a=007`.

[19] D C Licciardello and D J Thouless. Conductivity and mobility edges for two-dimensional disordered systems. *Journal of Physics C: Solid State Physics*, 8 (24):4157, 1975. URL `http://stacks.iop.org/0022-3719/8/i=24/a=009`.

[20] A. MacKinnon and B. Kramer. One-parameter scaling of localization length and conductance in disordered systems. *Phys. Rev. Lett.*, 47:1546–1549, Nov 1981. doi: 10.1103/PhysRevLett.47.1546. URL `https://link.aps.org/doi/10.1103/PhysRevLett.47.1546`.

[21] P. Prelovsek. Conductor-insulator transition in the anderson model of a disordered solid. *Phys. Rev. B*, 23:1304–1319, Feb 1981. doi: 10.1103/PhysRevB.23.1304. URL `https://link.aps.org/doi/10.1103/PhysRevB.23.1304`.

[22] Sanjoy Sarker and Eytan Domany. Scaling theory of anderson localization: A renormalization-group approach. *Phys. Rev. B*, 23: 6018–6036, Jun 1981. doi: 10.1103/PhysRevB.23.6018. URL `https://link.aps.org/doi/10.1103/PhysRevB.23.6018`.

[23] D. Vollhardt and P. Wölfle. Scaling equations from a self-consistent theory of anderson localization. *Phys. Rev. Lett.*, 48: 699–702, Mar 1982. doi: 10.1103/PhysRevLett.48.699. URL `https://link.aps.org/doi/10.1103/PhysRevLett.48.699`.

[24] W. Götze. The mobility of a quantum particle in a three-dimensional random potential. *Philosophical Magazine B*, 43 (2):219–250, 1981. doi: 10.1080/13642818108221896. URL `https://doi.org/10.1080/13642818108221896`.

[25] A. MacKinnon and B. Kramer. The scaling theory of electrons in disordered solids: Additional numerical results. *Zeitschrift für Physik B Condensed Matter*, 53(1):1–13, Mar 1983. ISSN 1431-584X. doi: 10.1007/BF01578242. URL `https://doi.org/10.1007/BF01578242`.

[26] B. R. Bulka, B. Kramer, and A. MacKinnon. Mobility edge in the three dimensional anderson model. *Physik B Condensed Matter*, 60:13–17, 1985. URL `https://doi.org/10.1007/BF01312638`.

[27] M. Schreiber. Fractal character of eigenstates in weakly disordered three-dimensional systems. *Phys. Rev. B*, 31:6146–6149, May 1985. doi: 10.1103/PhysRevB.31.6146. URL `https://link.aps.org/doi/10.1103/PhysRevB.31.6146`.

[28] E. N. Economou and C. M. Soukoulis. Connection of localization with the problem of the bound state in a potential well. *Phys. Rev. B*, 28:1093–1094, Jul 1983. doi: 10.1103/PhysRevB.28.1093. URL `https://link.aps.org/doi/10.1103/PhysRevB.28.1093`.

[29] E. N. Economou, C. M. Soukoulis, and A. D. Zdetsis. Localized states in disordered systems as bound states in potential wells. *Phys. Rev. B*, 30:1686–1694, Aug 1984. doi: 10.1103/PhysRevB.30.1686. URL `https://link.aps.org/doi/10.1103/PhysRevB.30.1686`.

[30] B. Bulka, M. Schreiber, and B. Kramer. Localization, quantum interference, and the metal-insulator transition. *Zeitschrift für Physik B Condensed Matter*, 66(1):21–30, Mar 1987. ISSN 1431-584X. doi: 10.1007/BF01312758. URL `https://doi.org/10.1007/BF01312758`.

[31] Patrick A. Lee. Real-space scaling studies of localization. *Phys. Rev. Lett.*, 42:1492–1494, May 1979. doi: 10.1103/PhysRevLett.42.1492. URL `https://link.aps.org/doi/10.1103/PhysRevLett.42.1492`.

[32] D. Vollhardt and P. Wölfle. Diagrammatic, self-consistent treatment of the anderson localization problem in $d \leq 2$ dimensions. *Phys. Rev. B*, 22:4666–4679, Nov 1980. doi: 10.1103/PhysRevB.22.4666. URL `https://link.aps.org/doi/10.1103/PhysRevB.22.4666`.

[33] D. Vollhardt and P. Wölfle. Anderson localization in $d \leq 2$ dimensions: A self-consistent diagrammatic theory. *Phys. Rev. Lett.*, 45:842–846, Sep 1980. doi: 10.1103/PhysRevLett.45.842. URL `https://link.aps.org/doi/10.1103/PhysRevLett.45.842`.

[34] Franz Wegner. The mobility edge problem: Continuous symmetry and a conjecture. *Zeitschrift für Physik B Condensed Matter*, 35(3):207–210, Sep 1979. ISSN 1431-584X. doi: 10.1007/BF01319839. URL `https://doi.org/10.1007/BF01319839`.

[35] K.B. Efetov. Supersymmetry and theory of disordered metals. *Advances in Physics*, 32(1):53–127, 1983. doi: 10.1080/00018738300101531. URL `https://doi.org/10.1080/00018738300101531`.

[36] Shinobu Hikami. Localization, Nonlinear $\sigma$ Model and String Theory. *Progress of Theoretical Physics Supplement*, 107:213–227, 01 1992. ISSN 0375-9687. doi: 10.1143/PTPS.107.213. URL `https://doi.org/10.1143/PTPS.107.213`.

[37] Eugene P. Wigner. On a class of analytic functions from the quantum theory of collisions. 53(1):36–67, 1951. ISSN 0003486X. doi: 10.2307/1969342. URL `http://www.jstor.org/stable/1969342`.

[38] Freeman J. Dyson. The threefold way. algebraic structure of symmetry groups and ensembles in quantum mechanics. *Journal of Mathematical Physics*, 3(6):1199–1215, 1962. doi: 10.1063/1.1703863. URL `https://doi.org/10.1063/1.1703863`.

[39] E. Hofstetter and M. Schreiber. Statistical properties of the eigenvalue spectrum of the three-dimensional anderson hamiltonian. *Phys. Rev. B*, 48:16979–16985, Dec 1993. doi: 10.1103/PhysRevB.48.16979. URL `https://link.aps.org/doi/10.1103/PhysRevB.48.16979`.

[40] Nevill Francis Mott and Edward A Davis. *Electronic Processes in Non-Crystalline Materials.* Oxford : Oxford University Press, 2nd ed edition, 2012. ISBN 9780191023286. URL `http://qut.eblib.com.au/patron/FullRecord.aspx?p=1507491`. Description based upon print version of record.

[41] I. Kh. Zharekeshev and B. Kramer. Scaling of level statistics at the disorder-induced metal-insulator transition. *Phys. Rev. B*, 51: 17239–17242, Jun 1995. doi: 10.1103/PhysRevB.51.17239. URL `https://link.aps.org/doi/10.1103/PhysRevB.51.17239`.

[42] Isa Kh. Zharekeshev and Bernhard Kramer. Asymptotics of universal probability of neighboring level spacings at the anderson transition. *Phys. Rev. Lett.*, 79:717–720, Jul 1997. doi: 10.1103/PhysRevLett.79.717. URL `https://link.aps.org/doi/10.1103/PhysRevLett.79.717`.

[43] Imre Varga, Etienne Hofstetter, Michael Schreiber, and János Pipek. Shape analysis of the level-spacing distribution around the metal-insulator transition in the three-dimensional anderson model. *Phys. Rev. B*, 52:7783–7786, Sep 1995. doi: 10.1103/PhysRevB.52.7783. URL `https://link.aps.org/doi/10.1103/PhysRevB.52.7783`.

[44] Arkady G. Aronov, Vladimir E. Kravtsov, and Igor V. Lerner. Spectral correlations in disordered electronic systems: Crossover from metal to insulator regime. *Phys. Rev. Lett.*, 74:1174–1177, Feb 1995. doi: 10.1103/PhysRevLett.74.1174. URL `https://link.aps.org/doi/10.1103/PhysRevLett.74.1174`.

[45] C Castellani and L Peliti. *Journal of Physics A: Mathematical and General*, 19(8):L429–L432, jun 1986. doi: 10.1088/0305-4470/19/8/004. URL `https://doi.org/10.1088`.

[46] Bodo Huckestein. Scaling theory of the integer quantum hall effect. *Rev. Mod. Phys.*, 67:357–396, Apr 1995. doi: 10.1103/RevModPhys.67.357. URL `https://link.aps.org/doi/10.1103/RevModPhys.67.357`.

[47] MARTIN JANSSEN. Multifractal analysis of broadly-distributed observables at criticality. *International Journal of Modern Physics B*, 08(08):943–984, 1994. doi: 10.1142/S021797929400049X. URL `https://doi.org/10.1142/S021797929400049X`.

[48] Matthew S. Foster, Shinsei Ryu, and Andreas W. W. Ludwig. Termination of typical wave-function multifractal spectra at the anderson metal-insulator transition: Field theory description using the functional renormalization group. *Phys. Rev. B*, 80:075101, Aug 2009. doi: 10.1103/PhysRevB.80.075101. URL `https://link.aps.org/doi/10.1103/PhysRevB.80.075101`.

[49] Renate Gade and Franz Wegner. The n = 0 replica limit of u(n) and u(n)so(n) models. *Nuclear Physics B*, 360(2):213 – 218, 1991. ISSN 0550-3213. doi: https://doi.org/10.1016/0550-3213(91)90401-I. URL `http://www.sciencedirect.com/science/article/pii/055032139190401I`.

[50] Renate Gade. Anderson localization for sublattice models. *Nuclear Physics B*, 398(3):499 – 515, 1993. ISSN 0550-3213. doi: https://doi.org/10.1016/0550-3213(93)90601-K. URL `http://www.sciencedirect.com/science/article/pii/055032139390601K`.

[51] Alexander Altland and Martin R. Zirnbauer. Nonstandard symmetry classes in mesoscopic normal-superconducting hybrid structures. *Phys. Rev. B*, 55:1142–1161, Jan 1997. doi: 10.1103/PhysRevB.55.1142. URL `https://link.aps.org/doi/10.1103/PhysRevB.55.1142`.

[52] Martin R. Zirnbauer. Riemannian symmetric superspaces and their origin in random-matrix theory. *Journal of Mathematical Physics*, 37(10):4986–5018, 1996. doi: 10.1063/1.531675. URL `https://doi.org/10.1063/1.531675`.

[53] Eduardo V. Castro, M. Pilar López-Sancho, and María A. H. Vozmediano. Anderson localization and topological transition in chern insulators. *Phys. Rev. B*, 92:085410, Aug 2015. doi: 10.1103/PhysRevB.92.085410. URL `https://link.aps.org/doi/10.1103/PhysRevB.92.085410`.

[54] H. Grussbach and M. Schreiber. Determination of the mobility edge in the anderson model of localization in three dimensions by multifractal analysis. *Phys. Rev. B*, 51:663–666, Jan 1995. doi: 10.1103/PhysRevB.51.663. URL `https://link.aps.org/doi/10.1103/PhysRevB.51.663`.

[55] Franz Wegner. Four-loop-order $\beta$-function of nonlinear $\sigma$-models in symmetric spaces. *Nuclear Physics B*, 316(3):663 – 678, 1989. ISSN 0550-3213. doi: https://doi.org/10.1016/0550-3213(89)90063-1. URL `http://www.sciencedirect.com/science/article/pii/0550321389900631`.

[56] Keith Slevin and Tomi Ohtsuki. Critical exponent for the anderson transition in the three-dimensional orthogonal universality class. *New Journal of Physics*, 16(1):015012, jan 2014. doi: 10.1088/1367-2630/16/1/015012. URL `https://doi.org/10.1088`.

[57] Keith Slevin and Tomi Ohtsuki. Corrections to scaling at the anderson transition. *Phys. Rev. Lett.*, 82:382–385, Jan 1999. doi: 10.1103/PhysRevLett.82.382. URL `https://link.aps.org/doi/10.1103/PhysRevLett.82.382`.

[58] Alberto Rodriguez, Louella J. Vasquez, Keith Slevin, and Rudolf A. Römer. Multifractal finite-size scaling and universality at the anderson transition. *Phys. Rev. B*, 84:134209, Oct 2011. doi: 10.1103/PhysRevB.84.134209. URL `https://link.aps.org/doi/10.1103/PhysRevB.84.134209`.

[59] Alberto Rodriguez, Louella J. Vasquez, Keith Slevin, and Rudolf A. Römer. Critical parameters from a generalized multifractal analysis at the anderson transition. *Phys. Rev. Lett.*, 105:

046403, Jul 2010. doi: 10.1103/PhysRevLett.105.046403. URL https://link.aps.org/doi/10.1103/PhysRevLett.105.046403.

[60] E. Tarquini, G. Biroli, and M. Tarzia. Critical properties of the anderson localization transition and the high-dimensional limit. *Phys. Rev. B*, 95:094204, Mar 2017. doi: 10.1103/PhysRevB.95.094204. URL https://link.aps.org/doi/10.1103/PhysRevB.95.094204.

[61] Yoshiki Ueoka and Keith Slevin. Dimensional dependence of critical exponent of the anderson transition in the orthogonal universality class. *Journal of the Physical Society of Japan*, 83(8):084711, 2014. doi: 10.7566/JPSJ.83.084711. URL https://doi.org/10.7566/JPSJ.83.084711.

[62] J. M. Deutsch. Quantum statistical mechanics in a closed system. *Phys. Rev. A*, 43:2046–2049, Feb 1991. doi: 10.1103/PhysRevA.43.2046. URL https://link.aps.org/doi/10.1103/PhysRevA.43.2046.

[63] Mark Srednicki. Chaos and quantum thermalization. *Phys. Rev. E*, 50:888–901, Aug 1994. doi: 10.1103/PhysRevE.50.888. URL https://link.aps.org/doi/10.1103/PhysRevE.50.888.

[64] Rahul Nandkishore and David A. Huse. Many-body localization and thermalization in quantum statistical mechanics. *Annual Review of Condensed Matter Physics*, 6(1):15–38, 2015. doi: 10.1146/annurev-conmatphys-031214-014726. URL https://doi.org/10.1146/annurev-conmatphys-031214-014726.

[65] Ehud Altman and Ronen Vosk. Universal dynamics and renormalization in many-body-localized systems. *Annual Review of Condensed Matter Physics*, 6(1):383–409, 2015. doi: 10.1146/annurev-conmatphys-031214-014701. URL https://doi.org/10.1146/annurev-conmatphys-031214-014701.

[66] John Z. Imbrie. Diagonalization and many-body localization for a disordered quantum spin chain. *Phys. Rev. Lett.*, 117:

027201, Jul 2016. doi: 10.1103/PhysRevLett.117.027201. URL
`https://link.aps.org/doi/10.1103/PhysRevLett.117.027201`.

[67] I. V. Gornyi, A. D. Mirlin, and D. G. Polyakov. Interacting electrons in
disordered wires: Anderson localization and low-$t$ transport. *Phys. Rev.
Lett.*, 95:206603, Nov 2005. doi: 10.1103/PhysRevLett.95.206603. URL
`https://link.aps.org/doi/10.1103/PhysRevLett.95.206603`.

[68] Wojciech De Roeck, Francois Huveneers, Markus Müller, and Mauro
Schiulaz. Absence of many-body mobility edges. *Phys. Rev. B*,
93:014203, Jan 2016. doi: 10.1103/PhysRevB.93.014203. URL
`https://link.aps.org/doi/10.1103/PhysRevB.93.014203`.

[69] James R. Garrison, Ryan V. Mishmash, and Matthew P. A. Fisher. Par-
tial breakdown of quantum thermalization in a hubbard-like model. *Phys.
Rev. B*, 95:054204, Feb 2017. doi: 10.1103/PhysRevB.95.054204. URL
`https://link.aps.org/doi/10.1103/PhysRevB.95.054204`.

[70] I. Vakulchyk, I. Yusipov, M. Ivanchenko, S. Flach, and S. Denisov. Signa-
tures of many-body localization in steady states of open quantum systems.
*Phys. Rev. B*, 98:020202, Jul 2018. doi: 10.1103/PhysRevB.98.020202. URL
`https://link.aps.org/doi/10.1103/PhysRevB.98.020202`.

[71] A L Efros and B I Shklovskii. Coulomb gap and low temperature conductivity
of disordered systems. *Journal of Physics C: Solid State Physics*, 8(4):L49–L51,
feb 1975. doi: 10.1088/0022-3719/8/4/003. URL `https://doi.org/10.1088`.

[72] A.A. Gogolin. Electron localization and hopping conductivity in one-
dimensional disordered systems. *Physics Reports*, 86(1):1 – 53, 1982.
ISSN 0370-1573. doi: https://doi.org/10.1016/0370-1573(82)90069-2. URL
`http://www.sciencedirect.com/science/article/pii/0370157382900692`.

[73] A. B. Fowler, A. Hartstein, and R. A. Webb. Conductance in
restricted-dimensionality accumulation layers. *Phys. Rev. Lett.*,

48:196–199, Jan 1982. doi: 10.1103/PhysRevLett.48.196. URL `https://link.aps.org/doi/10.1103/PhysRevLett.48.196`.

[74] C. P. Umbach, S. Washburn, R. B. Laibowitz, and R. A. Webb. Magnetoresistance of small, quasi-one-dimensional, normal-metal rings and lines. *Phys. Rev. B*, 30:4048–4051, Oct 1984. doi: 10.1103/PhysRevB.30.4048. URL `https://link.aps.org/doi/10.1103/PhysRevB.30.4048`.

[75] J. C. Licini, D. J. Bishop, M. A. Kastner, and J. Melngailis. Aperiodic magnetoresistance oscillations in narrow inversion layers in si. *Phys. Rev. Lett.*, 55:2987–2990, Dec 1985. doi: 10.1103/PhysRevLett.55.2987. URL `https://link.aps.org/doi/10.1103/PhysRevLett.55.2987`.

[76] R. G. Wheeler, K. K. Choi, A. Goel, R. Wisnieff, and D. E. Prober. Localization and electron-electron interaction effects in submicron-width inversion layers. *Phys. Rev. Lett.*, 49:1674–1677, Nov 1982. doi: 10.1103/PhysRevLett.49.1674. URL `https://link.aps.org/doi/10.1103/PhysRevLett.49.1674`.

[77] P. A. Lee, A. Douglas Stone, and H. Fukuyama. Universal conductance fluctuations in metals: Effects of finite temperature, interactions, and magnetic field. *Phys. Rev. B*, 35:1039–1070, Jan 1987. doi: 10.1103/PhysRevB.35.1039. URL `https://link.aps.org/doi/10.1103/PhysRevB.35.1039`.

[78] J. I. Pascual, J. Méndez, J. Gómez-Herrero, A. M. Baró, N. Garcia, Uzi Landman, W. D. Luedtke, E. N. Bogachek, and H. P. Cheng. Properties of metallic nanowires: From conductance quantization to localization. *Science*, 267(5205): 1793–1795, 1995. ISSN 0036-8075. doi: 10.1126/science.267.5205.1793. URL `https://science.sciencemag.org/content/267/5205/1793`.

[79] C. Gómez-Navarro, P. J. De Pablo, J. Gómez-Herrero, B. Biel, F. J. Garcia-Vidal, A. Rubio, and F. Flores. Tuning the conductance of single-walled carbon nanotubes by ion irradiation in the anderson localization regime. *Nat. Mater.*, 4:534–539, 2005. URL `https://doi.org/10.1038/nmat1414`.

[80] Gerd Bergmann. Weak localization in thin films: a time-of-flight experiment with conduction electrons. *Physics Reports*, 107(1):1 – 58, 1984. ISSN 0370-1573. doi: https://doi.org/10.1016/0370-1573(84)90103-0. URL `http://www.sciencedirect.com/science/article/pii/0370157384901030`.

[81] G. J. Dolan and D. D. Osheroff. Nonmetallic conduction in thin metal films at low temperatures. *Phys. Rev. Lett.*, 43: 721–724, Sep 1979. doi: 10.1103/PhysRevLett.43.721. URL `https://link.aps.org/doi/10.1103/PhysRevLett.43.721`.

[82] R. S. Markiewicz and L. A. Harris. Two-dimensional resistivity of ultrathin metal films. *Phys. Rev. Lett.*, 46:1149–1153, Apr 1981. doi: 10.1103/PhysRevLett.46.1149. URL `https://link.aps.org/doi/10.1103/PhysRevLett.46.1149`.

[83] Gerd Bergmann. Quantitative analysis of weak localization in thin mg films by magnetoresistance measurements. *Phys. Rev. B*, 25:2937–2939, Feb 1982. doi: 10.1103/PhysRevB.25.2937. URL `https://link.aps.org/doi/10.1103/PhysRevB.25.2937`.

[84] Gerd Bergmann. Measurement of the magnetic scattering time by weak localization. *Phys. Rev. Lett.*, 49:162–164, Jul 1982. doi: 10.1103/PhysRevLett.49.162. URL `https://link.aps.org/doi/10.1103/PhysRevLett.49.162`.

[85] L. Van den dries, C. Van Haesendonck, Y. Bruynseraede, and G. Deutscher. Two-dimensional localization in thin copper films. *Phys. Rev. Lett.*, 46:565–568, Feb 1981. doi: 10.1103/PhysRevLett.46.565. URL `https://link.aps.org/doi/10.1103/PhysRevLett.46.565`.

[86] Isam Manai, Jean-Fran çois Clément, Radu Chicireanu, Clément Hainaut, Jean Claude Garreau, Pascal Szriftgiser, and Dominique Delande. Experimental observation of two-dimensional anderson localization with the atomic kicked rotor. *Phys. Rev. Lett.*, 115:

240603, Dec 2015. doi: 10.1103/PhysRevLett.115.240603. URL `https://link.aps.org/doi/10.1103/PhysRevLett.115.240603`.

[87] H. Eschrig. D. m. finlayson (ed.). localization and interaction in disordered metals and doped semiconductors. proc. 31st scottish universities summer school in physics. edinburgh university press and redwood burn ltd, trowbridge, 1986; xv, 393 pages, 202 figures, 5 tables, isbn 0-905945-14-x. *Crystal Research and Technology*, 23(9):1084–1084, 1988. doi: 10.1002/crat.2170230905. URL `https://onlinelibrary.wiley.com/doi/abs/10.1002/crat.2170230905`.

[88] Shingo Katsumoto, Fumio Komori, Naokatsu Sano, and Shun-ichi Kobayashi. Fine tuning of metal-insulator transition in al0.3ga0.7as using persistent photoconductivity. *Journal of the Physical Society of Japan*, 56(7):2259–2262, 1987. doi: 10.1143/JPSJ.56.2259. URL `https://doi.org/10.1143/JPSJ.56.2259`.

[89] T. Siegrist, P. Jost, H. Volker, M. Woda, P. Merkelbach, C. Schlockermann, and M. Wuttig. Disorder-induced localization in crystalline phasechange materials. *Nature Materials*, 10:202 EP –, Jan 2011. URL `https://doi.org/10.1038/nmat2934`. Article.

[90] W. Zhang, A. Thiess, P. Zalden, R. Zeller, P. H. Dederichs, J.-Y. Raty, M. Wuttig, S. Blügel, and R. Mazzarello. Role of vacancies in metal-insulator transitions of crystalline phase-change materials. *Nature Materials*, 11:952 EP –, Oct 2012. URL `https://doi.org/10.1038/nmat3456`. Article.

[91] Peter Jost, Hanno Volker, Annika Poitz, Christian Poltorak, Peter Zalden, Tobias Schäfer, Felix R. L. Lange, Rüdiger M. Schmidt, Bernd Holländer, Matti R. Wirtssohn, and Matthias Wuttig. Disorder-induced localization in crystalline pseudo-binary gete–sb2te3 alloys between ge3sb2te6 and gete. *Advanced Functional Materials*, 25(40):6399–6406, 2015. doi: 10.1002/adfm.201500848. URL `https://onlinelibrary.wiley.com/doi/abs/10.1002/adfm.201500848`.

[92] A J Williams, T M McQueen, V Ksenofontov, C Felser, and R J Cava. The metal–insulator transition in fe1.01-xCuxSe. *Journal of Physics: Condensed Matter*, 21(30):305701, jul 2009. doi: 10.1088/0953-8984/21/30/305701. URL `https://doi.org/10.1088`.

[93] Tianping Ying, Yueqiang Gu, Xiao Chen, Xinbo Wang, Shifeng Jin, Linlin Zhao, Wei Zhang, and Xiaolong Chen. Anderson localization of electrons in single crystals: Lixfe7se8. *Science Advances*, 2(2), 2016. doi: 10.1126/sciadv.1501283. URL `https://advances.sciencemag.org/content/2/2/e1501283`.

[94] Klaus von Klitzing. The quantized hall effect. *Rev. Mod. Phys.*, 58:519–531, Jul 1986. doi: 10.1103/RevModPhys.58.519. URL `https://link.aps.org/doi/10.1103/RevModPhys.58.519`.

[95] A. M. M. Pruisken. Universal singularities in the integral quantum hall effect. *Phys. Rev. Lett.*, 61:1297–1300, Sep 1988. doi: 10.1103/PhysRevLett.61.1297. URL `https://link.aps.org/doi/10.1103/PhysRevLett.61.1297`.

[96] Wanli Li, C. L. Vicente, J. S. Xia, W. Pan, D. C. Tsui, L. N. Pfeiffer, and K. W. West. Scaling in plateau-to-plateau transition: A direct connection of quantum hall systems with the anderson localization model. *Phys. Rev. Lett.*, 102:216801, May 2009. doi: 10.1103/PhysRevLett.102.216801. URL `https://link.aps.org/doi/10.1103/PhysRevLett.102.216801`.

[97] Keith Slevin and Tomi Ohtsuki. Critical exponent for the quantum hall transition. *Phys. Rev. B*, 80:041304, Jul 2009. doi: 10.1103/PhysRevB.80.041304. URL `https://link.aps.org/doi/10.1103/PhysRevB.80.041304`.

[98] H. Obuse, A. R. Subramaniam, A. Furusaki, I. A. Gruzberg, and A. W. W. Ludwig. Conformal invariance, multifractality, and finite-size scaling at anderson localization transitions in two dimensions. *Phys. Rev. B*, 82:035309, Jul 2010. doi: 10.1103/PhysRevB.82.035309. URL `https://link.aps.org/doi/10.1103/PhysRevB.82.035309`.

[99] M. Amado, A. V. Malyshev, A. Sedrakyan, and F. Domínguez-Adame. Numerical study of the localization length critical index in a network model of plateau-plateau transitions in the quantum hall effect. *Phys. Rev. Lett.*, 107:066402, Aug 2011. doi: 10.1103/PhysRevLett.107.066402. URL `https://link.aps.org/doi/10.1103/PhysRevLett.107.066402`.

[100] I. C. Fulga, F. Hassler, A. R. Akhmerov, and C. W. J. Beenakker. Topological quantum number and critical exponent from conductance fluctuations at the quantum hall plateau transition. *Phys. Rev. B*, 84:245447, Dec 2011. doi: 10.1103/PhysRevB.84.245447. URL `https://link.aps.org/doi/10.1103/PhysRevB.84.245447`.

[101] Hideaki Obuse, Ilya A. Gruzberg, and Ferdinand Evers. Finite-size effects and irrelevant corrections to scaling near the integer quantum hall transition. *Phys. Rev. Lett.*, 109:206804, Nov 2012. doi: 10.1103/PhysRevLett.109.206804. URL `https://link.aps.org/doi/10.1103/PhysRevLett.109.206804`.

[102] J T Chalker and P D Coddington. Percolation, quantum tunnelling and the integer hall effect. *Journal of Physics C: Solid State Physics*, 21(14):2665–2679, may 1988. doi: 10.1088/0022-3719/21/14/008. URL `https://doi.org/10.1088`.

[103] Meint P. Van Albada and Ad Lagendijk. Observation of weak localization of light in a random medium. *Phys. Rev. Lett.*, 55:2692–2695, Dec 1985. doi: 10.1103/PhysRevLett.55.2692. URL `https://link.aps.org/doi/10.1103/PhysRevLett.55.2692`.

[104] M. Kaveh, M. Rosenbluh, I. Edrei, and I. Freund. Weak localization and light scattering from disordered solids. *Phys. Rev. Lett.*, 57:2049–2052, Oct 1986. doi: 10.1103/PhysRevLett.57.2049. URL `https://link.aps.org/doi/10.1103/PhysRevLett.57.2049`.

[105] Meint P. van Albada, Martin B. van der Mark, and Ad Lagendijk. Observation of weak localization of light in a finite slab:

Anisotropy effects and light path classification. *Phys. Rev. Lett.*, 58:361–364, Jan 1987. doi: 10.1103/PhysRevLett.58.361. URL https://link.aps.org/doi/10.1103/PhysRevLett.58.361.

[106] Shanjin He and J. D. Maynard. Detailed measurements of inelastic scattering in anderson localization. *Phys. Rev. Lett.*, 57: 3171–3174, Dec 1986. doi: 10.1103/PhysRevLett.57.3171. URL https://link.aps.org/doi/10.1103/PhysRevLett.57.3171.

[107] Rachida Dalichaouch, J. P. Armstrong, S. Schultz, P. M. Platzman, and S. L. McCall. Microwave localization by two-dimensional random scattering. *Nature*, 354(6348):53–55, 1991. ISSN 1476-4687. doi: 10.1038/354053a0. URL https://doi.org/10.1038/354053a0.

[108] A. A. Chabanov, M. Stoytchev, and A. Z. Genack. Statistical signatures of photon localization. *Nature*, 404(6780):850–853, 2000. ISSN 1476-4687. doi: 10.1038/35009055. URL https://doi.org/10.1038/35009055.

[109] A. A. Chabanov, Z. Q. Zhang, and A. Z. Genack. Breakdown of diffusion in dynamics of extended waves in mesoscopic media. *Phys. Rev. Lett.*, 90:203903, May 2003. doi: 10.1103/PhysRevLett.90.203903. URL https://link.aps.org/doi/10.1103/PhysRevLett.90.203903.

[110] Tal Schwartz, Guy Bartal, Shmuel Fishman, and Mordechai Segev. Transport and anderson localization in disordered two-dimensional photonic lattices. *Nature*, 446:52 EP –, Mar 2007. URL https://doi.org/10.1038/nature05623.

[111] B. Juliette, J Vincen, Z. Zhanchun, A. Bernard, B. Hambrech, P Lugan, D. Clemen, L. Sanchez-Palencia, P. Bouye, and A. Aspec. Direct observation of anderson localization of matter waves in a controlled disorder. *Nature*, 453: 891–894, 2008.

[112] Diederik S. Wiersma, Paolo Bartolini, Ad Lagendijk, and Roberto Righini. Localization of light in a disordered medium. *Nature*, 390(6661):671–673, 1997. ISSN 1476-4687. doi: 10.1038/37757. URL `https://doi.org/10.1038/37757`.

[113] Martin Störzer, Peter Gross, Christof M. Aegerter, and Georg Maret. Observation of the critical regime near anderson localization of light. *Phys. Rev. Lett.*, 96:063904, Feb 2006. doi: 10.1103/PhysRevLett.96.063904. URL `https://link.aps.org/doi/10.1103/PhysRevLett.96.063904`.

[114] C. M. Aegerter, M. Störzer, and G. Maret. Experimental determination of critical exponents in anderson localisation of light. *Europhys. Lett.*, 75(4):562–568, 2006. doi: 10.1209/epl/i2006-10144-3. URL `https://doi.org/10.1209/epl/i2006-10144-3`.

[115] Hefei Hu, A. Strybulevych, J. H. Page, S. E. Skipetrov, and B. A. van Tiggelen. Localization of ultrasound in a three-dimensional elastic network. *Nature Physics*, 4:945 EP –, Oct 2008. URL `https://doi.org/10.1038/nphys1101`.

[116] Sajeev John, H. Sompolinsky, and Michael J. Stephen. Localization in a disordered elastic medium near two dimensions. *Phys. Rev. B*, 27:5592–5603, May 1983. doi: 10.1103/PhysRevB.27.5592. URL `https://link.aps.org/doi/10.1103/PhysRevB.27.5592`.

[117] T. R. Kirkpatrick. Localization of acoustic waves. *Phys. Rev. B*, 31:5746–5755, May 1985. doi: 10.1103/PhysRevB.31.5746. URL `https://link.aps.org/doi/10.1103/PhysRevB.31.5746`.

[118] Martin Hirsekorn. Small-size sonic crystals with strong attenuation bands in the audible frequency range. *Applied Physics Letters*, 84(17):3364–3366, 2004. doi: 10.1063/1.1723688. URL `https://doi.org/10.1063/1.1723688`.

[119] Nicholas Fang, Dongjuan Xi, Jianyi Xu, Muralidhar Ambati, Werayut Srituravanich, Cheng Sun, and Xiang Zhang. Ultrasonic metamaterials with neg-

ative modulus. *Nature Materials*, 5(6):452–456, 2006. ISSN 1476-4660. doi: 10.1038/nmat1644. URL `https://doi.org/10.1038/nmat1644`.

[120] Zhi-Yong Tao, Ting Liu, Huan Liu, and Ya-Xian Fan. Antisymmetric localization by a defect in an acoustic band-gap structure. *Phys. Rev. Applied*, 11:024033, Feb 2019. doi: 10.1103/PhysRevApplied.11.024033. URL `https://link.aps.org/doi/10.1103/PhysRevApplied.11.024033`.

[121] E. Akkermans and R. Maynard. Weak localization and anharmonicity of phonons. *Phys. Rev. B*, 32:7850–7862, Dec 1985. doi: 10.1103/PhysRevB.32.7850. URL `https://link.aps.org/doi/10.1103/PhysRevB.32.7850`.

[122] J. E. Graebner, B. Golding, and L. C. Allen. Phonon localization in glasses. *Phys. Rev. B*, 34:5696–5701, Oct 1986. doi: 10.1103/PhysRevB.34.5696. URL `https://link.aps.org/doi/10.1103/PhysRevB.34.5696`.

[123] Walter Schirmacher and Michael Wagener. Vibrational anomalies and phonon localization in glasses. *Solid State Communications*, 86(9):597 – 603, 1993. ISSN 0038-1098. doi: https://doi.org/10.1016/0038-1098(93)90147-F. URL `http://www.sciencedirect.com/science/article/pii/003810989390147F`.

[124] Walter Schirmacher, Gregor Diezemann, and Carl Ganter. Harmonic vibrational excitations in disordered solids and the "boson peak". *Phys. Rev. Lett.*, 81:136–139, Jul 1998. doi: 10.1103/PhysRevLett.81.136. URL `https://link.aps.org/doi/10.1103/PhysRevLett.81.136`.

[125] Jan W. Kantelhardt, Armin Bunde, and Ludwig Schweitzer. Extended fractons and localized phonons on percolation clusters. *Phys. Rev. Lett.*, 81:4907–4910, Nov 1998. doi: 10.1103/PhysRevLett.81.4907. URL `https://link.aps.org/doi/10.1103/PhysRevLett.81.4907`.

[126] J. J. Ludlam, S. N. Taraskin, and S. R. Elliott. Disorder-induced vibrational localization. *Phys. Rev. B*, 67:132203,

Apr 2003. doi: 10.1103/PhysRevB.67.132203. URL https://link.aps.org/doi/10.1103/PhysRevB.67.132203.

[127] L. D. Hicks and M. S. Dresselhaus. Effect of quantum-well structures on the thermoelectric figure of merit. *Phys. Rev. B*, 47: 12727–12731, May 1993. doi: 10.1103/PhysRevB.47.12727. URL https://link.aps.org/doi/10.1103/PhysRevB.47.12727.

[128] Woochul Kim, Joshua Zide, Arthur Gossard, Dmitri Klenov, Susanne Stemmer, Ali Shakouri, and Arun Majumdar. Thermal conductivity reduction and thermoelectric figure of merit increase by embedding nanoparticles in crystalline semiconductors. *Phys. Rev. Lett.*, 96:045901, Feb 2006. doi: 10.1103/PhysRevLett.96.045901. URL https://link.aps.org/doi/10.1103/PhysRevLett.96.045901.

[129] R Venkatasubramanian, E Siivola, T Colpitts, and B OQuinn. Thin-film thermoelectric devices with high room-temperature figures of merit. *Nature*, 413: 597–602, 2001.

[130] T.c Harman, P.J Taylor, M Walsh, and B.E LaForge. Quantum dot superlattice thermoelectric materials and devices. *Science*, 297:2229–2232, 2002.

[131] Bin Liang, Bo Yuan, and Jian-chun Cheng. Acoustic diode: Rectification of acoustic energy flux in one-dimensional systems. *Phys. Rev. Lett.*, 103:104301, Sep 2009. doi: 10.1103/PhysRevLett.103.104301. URL https://link.aps.org/doi/10.1103/PhysRevLett.103.104301.

[132] B Liang, X.S Guo, D Zhang, and J.C Cheng. An acoustic rectifier. *Nature Mater*, 9, 2010.

[133] M. Trigo, A. Bruchhausen, A. Fainstein, B. Jusserand, and V. Thierry-Mieg. Confinement of acoustical vibrations in a semiconductor planar phonon cavity. *Phys. Rev. Lett.*, 89:227402, Nov 2002. doi: 10.1103/PhysRevLett.89.227402. URL https://link.aps.org/doi/10.1103/PhysRevLett.89.227402.

147

[134] Matt Eichenfield, Ryan M Chan, Jasper, J Kerry, and Painter Osker. Optomechanical crystals. *Nature*, 462:78–82, 2009.

[135] I. E. Psarobas, N. Papanikolaou, N. Stefanou, B. Djafari-Rouhani, B. Bonello, and V. Laude. Enhanced acousto-optic interactions in a one-dimensional phoxonic cavity. *Phys. Rev. B*, 82: 174303, Nov 2010. doi: 10.1103/PhysRevB.82.174303. URL `https://link.aps.org/doi/10.1103/PhysRevB.82.174303`.

[136] A. Fainstein, N. D. Lanzillotti-Kimura, B. Jusserand, and B. Perrin. Strong optical-mechanical coupling in a vertical gaas/alas microcavity for subterahertz phonons and near-infrared light. *Phys. Rev. Lett.*, 110:037403, Jan 2013. doi: 10.1103/PhysRevLett.110.037403. URL `https://link.aps.org/doi/10.1103/PhysRevLett.110.037403`.

[137] E. Gavartin, R. Braive, I. Sagnes, O. Arcizet, A. Beveratos, T. J. Kippenberg, and I. Robert-Philip. Optomechanical coupling in a two-dimensional photonic crystal defect cavity. *Phys. Rev. Lett.*, 106: 203902, May 2011. doi: 10.1103/PhysRevLett.106.203902. URL `https://link.aps.org/doi/10.1103/PhysRevLett.106.203902`.

[138] A.A. Maradudin. Theoretical and experimental aspects of the effects of point defects and disorder on the vibrations of crystals*—1. volume 18 of *Solid State Physics*, pages 273 – 420. Academic Press, 1966. doi: http://dx.doi.org/10.1016/S0081-1947(08)60350-1. URL `//www.sciencedirect.com/science/article/pii/S0081194708603501`.

[139] B Kramer and A MacKinnon. Localization: theory and experiment. *Reports on Progress in Physics*, 56(12):1469–1564, dec 1993. doi: 10.1088/0034-4885/56/12/001. URL `https://doi.org/10.1088`.

[140] R.N. SILVER and H. RÖDER. Densities of states of mega-dimensional hamiltonian matrices. *International Journal of Modern Physics*

C, 05(04):735–753, 1994. doi: 10.1142/S0129183194000842. URL https://doi.org/10.1142/S0129183194000842.

[141] R. N. Silver and H. Röder. Calculation of densities of states and spectral functions by chebyshev recursion and maximum entropy. *Phys. Rev. E*, 56:4822–4829, Oct 1997. doi: 10.1103/PhysRevE.56.4822. URL http://link.aps.org/doi/10.1103/PhysRevE.56.4822.

[142] G. Schubert and H. Fehske. *Quantum and Semi-classical Percolation and Breakdown in Disordered Solids, Lecture Notes in Physics.* Springer Berlin Heidelberg, 2009.

[143] B. Kramer and M. Schreiber. *K. H. Hoffmann and M. Schreiber (eds.) in Computational Physics.* Springer, Berlin, 1996.

[144] A. MacKinnon and B. Kramer. *Z. Phys. B*, 53:1–13, 1983.

[145] B. Kramer, A. MacKinnon, T. Ohtsuki, and K. Slevin. *Int. J. Mod. Phys. B*, 24:1841, 2010.

[146] P. Markos. *Acta Physica Slovaca*, 56:561, 2006.

[147] Eytan Domany and Sanjoy Sarker. Renormalization-group study of anderson localization. *Phys. Rev. B*, 20:4726–4729, Dec 1979. doi: 10.1103/PhysRevB.20.4726. URL http://link.aps.org/doi/10.1103/PhysRevB.20.4726.

[148] L. Root and J. L. Skinner. Renormalization-group approach to quantum percolation and anderson localization. *Phys. Rev. B*, 33:7738–7742, Jun 1986. doi: 10.1103/PhysRevB.33.7738. URL http://link.aps.org/doi/10.1103/PhysRevB.33.7738.

[149] A. Singh and W. L. McMillan. *J. Phys. C*, 18:2097, 1985.

[150] Freeman J. Dyson. The dynamics of a disordered linear chain. *Phys. Rev.*, 92:1331–1338, Dec 1953. doi: 10.1103/PhysRev.92.1331. URL http://link.aps.org/doi/10.1103/PhysRev.92.1331.

[151] Richard Bellman. Dynamics of a disordered linear chain. *Phys. Rev.*, 101:19–19, Jan 1956. doi: 10.1103/PhysRev.101.19. URL `http://link.aps.org/doi/10.1103/PhysRev.101.19`.

[152] Elliott W. Montroll and Renfrey B. Potts. Effect of defects on lattice vibrations. *Phys. Rev.*, 100:525–543, Oct 1955. doi: 10.1103/PhysRev.100.525. URL `http://link.aps.org/doi/10.1103/PhysRev.100.525`.

[153] George Weiss and Alexei Maradudin. Thermodynamic properties of a disordered lattice. *Journal of Physics and Chemistry of Solids*, 7(4):327 – 344, 1958. ISSN 0022-3697. doi: http://dx.doi.org/10.1016/0022-3697(58)90283-X. URL `http://www.sciencedirect.com/science/article/pii/002236975890283X`.

[154] Elliott, D. W. Taylor, and Rudolf Ernst Peierls. Vibrations of random dilute alloys. *Proceedings of the Royal Society of London*, 296(1445):161–188, 1967. doi: 10.1098/rspa.1967.0012. URL `https://royalsocietypublishing.org/doi/abs/10.1098/rspa.1967.0012`.

[155] R. W. Davies and J. S. Langer. Self-consistent field approximation for the frequency spectrum of a disordered chain. *Phys. Rev.*, 131:163–166, Jul 1963. doi: 10.1103/PhysRev.131.163. URL `http://link.aps.org/doi/10.1103/PhysRev.131.163`.

[156] Melvin Lax. Multiple scattering of waves. *Rev. Mod. Phys.*, 23:287–310, Oct 1951. doi: 10.1103/RevModPhys.23.287. URL `http://link.aps.org/doi/10.1103/RevModPhys.23.287`.

[157] D. W. Taylor. Vibrational properties of imperfect crystals with large defect concentrations. *Phys. Rev.*, 156:1017–1029, Apr 1967. doi: 10.1103/PhysRev.156.1017. URL `https://link.aps.org/doi/10.1103/PhysRev.156.1017`.

[158] Qian-Jin Chu and Zhao-Qing Zhang. Localization of phonons in mixed crystals. *Phys. Rev. B*, 38:4906–4915, Sep 1988. doi: 10.1103/PhysRevB.38.4906. URL `http://link.aps.org/doi/10.1103/PhysRevB.38.4906`.

[159] W. A. Kamitakahara and D. W. Taylor. Comparison of single-site approximations for the lattice dynamics of mass-disordered alloys. *Phys. Rev. B*, 10:1190–1199, Aug 1974. doi: 10.1103/PhysRevB.10.1190. URL `http://link.aps.org/doi/10.1103/PhysRevB.10.1190`.

[160] A Mookerjee. A new formalism for the study of configuration-averaged properties of disordered systems. *Journal of Physics C: Solid State Physics*, 6(10): L205, 1973. URL `http://stacks.iop.org/0022-3719/6/i=10/a=003`.

[161] M Yussouff and A Mookerjee. Phonon frequency spectrum in random binary alloys. *Journal of Physics C: Solid State Physics*, 17(6):1009, 1984. URL `http://stacks.iop.org/0022-3719/17/i=6/a=010`.

[162] Theodore Kaplan, P. L. Leath, L. J. Gray, and H. W. Diehl. Self-consistent cluster theory for systems with off-diagonal disorder. *Phys. Rev. B*, 21:4230–4246, May 1980. doi: 10.1103/PhysRevB.21.4230. URL `http://link.aps.org/doi/10.1103/PhysRevB.21.4230`.

[163] Robert Mills and Pisistha Ratanavararaksa. Analytic approximation for substitutional alloys. *Phys. Rev. B*, 18:5291–5308, Nov 1978. doi: 10.1103/PhysRevB.18.5291. URL `http://link.aps.org/doi/10.1103/PhysRevB.18.5291`.

[164] Subhradip Ghosh, P. L. Leath, and Morrel H. Cohen. Phonons in random alloys: The itinerant coherent-potential approximation. *Phys. Rev. B*, 66:214206, Dec 2002. doi: 10.1103/PhysRevB.66.214206. URL `https://link.aps.org/doi/10.1103/PhysRevB.66.214206`.

[165] J. Kroha, C. M. Soukoulis, and P. Wölfle. Localization of classical waves in a random medium: A self-consistent theory. *Phys. Rev.*

*B*, 47:11093–11096, May 1993. doi: 10.1103/PhysRevB.47.11093. URL https://link.aps.org/doi/10.1103/PhysRevB.47.11093.

[166] P. DEAN. The vibrational properties of disordered systems: Numerical studies. *Rev. Mod. Phys.*, 44:127–168, Apr 1972. doi: 10.1103/RevModPhys.44.127. URL http://link.aps.org/doi/10.1103/RevModPhys.44.127.

[167] Daniel N. Payton and William M. Visscher. Dynamics of disordered harmonic lattices. i. normal-mode frequency spectra for randomly disordered isotopic binary lattices. *Phys. Rev.*, 154:802–811, Feb 1967. doi: 10.1103/PhysRev.154.802. URL https://link.aps.org/doi/10.1103/PhysRev.154.802.

[168] S. D. Pinski, W. Schirmacher, and R. A. Römer. Anderson universality in a model of disordered phonons. *EPL (Europhysics Letters)*, 97(1):16007, 2012. URL http://stacks.iop.org/0295-5075/97/i=1/a=16007.

[169] Cécile Monthus and Thomas Garel. Anderson localization of phonons in dimension $d = 1, 2, 3$: Finite-size properties of the inverse participation ratios of eigenstates. *Phys. Rev. B*, 81:224208, Jun 2010. doi: 10.1103/PhysRevB.81.224208. URL https://link.aps.org/doi/10.1103/PhysRevB.81.224208.

[170] Thomas Maier, Mark Jarrell, Thomas Pruschke, and Matthias H. Hettler. Quantum cluster theories. *Rev. Mod. Phys.*, 77:1027–1080, Oct 2005. doi: 10.1103/RevModPhys.77.1027. URL https://link.aps.org/doi/10.1103/RevModPhys.77.1027.

[171] C. E. Ekuma, H. Terletska, K.-M. Tam, Z.-Y. Meng, J. Moreno, and M. Jarrell. Typical medium dynamical cluster approximation for the study of anderson localization in three dimensions. *Phys. Rev. B*, 89:081107, Feb 2014. doi: 10.1103/PhysRevB.89.081107. URL https://link.aps.org/doi/10.1103/PhysRevB.89.081107.

[172] H. Terletska, C. E. Ekuma, C. Moore, K.-M. Tam, J. Moreno, and M. Jarrell. Study of off-diagonal disorder using the typical medium dynamical cluster approximation. *Phys. Rev. B*, 90: 094208, Sep 2014. doi: 10.1103/PhysRevB.90.094208. URL `https://link.aps.org/doi/10.1103/PhysRevB.90.094208`.

[173] Yi Zhang, R. Nelson, Elisha Siddiqui, K.-M. Tam, U. Yu, T. Berlijn, W. Ku, N. S. Vidhyadhiraja, J. Moreno, and M. Jarrell. Generalized multiband typical medium dynamical cluster approximation: Application to (ga,mn)n. *Phys. Rev. B*, 94:224208, Dec 2016. doi: 10.1103/PhysRevB.94.224208. URL `https://link.aps.org/doi/10.1103/PhysRevB.94.224208`.

[174] V. Dobrosavljević, A. A. Pastor, and B. K. Nikolić. Typical medium theory of anderson localization: A local order parameter approach to strong-disorder effects. *EPL (Europhysics Letters)*, 62(1):76, 2003. URL `http://stacks.iop.org/0295-5075/62/i=1/a=076`.

[175] R. N. Aiyer, R. J. Elliott, J. A. Krumhansl, and P. L. Leath. Pair effects and self-consistent corrections in disordered alloys. *Phys. Rev.*, 181:1006–1014, May 1969. doi: 10.1103/PhysRev.181.1006. URL `http://link.aps.org/doi/10.1103/PhysRev.181.1006`.

[176] H Terletska, Y Zhang, K-M Tam, T Berlijn, L Chioncel, N. S Vidhyadhiraja, and M Jarrell. Quantum cluster typical medium method for the study of localization in strongly disordered electronic systems. *Appl. Sci.*, 8:2401, 2018.

[177] J. S. Langer. Frequency spectrum of a disordered one-dimensional lattice. *Journal of Mathematical Physics*, 2(4):584–591, 1961. doi: 10.1063/1.1703742. URL `https://doi.org/10.1063/1.1703742`.

[178] Charles W. Myles and John D. Dow. Theory of alloys. i. embedded-cluster calculations of phonon spectra for a one-dimensional binary alloy. *Phys.*

*Rev. B*, 19:4939–4951, May 1979. doi: 10.1103/PhysRevB.19.4939. URL `http://link.aps.org/doi/10.1103/PhysRevB.19.4939`.

[179] M. Jarrell and H. R. Krishnamurthy. Systematic and causal corrections to the coherent potential approximation. *Phys. Rev. B*, 63:125102, Mar 2001. doi: 10.1103/PhysRevB.63.125102. URL `https://link.aps.org/doi/10.1103/PhysRevB.63.125102`.

[180] N Mott. The mobility edge since 1967. *Journal of Physics C: Solid State Physics*, 20(21):3075, 1987. URL `http://stacks.iop.org/0022-3719/20/i=21/a=008`.

[181] G Semeghini, M Landini, P Castilho, S Roy, G Spagnolli, A Trenkwalder, M Fattori, M lnguscio, and G Modugno. Measurement of the mobility edge for 3d anderson localization. *Nature Phys.*, 11(21):554, 2015. URL `http://stacks.iop.org/0022-3719/20/i=21/a=008`.

[182] Ross T. Howie, Ioan B. Magdău, Alexander F. Goncharov, Graeme J. Ackland, and Eugene Gregoryanz. Phonon localization by mass disorder in dense hydrogen-deuterium binary alloy. *Phys. Rev. Lett.*, 113:175501, Oct 2014. doi: 10.1103/PhysRevLett.113.175501. URL `https://link.aps.org/doi/10.1103/PhysRevLett.113.175501`.

[183] C.-K. Peng, S. V. Buldyrev, A. L. Goldberger, S. Havlin, F. Sciortino, M. Simons, and H. E. Stanley. Long-range correlations in nucleotide sequences. *Nature*, 356(6365):168–170, 1992. ISSN 1476-4687. doi: 10.1038/356168a0. URL `https://doi.org/10.1038/356168a0`.

[184] Dirk Holste, Ivo Grosse, and Hanspeter Herzel. Statistical analysis of the dna sequence of human chromosome 22. *Phys. Rev. E*, 64:041917, Sep 2001. doi: 10.1103/PhysRevE.64.041917. URL `https://link.aps.org/doi/10.1103/PhysRevE.64.041917`.

[185] Qiuzi Li, E. H. Hwang, E. Rossi, and S. Das Sarma. Theory of 2d transport in graphene for correlated disorder. *Phys. Rev. Lett.*, 107:156601, Oct 2011. doi: 10.1103/PhysRevLett.107.156601. URL `https://link.aps.org/doi/10.1103/PhysRevLett.107.156601`.

[186] Tohru Kawarabayashi, Yasuhiro Hatsugai, and Hideo Aoki. Quantum hall plateau transition in graphene with spatially correlated random hopping. *Phys. Rev. Lett.*, 103:156804, Oct 2009. doi: 10.1103/PhysRevLett.103.156804. URL `https://link.aps.org/doi/10.1103/PhysRevLett.103.156804`.

[187] Tohru Kawarabayashi, Yoshiyuki Ono, Tomi Ohtsuki, Stefan Kettemann, Alexander Struck, and Bernhard Kramer. Unconventional conductance plateau transitions in quantum hall wires with spatially correlated disorder. *Phys. Rev. B*, 75:235317, Jun 2007. doi: 10.1103/PhysRevB.75.235317. URL `https://link.aps.org/doi/10.1103/PhysRevB.75.235317`.

[188] Adrian Girschik, Florian Libisch, and Stefan Rotter. Topological insulator in the presence of spatially correlated disorder. *Phys. Rev. B*, 88:014201, Jul 2013. doi: 10.1103/PhysRevB.88.014201. URL `https://link.aps.org/doi/10.1103/PhysRevB.88.014201`.

[189] D Clément, A F Varón, J A Retter, L Sanchez-Palencia, A Aspect, and P Bouyer. Experimental study of the transport of coherent interacting matter-waves in a 1d random potential induced by laser speckle. *New Journal of Physics*, 8(8):165–165, aug 2006. doi: 10.1088/1367-2630/8/8/165. URL `https://doi.org/10.1088`.

[190] V. Bellani, E. Diez, R. Hey, L. Toni, L. Tarricone, G. B. Parravicini, F. Domínguez-Adame, and R. Gómez-Alcalá. Experimental evidence of delocalized states in random dimer superlattices. *Phys. Rev. Lett.*, 82:2159–2162, Mar 1999. doi: 10.1103/PhysRevLett.82.2159. URL `https://link.aps.org/doi/10.1103/PhysRevLett.82.2159`.

[191] G Berthet, L Lavoine, M.K Parit, A Brolis, A Boisse, and T Bourdel. Observation of the algebraic localization-delocalization transition in a 1d disordered potential with a bias force. *arXiv:1908.01511*. URL `https://arxiv.org/abs/1908.01511`.

[192] David H. Dunlap, H-L. Wu, and Philip W. Phillips. Absence of localization in a random-dimer model. *Phys. Rev. Lett.*, 65:88–91, Jul 1990. doi: 10.1103/PhysRevLett.65.88. URL `https://link.aps.org/doi/10.1103/PhysRevLett.65.88`.

[193] H.-L. Wu and Philip Phillips. Polyaniline is a random-dimer model: A new transport mechanism for conducting polymers. *Phys. Rev. Lett.*, 66:1366–1369, Mar 1991. doi: 10.1103/PhysRevLett.66.1366. URL `https://link.aps.org/doi/10.1103/PhysRevLett.66.1366`.

[194] S.N. Evangelou and D.E. Katsanos. Super-diffusion in random chains with correlated disorder. *Physics Letters A*, 164(5):456 – 464, 1992. ISSN 0375-9601. doi: https://doi.org/10.1016/0375-9601(92)90114-2. URL `http://www.sciencedirect.com/science/article/pii/0375960192901142`.

[195] J. Heinrichs. Localization, antilocalization, and delocalization in one-dimensional disordered lattices. *Phys. Rev. B*, 51: 5699–5710, Mar 1995. doi: 10.1103/PhysRevB.51.5699. URL `https://link.aps.org/doi/10.1103/PhysRevB.51.5699`.

[196] E. N. Economou, C. M. Soukoulis, and M. H. Cohen. Localization for correlated binary-alloy disorder. *Phys. Rev. B*, 37: 4399–4407, Mar 1988. doi: 10.1103/PhysRevB.37.4399. URL `https://link.aps.org/doi/10.1103/PhysRevB.37.4399`.

[197] A Bovier. Perturbation theory for the random dimer model. *Journal of Physics A: Mathematical and General*, 25(5):1021–1029, mar 1992. doi: 10.1088/0305-4470/25/5/011. URL `https://doi.org/10.1088`.

[198] J C Flores and M Hilke. Absence of localization in disordered systems with local correlation. *Journal of Physics A: Mathematical and General*, 26(24):L1255–L1259, dec 1993. doi: 10.1088/0305-4470/26/24/002. URL `https://doi.org/10.1088`.

[199] J C Flores. Transport in models with correlated diagonal and off-diagonal disorder. *Journal of Physics: Condensed Matter*, 1(44):8471–8479, nov 1989. doi: 10.1088/0953-8984/1/44/017. URL `https://doi.org/10.1088`.

[200] Pedro Carpena, Pedro Bernaola-Galván, Plamen Ch Ivanov, and H. Eugene Stanley. Metal-insulator transition in chains with correlated disorder. *Nature*, 418(6901):955–959, 2002. ISSN 1476-4687. doi: 10.1038/nature00948. URL `https://doi.org/10.1038/nature00948`.

[201] Francisco A. B. F. de Moura and Marcelo L. Lyra. Delocalization in the 1d anderson model with long-range correlated disorder. *Phys. Rev. Lett.*, 81:3735–3738, Oct 1998. doi: 10.1103/PhysRevLett.81.3735. URL `https://link.aps.org/doi/10.1103/PhysRevLett.81.3735`.

[202] Sajeev John and Michael J. Stephen. Wave propagation and localization in a long-range correlated random potential. *Phys. Rev. B*, 28:6358–6368, Dec 1983. doi: 10.1103/PhysRevB.28.6358. URL `https://link.aps.org/doi/10.1103/PhysRevB.28.6358`.

[203] Wasim Raja Mondal, N. S. Vidhyadhiraja, T. Berlijn, Juana Moreno, and M. Jarrell. Localization of phonons in mass-disordered alloys: A typical medium dynamical cluster approach. *Phys. Rev. B*, 96:014203, Jul 2017. doi: 10.1103/PhysRevB.96.014203. URL `https://link.aps.org/doi/10.1103/PhysRevB.96.014203`.

[204] Wasim Raja Mondal, T. Berlijn, M. Jarrell, and N. S. Vidhyadhiraja. Phonon localization in binary alloys with diagonal and off-diagonal disorder: A cluster green's function approach. *Phys. Rev.*

*B*, 99:134203, Apr 2019. doi: 10.1103/PhysRevB.99.134203. URL
`https://link.aps.org/doi/10.1103/PhysRevB.99.134203`.

[205] N Mott. The mobility edge since 1967. *Journal of Physics C: Solid State Physics*, 20(21):3075–3102, jul 1987. doi: 10.1088/0022-3719/20/21/008. URL `https://doi.org/10.1088`.

[206] G. Semeghini, M. Landini, P. Castilho, S. Roy, G. Spagnolli, A. Trenkwalder, M. Fattori, M. Inguscio, and G. Modugno. Measurement of the mobility edge for 3d anderson localization. *Nature Physics*, 11:554 EP –, Jun 2015. URL `https://doi.org/10.1038/nphys3339`. Article.

[207] Theodore Kaplan and Mark Mostoller. Force constant and mass disorder in vibrational systems in the coherent-potential approximation. *Phys. Rev. B*, 9:1783–1791, Feb 1974. doi: 10.1103/PhysRevB.9.1783. URL `https://link.aps.org/doi/10.1103/PhysRevB.9.1783`.

[208] Theodore Kaplan and L. J. Gray. Elementary excitations in random substitutional alloys. *Phys. Rev. B*, 14:3462–3470, Oct 1976. doi: 10.1103/PhysRevB.14.3462. URL `https://link.aps.org/doi/10.1103/PhysRevB.14.3462`.

[209] L. J. Gray and Theodore Kaplan. Self-consistent theory for random alloys with short-range order. *Phys. Rev. B*, 24:1872–1882, Aug 1981. doi: 10.1103/PhysRevB.24.1872. URL `https://link.aps.org/doi/10.1103/PhysRevB.24.1872`.

[210] G Grunewald. Inclusion of force constant and mass disorder in a self-consistent theory of phonons in high concentration alloys. *Journal of Physics F: Metal Physics*, 6(6):999, 1976. URL `http://stacks.iop.org/0305-4608/6/i=6/a=014`.

[211] A Mookerjee and R Pratap Singh. Vibrational properties of ni x pt 1-x alloys. *Journal of Physics C: Solid State Physics*, 18(22):4261, 1985. URL http://stacks.iop.org/0022-3719/18/i=22/a=010.

[212] Daniel N. Payton and William M. Visscher. Dynamics of disordered harmonic lattices. iii. normal-mode spectra for abnormal arrays. *Phys. Rev.*, 175:1201–1207, Nov 1968. doi: 10.1103/PhysRev.175.1201. URL https://link.aps.org/doi/10.1103/PhysRev.175.1201.

[213] J. A. Blackman, D. M. Esterling, and N. F. Berk. Generalized locator—coherent-potential approach to binary alloys. *Phys. Rev. B*, 4:2412–2428, Oct 1971. doi: 10.1103/PhysRevB.4.2412. URL https://link.aps.org/doi/10.1103/PhysRevB.4.2412.

[214] S D Pinski and R A Roemer. Study of the localization-delocalization transition for phonons via transfer matrix method techniques. *Journal of Physics: Conference Series*, 286(1):012025, 2011. URL http://stacks.iop.org/1742-6596/286/i=1/a=012025.

[215] Y. M. Beltukov, V. I. Kozub, and D. A. Parshin. Ioffe-regel criterion and diffusion of vibrations in random lattices. *Phys. Rev. B*, 87:134203, Apr 2013. doi: 10.1103/PhysRevB.87.134203. URL https://link.aps.org/doi/10.1103/PhysRevB.87.134203.

[216] Matthew D. Gratale, Peter J. Yunker, Ke Chen, Tim Still, Kevin B. Aptowicz, and A. G. Yodh. Phonons in two-dimensional colloidal crystals with bond-strength disorder. *Phys. Rev. E*, 87: 052301, May 2013. doi: 10.1103/PhysRevE.87.052301. URL https://link.aps.org/doi/10.1103/PhysRevE.87.052301.

[217] D. Kaya, N.L Green, C.E Maloney, and M.F Islam. Normal modes and density of states in disordered colliodial solids. *Science*, 329:656–658, August 2010.

[218] Y. Tsunoda, N. Kunitomi, N. Wakabayashi, R. M. Nicklow, and H. G. Smith. Phonon dispersion relations in the disordered $ni_{1-x}pt_x$ system. *Phys. Rev. B*, 19:2876–2885, Mar 1979. doi: 10.1103/PhysRevB.19.2876. URL `http://link.aps.org/doi/10.1103/PhysRevB.19.2876`.

[219] M. E. Manley, J. W. Lynn, D. L. Abernathy, E. D. Specht, O. Delaire, A. R. Bishop, R. Sahul, and J. D. Budai. Phonon localization drives polar nanoregions in a relaxor ferroelectric. *Nature Communications*, 5:3683 EP –, Apr 2014. URL `https://doi.org/10.1038/ncomms4683`. Article.

[220] Sanli Faez, Anatoliy Strybulevych, John H. Page, Ad Lagendijk, and Bart A. van Tiggelen. Observation of multifractality in anderson localization of ultrasound. *Phys. Rev. Lett.*, 103: 155703, Oct 2009. doi: 10.1103/PhysRevLett.103.155703. URL `https://link.aps.org/doi/10.1103/PhysRevLett.103.155703`.

[221] S. D. Pinski, W. Schirmacher, and R. A. Römer. Anderson universality in a model of disordered phonons. *EPL (Europhysics Letters)*, 97(1):16007, jan 2012. doi: 10.1209/0295-5075/97/16007. URL `https://doi.org/10.1209`.

[222] S. E. Skipetrov and I. M. Sokolov. Absence of anderson localization of light in a random ensemble of point scatterers. *Phys. Rev. Lett.*, 112:023905, Jan 2014. doi: 10.1103/PhysRevLett.112.023905. URL `https://link.aps.org/doi/10.1103/PhysRevLett.112.023905`.

[223] S. E. Skipetrov and Y. M. Beltukov. Anderson transition for elastic waves in three dimensions. *Phys. Rev. B*, 98: 064206, Aug 2018. doi: 10.1103/PhysRevB.98.064206. URL `https://link.aps.org/doi/10.1103/PhysRevB.98.064206`.

[224] Yi Zhang, Hanna Terletska, C. Moore, Chinedu Ekuma, Ka-Ming Tam, Tom Berlijn, Wei Ku, Juana Moreno, and Mark Jarrell. Study of multiband disordered systems using the typical medium dynamical cluster approximation.

*Phys. Rev. B*, 92:205111, Nov 2015. doi: 10.1103/PhysRevB.92.205111. URL https://link.aps.org/doi/10.1103/PhysRevB.92.205111.